CYTOTOXICITY STUDIES ON METALLO-SALENS AND THEIR APPLICATIONS IN GENE DELIVERY

by

GETACHEW ABEBE WOLDEMARIAM

Presented to the Faculty of the Graduate School of

The University of Texas at Arlington in Partial Fulfillment

of the Requirements

for the Degree of

DOCTOR OF PHILOSOPHY

THE UNIVERSITY OF TEXAS AT ARLINGTON

December 2008

ACKNOWLEDGEMENTS

I would like to express my heartfelt gratitude to my research advisor Prof. Subhrangsu S. Mandal for his support and guidance during my graduate research work. I would like to extend my sincere appreciation for my current research committee members Prof. Frederick MacDonnell and Prof. Jongyun Heo for their valuable advice, and patience. I also thank my former committee members Prof. Edward Bellion and Prof. Richard Guan for their help.

I would like to thank Dr. Ansari for his helpful suggestions during my writing process in editing and formatting. I would also thank him and James Grants for their help with some of the experiments described in Chapter III. I would like to thank all the wonderful people at our department who help me during my stay at UTA, especially Dr. Brian, Ruth, Jill, Jim, Debby, Autumn, Nancy, Yvonne, Chuck and Rita. I am also thankful for Prof. Zoltan Schelly for allowing us to use his laboratory and Dr. Reddy from his laboratory for helping with DLS measurement. I would like to thank Prof. Krishnan Rajeshwar and Dr. Maryl Osagi for the collaborative work. I would also like to thank our laboratory members, Bibhu, Bogala, Sahba, Bishakha, Imiran, Bhawana, Katrina, and other friends Vihn, Sam, Ross, Abishake, Sabuji, Kennet, Diliki and Thamara for all good times we had. I thank Dr. Sushma for providing us with pLEGFP-N1 plasmid construct used in our experiments. I would like to sincerely thank TPEG for

providing me with tuition scholarship for my graduate work and department of chemistry and biochemistry for giving an opportunity to pursue my graduate study. I would like to thank all my siblings and my parents for their unwavering and loving support they have given me at all times. They are my true unsung heroes on whose shoulder I stand. God Bless you all!

December 2, 2008

ABSTRACT

CYTOTOXICITY STUDIES ON METALLO-SALENS AND THEIR APPLICATIONS IN GENE DELIVERY

Getachew A. Woldemariam, PhD.

The University of Texas at Arlington, 2008

Supervising Professor: Subhrangsu S. Mandal

Most of biological catalysts including nucleases are made of active metal centers. Metal complexes that are able to interact with DNA and RNA mimicking these natural nucleases will be valuable as therapeutic agents that target nucleic acids. Metal complexes have been used for very long time to treat different kinds of illnesses including cancer. Platinum based compounds are among the most widely used anticancer agents in clinical use. The first chapter of this dissertation highlights the roles of metal ions and their complexes with regard to biochemical activities, as enzyme inhibitors, anticancer agents and metallo-nucleases. Moreover, we will discuss the problems associated with the use of anticancer drugs like cisplatin and the steps taken to alleviate that using targeted drug delivery system. Although several drugs are in use for treating various illnesses genetic diseases which are not treatable by conventional therapeutics have recently been a target by gene therapy. This chapter also discusses the

types of gene delivery vehicles used and efforts made to optimize the process of transfection.

In chapter II we discuss the DNA cleavage activities of Fe(III)-salen, its mechanism of action on DNA and sequence specificity. We have found that Fe(III)-salen cleaves DNA in the presence of DTT in a sequence neutral fashion by generating free radicals as indicated by DNA cleavage inhibition experiments. *In vitro* transcription assay performed on naked DNA template shows that Fe(III)-salen inhibits transcription. Further we have analyzed the effects of this metal complex on cultured HEK293 cells and investigated the ability of the complex to affect cell viability and to cause apoptosis (programmed cell death). The cell viability study undertaken shows that Fe(III)-salen is a potent cytotoxic agent with IC_{50} value of 2 μM. We have found that the metal complex has the ability to kill cells via apoptotic process as observed by DAPI staining of the nucleus of the cell. We have studied the mechanism of action of apoptosis and we were able to determine that the metal complex causes apoptosis through intrinsic mitochondrial pathway.

In chapter III we have prepared a series of derivatives of Fe(III)-salen compounds. Initially, we synthesized several Fe(III)-salen derivatives by changing the bridging groups and introducing various hydroxy and methoxy functionalities into the salen moiety. We have investigated the effect bridging groups and substituents on the Fe(III)-salen mediated DNA cleavage properties. Our result showed that the DNA cleavage efficiency decreases as the bridging group is changed from ethylenediamine to *ortho*-pheynlenediamine to 2,3-diaminonaphthalene. Hydroxy-substituted Fe(III)-

salnaphens were more efficient on inducing DNA cleavage compared to corresponding methoxy derivatives. The cytotoxicity analysis of Fe(III)-salen derivatives showed that several compound induce efficient cell death towards MCF7 and HEK293 cells. Most interestingly, however, Fe(III)-salen complexes with lower DNA cleavage activity exhibited higher cytotoxicity. These results demonstrated that *in vitro* DNA clevage properties of the metallo-salen are not essential for their cytotoxicity. Similarly, we have also investigated the effect of 4, 4´-dialkoxy Fe(III)-salen complexes containing various long chain derivatives on HEK293 cells. Our result demonstrated that cytotoxicity of Fe(III)-salen lipid molecules is decreased with the increase in carbon chain length.

In Chapter IV we investigated the self-assembly properties and DNA transfection abilities of our novel long chain containing 4, 4´-dialkoxy Fe(III)-salen lipid complexes. Using dynamic light scattering, scanning electron microscopy and dye-encapsulation experiments, we demonstrated that Fe(III)-salen lipids self-assembled into hollow liposomal structures. We also showed that Fe(III)-salen liposomes form complexes with negatively charged DNA molecules forming lipid-DNA complexes. Moreover, One of the Fe(III)-salen liposome showed efficient DNA delivery (transfection) into cultured human cells.

TABLE OF CONTENTS

LIST OF ILLUSTRATIONS

LIST OF TABLES

LIST OF SCHEMES

LIST OF ABBREVIATIONS

ALS	Amyotrophic Lateral Sclerosis
AD	Alzheimer's Disease
Caspases	Cysteinyl-directed aspartate-specific protease
DAPI	4',6-diamidino-2-phenylindole
DHDAB	Dihexadecyldimethylammonium Bromide
DMSO	Dimethyl Sulfoxide
DOTAP	N-[1-(2,3-dioleyl)propyl]-N,N,N-trimethylammonium chloride
DOX	Doxorubicin
EDTA	Ethylenediaminetetraacetic Acid
DTT	Dithiothreitol
ESI-MS	Electrospray Ionization-Mass Spectrometry
5-FC	5(6)-carboxyfluorescein
FITC	Fluorescein Isothiocyanate
GFP	Green Fluorescent Protein
HEK293	Human Embryonic Kiney Cell 293
HD	Huntington's Disease
IR	Infra Red
IC_{50}	(Inhibitor concentration) the concentration of the drug, which leads to 50%inhibition of the cell growth

Im	Imidazole
Ind	Indazole
LUV	Large Unilamellar Vesicles
MDR	Multi Drug Resistance
MLV	Large Multilamellar Vesicles
NMR	Nuclear Magnetic Resonance
MMPP	Magnesium Monoperoxyphthalate
MRI	Magnetic Resonance Imaging
MTT	(3-4,5-dimethylthiazol-2-yl)-2,5-diphenyltetrazolium bromide
MVV	Multi Vesicular Vesicles
NAMI-A	ImH[*trans*-Ru(Cl)4(DMSO)Im]
PEG	Polyethylene Glycol
PD	Parkinson's Disease
PI	Propedium Iodide
SAINT-2	N-methyl-4(dioleyl)methylpyridinium
STZ	Streptozotocin
SUV	Small Unilamellar Vesicles
TBE	Tris-Boric acid EDTA
TE	Tris-EDTA
TF	Transcription Factor
TNF-α	Tumor Necrosis Factor-alpha

TRITC	Tetramethylrhodamine Isothiocyanate	dihexadecyl dimethyl ammonium bromide

CHAPTER I

INTRODUCTION

1.1 Metal-Complexes and Their Biochemical Significance

The history of metals usage in medicine to heal various illnesses goes back to 5000 years. Ancient Egyptians had used copper to sterilize water and iron for healing purpose while gold was used in China and Arabia to fight various diseases. However, the use of metals during ancient times for medicinal purpose was solely based on superstition. The first rational design of medicinal inorganic compounds had emerged during early 1900s when $K[Au(CN)_2]$ was used for treatment of tuberculosis, and antimony compounds was used for treating leishmaniasis and other gold salts were used as antibacterial compound.[1-10]

Metal ions and their positively charged complexes have the propensity to interact with negatively charged nucleic acids phosphate backbone and nitrogenous bases as well as carboxyl and sulfhydryl groups of proteins. Most of the active sites of enzymes in plant, animals and microbes are made of metal centers that play important role in catalysis. Therefore, it is not surprising that metals have the ability to inhibit many of the cellular enzymes by displacing the original metal due to mere similarity in size and charge. For instance, gallium in Ga^{+3} oxidation state has chemical property that is close to that of Fe^{3+} in terms of its electrical charge, ion diameter coordination

number and electron configuration. Gallium nitrate have been found to inhibit iron dependent M2 subunit of ribonucleotide reductase in mice. [9,11,12] Whereas the anthracyclin derivatives of copper such as bisdoxorubicine Cu(II) complexes (structure in Figure 1.1) has been shown to inhibit protein kinase C, an enzyme that phosphorylate other proteins as part of post-translational regulations. Bi^{3+} compounds have been used to treat gastrointestinal disorders and are known to target mainly proteins and enzymes like metallothion ins Zn^{2+} site and transferrin Fe^{3+} sites.[13,14] Moreover, platinum chloride was found to inhibit DNA polymerase enzyme while cisplatin and tetraplatin have been found to inhibit adenylate cyclase, an important enzyme that convert ATP to 3′, 5′-cyclic AMP molecule in the cell. [8, 15]

1.2 Metal Complexes as Anticancer Agents

Despite the ancient use of some metals for medicinal purposes, metal-based compounds attracted little attention until the serendipitous discovery of cisplatin. Most of the compounds commercialized by pharmaceutical companies come from natural products of plant origin as well as their synthetic organic analogs.[16, 17] However, natural products are usually scarce and their total synthesis is often difficult taking years to develop methodologies. On the other hand metal complexes are relatively simpler to make. They can easily be functionalized to improve their solubility and functions. Because of their diverse electronic and structural properties, metal-complexes have the tendency to interact with important cellular targets, nucleic acids, and proteins.

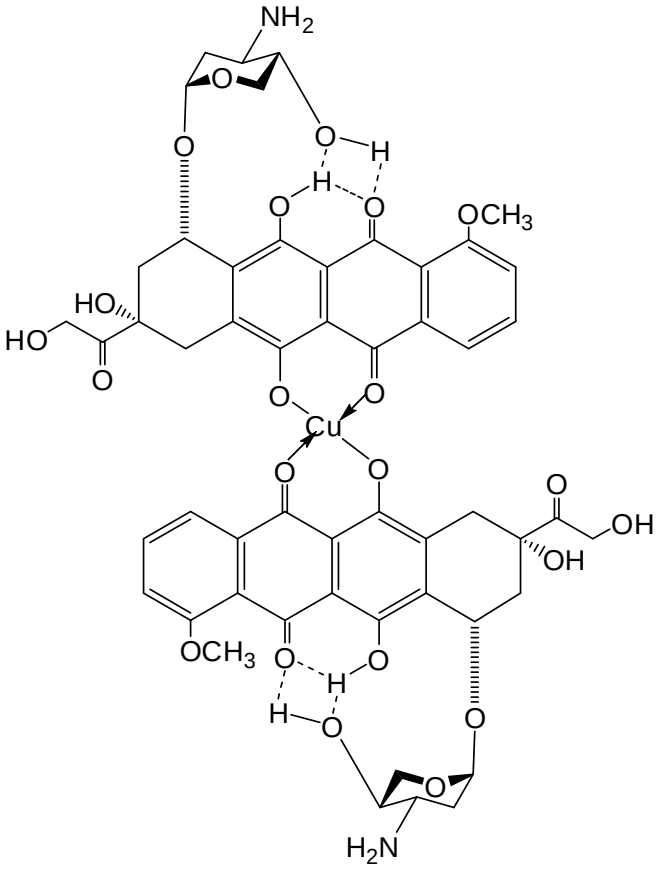

Figure 1.1 Structure of bisdoxorubicine Cu(II) complex.

Thus far the most common metal compounds used as anticancer agents are based on platinum, arsenic, antimony, bismuth, gold, vanadium, iron, rhodium, titanium, and gallium. Bismuth-6-mercaptopurine was the first antitumor compounds tested. Antimony (III) compounds with polydentate carboxylic acids have been shown to have anti-tumor activity in mice inoculated with S180 solid tumors. Vanadium was found to be an inhibitor of chemically induced mammary carcinogenesis; it is also inhibitor of terminal differentiation of murine erythroleukemia cells.[7, 18-20] Considering

the number of metals available there is huge potential to achieve compounds with novel properties that will have important therapeutic values. Amazing clinical success of cisplatin has paved the way for exploration of metal compounds as anticancer agent.

1.2.1 Platinum Based Complexes as Anticancer Agents

The first platinum-containing complex to be used in cancer treatment was cisplatin (*cis*-diamminedichloridoplatinum(II)). It was first synthesized in 1844 and known as Peyrone's chloride. More than about one and quarter century later Rosenberg reported the inhibitory activity of cisplatin on *E. coli* division.[21, 22] Cisplatin entered clinical trial in 1971 and within couples of decades it become the most widely used anticancer drug. Its success arises from the fact that it has very effective anticancer property especially against genitourinary tumors such as testicular cancer, bladder, head, neck, and small cell lung cancer (SCLC).[7, 23-26] Moreover, the possibility to be used in combination regiments as it has different toxicity from that of other anticancer drugs makes it even more attractive anticancer agent. However, the problem with the use of cisplatin is that cancer cells develop resistance to it. Significant side effects especially its toxicity on kidney (nephrotoxicity), neurotoxicity nausea, vomiting limited its clinical application and led to vigorous research to develop its analogs. Around 3000 platinum compounds have since been synthesized and evaluated for their anticancer properties. Thirty of those compounds had reached clinical trials and more than half of those have already been rejected.[9] Currently four of platinum based compounds in clinical use including cisplatin are carboplatin, oxaliplatin and nedaplatin (structure in Figure 1.2).[4] Although cisplatin is superior to carboplatin the latter has

lower toxicity.[9, 24, 25] On the other hand oxaliplatin has higher efficacy and lower toxicity compared to cisplatin and very good for treatment of ovarian, breast, head and neck cancers, malignant melanoma, glioblastoma and NSCLC and gives the best result in colorectal cancer.[7, 9]

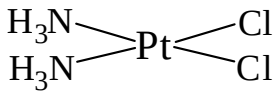

Cisplatin

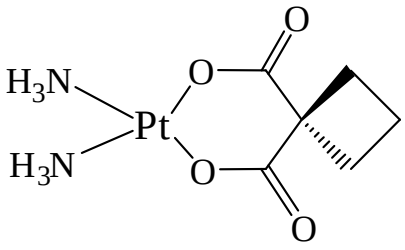

Carboplatin

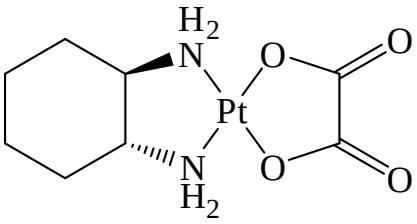

Oxaliplatin

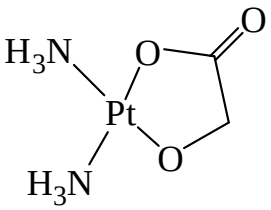

Nedaplatin

Figure 1.2 Some of the platinum based anticancer agents in clinical use.

1.2.2 Ruthenium Based Complexes as Anticancer Agents

Following the clinical success of platinum based complexes, several ruthenium based metal complexes have been prepared and *in vitro* interaction with DNA were studied.[28, 29] Moreover, the effects of these metal complexes on cancer cell lines were also analyzed and some have been found to be effect against cancers that have shown

resistance to cisplatin[29]. Two of promising compounds that made their way to phase II clinical trial are NAMI-A ([H_2Im]{trans-[Ru(III)Cl_4(dmso)(Him)]} and KP1019 inH[*trans*-$Ru^{III}Cl_4(in)_2$] shown (structures in Figure 1.3).[31, 32]

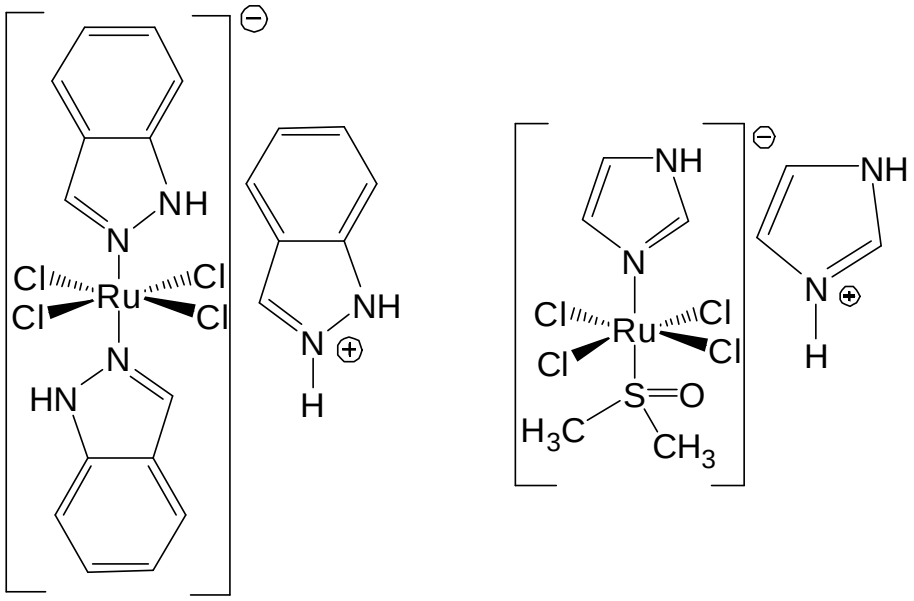

inH[*trans*-$R^{III}Cl_4(in)_2$] (KP1019)

imH[*trans*-$Ru^{III}Cl_4$(dmso-s)(im)] (NAMI-A)

Figure 1.3 Ruthenium based complexes anticancer agents KP1019 and NAMI-A, (in = indazole and im = imidazole).

Ruthenium based compounds are distinct from platinum based complexes in terms of mechanism of action, bio-distribution and toxicity, therefore expected to be active against those tumors that have shown resistance to platinum compounds.[31] Moreover, ruthenium compounds have been shown to exhibit anti-metastatic properties better than platinum compounds and they interact preferentially with proteins than DNA unlike the platinum compounds.[28] They also interact with nitric oxide (NO) molecule

implicated in tumor angiogenesis as well as blood albumin and transfferin an important plasma proteins.[34] For instance KP1019 has been found to be effective against colorectal cancers through mechanism of action different from that of platinum drugs.[29, 32] The uptake of these ruthenium complexes is facilitated by transferrin receptors which are over expressed on cancer cells compared to normal cells due to their higher than normal requirement of tumor cells for iron ion.[34] This will enhance the bio-distribution of ruthenium compounds in cancer cells compared to normal cells. It is believed that under hypoxic condition of tumor cells KP1029 is known to form Ru(II) and induces apoptosis through intrinsic mitochondrial pathway.[30-33]

1.3 Anticancer Drugs Induce Cell Death via Apoptosis

Life is at delicate balance between cell death and cell proliferation. Physiological cell death is as complex as cell proliferation; it is evolutionary conserved, genetically controlled process that is important for morphogenesis, embryonic development and for the maintenance of tissue homeostasis. Under physiological condition cells die primarily through apoptosis a term, which was first coined by Kerr in 1971.[63-65] Apoptosis is one of several kinds of programmed cell death that has been well studied and described. In eukaryotic tissues it serves many purposes in the cell by removing defective cells, by controlling the rate of proliferation in adult tissues and by helping to remove warn out cells and cells infected by microbes. It is well crafted enzymatically orchestrated natural cell death involving cells own participation in the death process. Failure in apoptosis results in cancer, systemic lupus and some viral

infections while abnormal apoptotic process causes neurodegenerative diseases like Alzheimer's, Parkinson's and amyotrophic lateral sclerosis (ALS), stroke, some autoimmune diseases.[66, 67]

In the early 90s, oncologists discovered that anti-cancer drugs kill cells through apoptosis and that modulation of apoptotic processes could induce resistance to cell death, i.e. a resistance to anticancer drugs.[68] Several classes of proteins involved in apoptosis signal transduction have been discovered afterwards. Some of the most important class of proteins found to regulate apoptotic processes was Bcl-2 family of proteins including Bcl-2 itself (Bcl-2, Bcl-XL, Bcl-w) which are anti-apoptotic. Meanwhile other Bcl-2 family members like Bax, Bak, Bik and Bok antagonize the previous class and they are pro-apoptotic.[69, 70] Apoptosis signals could be triggered by anticancer agents [71-73], hormones, cytokines and virus etc. and could occur through two main pathways, the intrinsic or mitochondrial pathway and the extrinsic pathway. In extrinsic pathway TNF-α (Tumor Necrosis Factor-alpha) and Fas ligand (FasL) receptors are involved in mediating the signaling cascade.[74] Perhaps the most relevant apoptotic pathway as far as anticancer drugs are concerned is the intrinsic or mitochondrial pathway where mitochondria and some of its proteins mediate the process of cell suicide.

On the outer surface of mitochondrial membrane of normal cells Bcl-2 protein is displayed preventing pro-apoptotic proteins from binding. When internal damage to the cell occurs either as a result of direct damage to mitochondria or genomic DNA by cytotoxic agents like cisplatin Bax (regulated by p53) and other related proteins, which

are pro-apoptotic, punch holes in the outer mitochondrial membrane causing cytochrome c to leak into cytosol. Cytochrome c is important protein whose primary function is to relay electrons between complex III and complex IV in mitochondrial membrane during oxidative phosphorylation. It is loosely associated with inner mitochondrial membrane but secluded in mitochondria at all times except during apoptosis.[75-77] Once cytochrome c is released into cytosol during apoptosis it binds to Apaf-1 (apoptotic protease activating factor 1) protein forming apoptosomes that activate caspase-9. Caspases (cysteinyl-directed aspartate-specific protease) are proteases that relay the apoptotic process (refer to pathway in Figure 1.4). There are several caspase enzymes and based on the type of role they play in apoptosis they are classified into two main categories. Caspase-2, 8, 9, 10 are considered to be initiators of apoptosis while Caspase-3, 6, 7 propagate apoptotic signal.[78, 79] The activation of caspase-9 by apoptosome complex leads to the activation of executioner caspases 3 and 7. The activation of these caspases in turn ultimately results in the enzymatic cascade that leads to nuclear condensation, cell membrane blebbing, shrinkage of cell and finally chromosomal DNA fragmentation into characteristic 200 bp which culminates in the generation of apoptotic bodies. It has been found that overexpression of the Bcl-2 or Bcl-XL block the release of cytochrome c preventing apoptosis and nullifying the effects of anticancer drugs.[80] In addition, modification of expression of oncogenes (myc, ras, jun, fos, etc) or tumor suppressor genes p53 also alter cell sensitivity to anticancer drugs.[7]

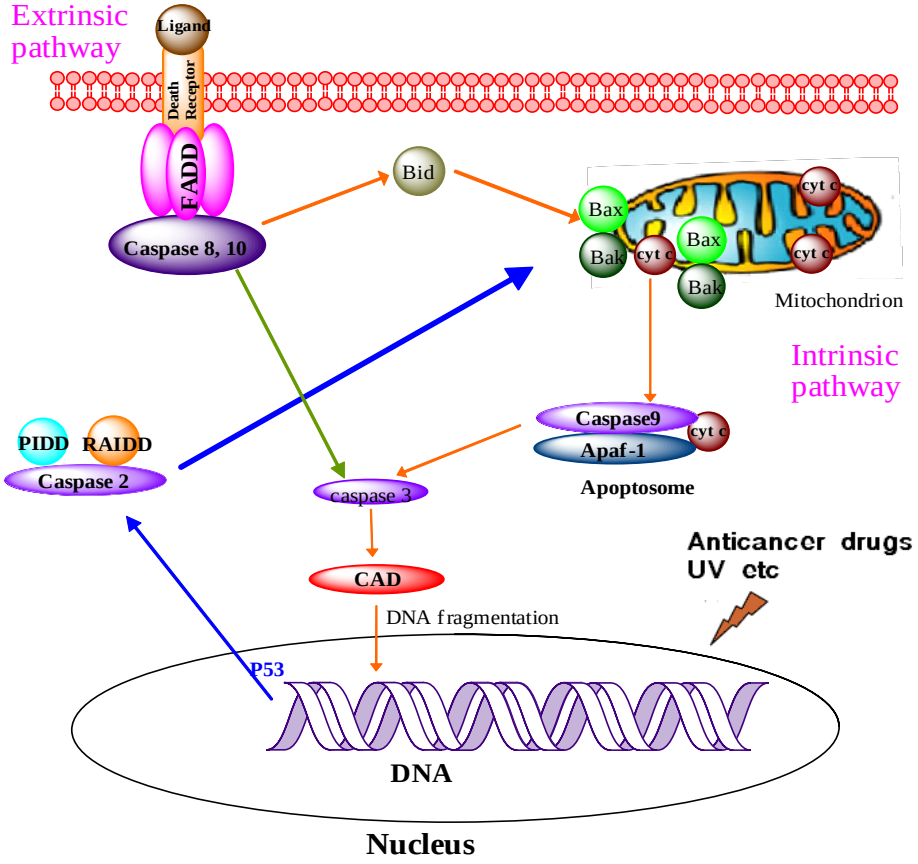

Figure 1.4 An overview of extrinsic and intrinsic apoptotic pathways.

1.4 Metallo-Salens

Transition metal-complexes of tetradentate ligand salen [N,N′-bis(salicylidene)ethylenediamine] are referred as metallo-salen. Co(II)-salen is most possibly first metallo-salen reported by Pfeiffer in 1930s.[34] He indicated that the Co(II)-salen is originally red but turns brown on standing.[35] Tsumaki showed the change in color is due to oxidation of the metal ion by oxygen which turns it brown that could be made to revert to red upon heating at 100 °C as it loses oxygen.[36] Since then several

metallo-salens and their derivatives have been synthesized and their structure characterized.[34-36] Metallo-salen has mostly been used as a catalysts for olefin epoxidation.[37,38] For example Manganese (III)-salen and its derivatives have been widely used. Beacuse many of the metallo-salen can be easily synthesized with different functionality, chirality and metallo-center, metallo-salens are popular choice in olefin oxidation especially in asymmetric oxidation.[43]

For example, derivatives of salen chromium (V) oxo complexes are active catalyst for the epoxidation of olefins in the presence of iodosylbenzene.[38] Similarly manganese (III) and ruthenium(III) salen complexes have also been found to oxidize various organic compounds.[39] Iron(III)-salen complex in the presence of iodosylbenzene has been used to effectively oxidize sulfides to sulfoxides.[37] Most importantly, Jacosen and co-workers made a break through in asymmetric epoxidation by introducing novel chiral manganese(III) salen complexes as efficient epoxidation catalyst (reaction in Scheme 1.1).[39-40]

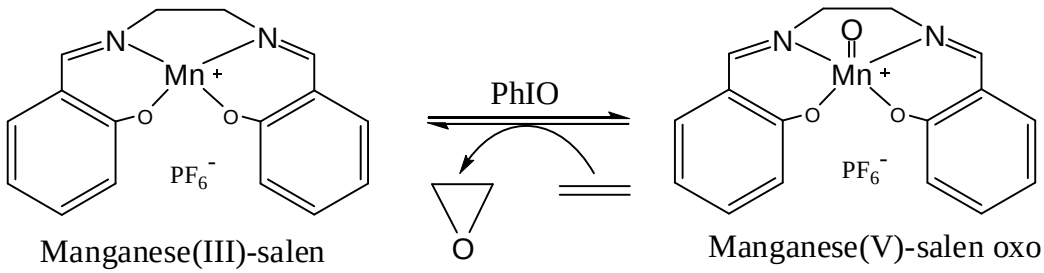

Manganese(III)-salen Manganese(V)-salen oxo

Scheme 1.1 Epoxidation reaction by Mn(III)-salen in the presence of iodosylarene.[41]

1.4.1 DNA Cleavage by Metallo-Salens

Deoxyribonucleic acid, DNA, is the genetic material that contains information about cellular events.[44] Metal complexes that can interact, damage or cleave DNA in predictable and sequence specific manner may play important role in gene regulation and drug discovery. The special class of the compound that interact and cleavae DNA are called chemical nucleases. Many different types of metal-complex based chemical nucleases have been developed and their interaction properties with DNA are well studied.[43] Metallo-salens are one such class of chemical nuclease that interact and damage DNA. Metallo-salens with positively charged metal center have advantage over other compounds because they mimic natural enzymes cofactors and not hindered by large negative charges on phosphodiester bonds to cause DNA strand scission.[42]

The most common mode of interactions of metal complexes with nucleic acids are direct binding via metal center or by non-covalent π-stacking interaction of aromatic group with DNA bases.[43, 45]

The predictable steric and electronic properties of metallo-salens make them attractive choice to study their effect on DNA.[43] By careful choice of the central metal ion and derivatives of salen ligands it is modulate theDNA interaction and cleavage properties of metal-complexes..[46] For example Cr(III) and Mn(III) salen complexes exert their DNA interaction properties differently. Although both complexes are water soluble because of their net positive charge they modify DNA differently. Manganese complex have the square-pyramidal geometry with one water axially ligated while chromium complex has octahedral geometry with two axially ligated water molecules.

Mn(III)-salen does direct strand scission in the presence of MMPP (magnesium monoperoxyphthalate) with selectivity at AT-rich region while such selectivity is clearly absent in chromium complex.[43, 47] On the other hand nickel salen binds DNA and RNA with GC sequence preference through unpaired guanines, which makes it quite different from other metal complexes in its mode of interaction.[47] The DNA cleavage efficiencies of various derivatives of Mn, Cu, Ni and Cr salens compounds (structure in Figure 1.5) were studied in detail and it was found that Mn(III) and Ni(II) derivatives cleaves DNA in the presence of MMPP while Cu(II) and Cr(III) derivatives failed to do so.[48] Similarly bis-8,8′-(para-trimethylammoniumphenyl)Ni(II)-salen was found cause oxidation of guanine residues that have high solvent accessibility in the presence of MMPP.[144]

Moreover, in addition to varying the central metal ion and observing the difference in DNA cleavage activities, twenty-six derivativates of manganese (III) salens were synthesized.[49] It was found that their DNA cleavage properties depend on the type of substituents and their positions on benzene ring.[49, 144] So far the DNA cleavage properties of metallo-salens as a function of varying metal center as well as substituent have been explored. However, very little has been done on their biochemical effects in cells or in animals.[139]

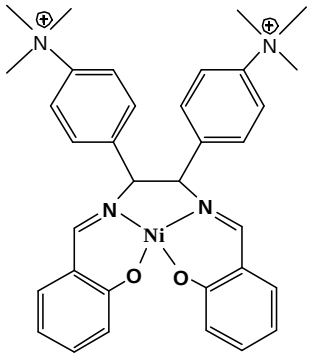

Bis-8,8'-(*p ara*-trimethylammoniumphenyl) Ni(II)-salen

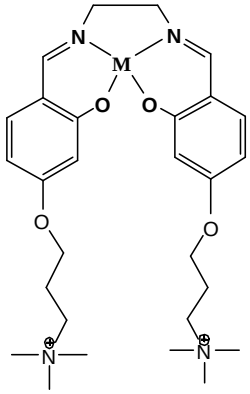

a. M = Mn(III) b. M = Ni(II)
c. M = Cu(II) d. M = Cr(III)

Bis-4,4'-(trimethylammoniumpropyloxy)-metal salen derivatives

Figure 1.5 Examples of metallo-salen based chemical nucleases.

1.4.2 Biochemical Activities of Metallo-Salens

Long before the discovery of insulin, many metal salts like salts of vanadium, chromium, manganese, tungsten, and molybdenum were found to exhibit insulin mimetic effects or have been found to improve the condition of humans with diabetes mellitus.[50] Nevertheless, metal ions are not readily incorporated into the cell and instead metal complexes of these ions have been studied for their efficacy. Notably derivatives of salen vanadium (V) oxo (structure in Figure 1.4) complex was found to exhibit normoglycemic effect in streptozotocin (STZ)-induced type 1 diabetic rats (STZ-rats) when given orally on daily bases.[50, 51]

Studies on cultured human cells have shown that $Cr(salen)(H_2O)_2ClO_4$ exhibited significant inhibition of lymphocyte proliferation as indicated by [^{3}H]-thymidine incorporation and cell viability assays. Nuclear fragmentation assay indicated that it caused nuclear condensation and fragmentation which is a hallmark of apoptosis.[52]

So far the most important biochemical activity of metalo-salen complexes comes from the use of manganese salen derivatives as superoxide dismutase and catalase mimetics. Superoxide dismutase and catalase are metallo-enzymes that perform dismutation reaction or detoxification of ROS (reactive oxygen species). [53] Reactive oxygen species includes superoxide anion ($O_2^{-\cdot}$), hydroxyl radical (·OH), nitric oxide (NO·) and hydrogen peroxide (H_2O_2). Superoxides and hydrogen peroxide are produced in biological systems by the partial reduction of molecular oxygen.[54] SOD catalyzes the removal of superioxide with oxygen and hydrogen peroxide as products while catalase is involved in the removal of hydrogen peroxide by converting it into oxygen and water.[55] Superoxide primarily arises from uncoupling of the mitochondrial electron transport chain during oxidative phosphorylation and other cellular events.[54-57] ROS if unchecked present a clear danger to the cell as they can easily react with many phosphatases containing thiol group and transcription factors like reducing factor-1, activator protein-1 and NFkB creating oxidative stress. Dysfunctional dismutation has been implicated in many of the neurodegenerative diseases and others like PD (Parkinson's disease), HD (Huntington's disease) AD (Alzheimer's disease), ALS (amyotrophic lateral sclerosis), epilepsy, stroke and trauma.[56-58]

The derivatives of manganese salen compounds EUK-134 and EUK-189 (structures in Figure 1.6) [58] are shown to have superoxide dismutase mimetic activity[58]. These compounds have been found to be neuroprotective including those of inflammatory autoimmune diseases like ischemia, epilepsy and amyotrophic lateral sclerosis.[59-60] It is low molecular weight, water soluble, cell permeable compound and has the ability to regenerate. In an *in vivo* trial EUK-134 has been found to reduce formation of peroxide lipids and erythema after UVA exposure.[61, 62]

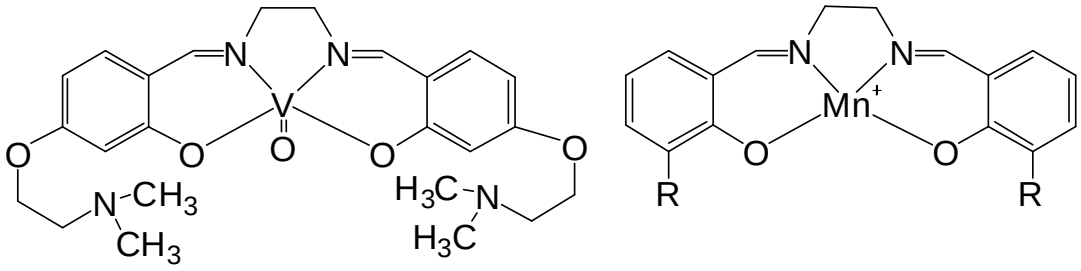

Salen vanadium (V) oxo derivative

EUK-134: R= OCH3

EUK-189: R= OCH_2CH_3

Figure 1.6 Chemical structures of some biochemically active metallo-salens.

1.5 Gene and Drug Delivery Vehicles and Liposomes

1.5.1 Various Types of Delivery Vehicles

One of the greatest challenges in the use of chemotherapeutic anticancer drugs and other drug for that matter are their lack of specificity for intended target which results in severe toxicity and side effect associated with taking the drugs, lack of

solubility in cellular aqueous condition, difficulty to cross cell membrane and degradability or absence of stability under physiological conditions.[81, 82] Similarly, many of the human genetic disorders may not be treated with drugs alone sufficiently and gene therapy is a necessity. However, delivery of genetic material to the required tissue and organ and its efficient expression is a measure hurdle that is hindering the process thus far.[83] The main objectives of drug and gene delivery vehicles are to deliver the right dose of substance to the right place at the right time for the right duration. There are several drug and gene delivery nanoscale vehicles currently in discovery stage, in clinical trial or already in use, which have ameliorated many of drugs associated side effects and also made gene therapy a possibility but far from the desired results.[84] Among the most common nanoscale delivery vehicles are liposomes, micelles, dendrimers, nanoparticles, nanotubes, bioconjugates, fullerens and nanoshells, nucleic acid nanoparticles, magnetic nanoparticles, and virus nanoparticles (cartoon representations in Figure 1.7). [83] They have the potential to increase the efficacy of drugs, lower drug toxicity and ability for sustained drug release over a very long period of time compared to taking bare drug. Moreover, these nanoscale materials not only they are valuable in drug and gene delivery but also they are effectively used or have a potential to be used as imaging and contrasting agent.

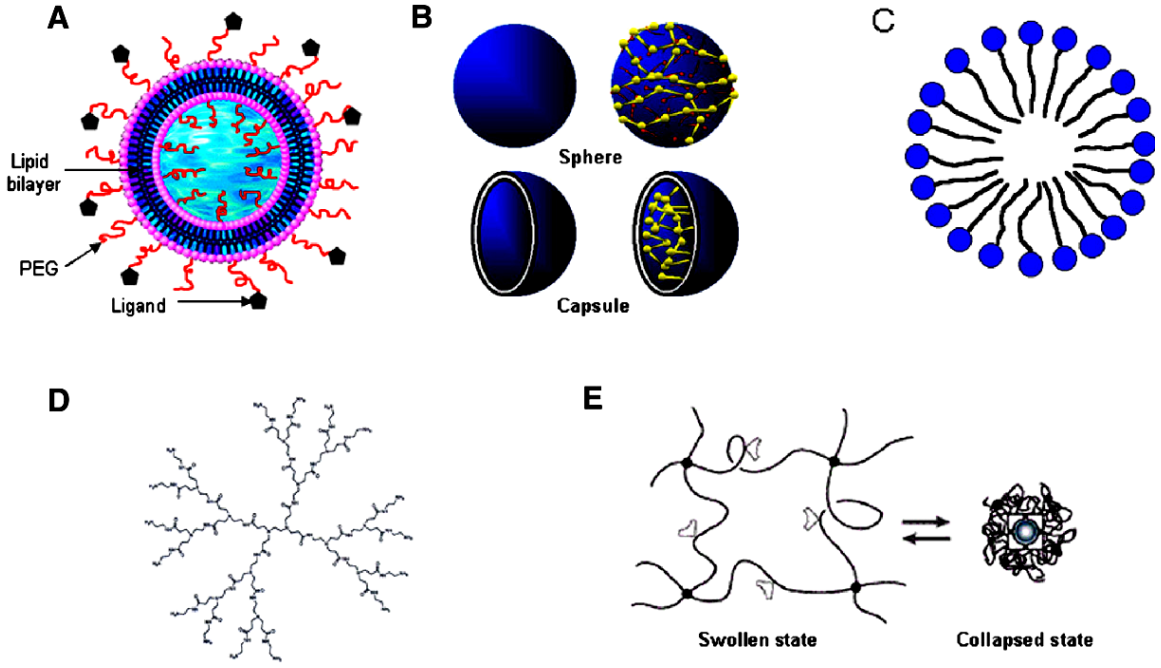

Figure 1.7 Schematic diagrams of liposomes (Panel A), nanoparticles and microparticles (Panel B), micelles (Panel C), dendrimer (Panel D), and hydrogel (Panel E). [83]

1.5.2 Applications of Liposomes

It was Alec Bangham almost half a century ago who first described that phospholipids form closed bilayer structure called liposomes, spherical vesicles that entrap water or other liquids and have similar structure of cell membrane. [85] Lipids are amphiphilic molecules that have polar head group and long chain of saturated or unsaturated hydrocarbons. The polar head group could be neutral, negatively charged (anionic liposomes) or positively charged (cationic liposomes, example DOTAP and

SAIN-2 (structures in Figure 1.8).[99] In liposome, the polar head group projects outward into the surrounding or entrapped aqueous media with hydrophobic chain between the two layers interacting. Liposome may have a single or several concentric lipid bilayers also known as lamellae.[85-87]

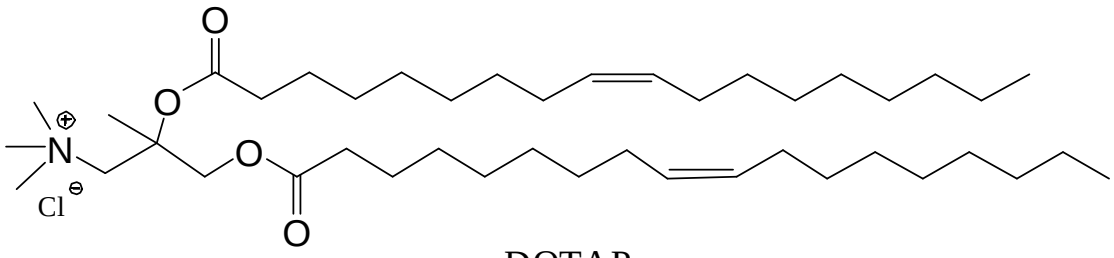

DOTAP

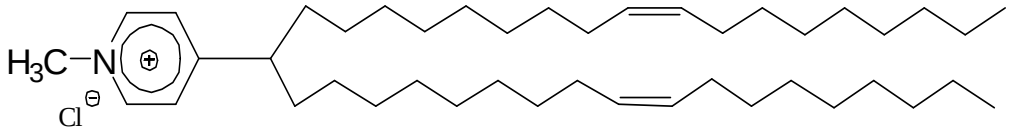

SAINT-2

Figure 1.8 Some common lipids constituting liposomes. DOTAP, N-[1-(2,3-dioleyl)propyl]-N,N,N-trimethylammonium chloride; SAINT-2, N-methyl-4(dioleyl)methylpyridinium.[99]

Therefore, liposomes could be small unilamellar vesicles (SUV), large unilamellar vesicles (LUV) and large multilamellar vesicles (MLV) or multivesicular vesicles (MVV) that enclose several small liposomes.[85, 86] Among the nanoscale drug delivery systems liposomes are the most clinically used particle to deliver cytotoxic drugs (see Table 1.1).[87] For example, liposome can carry about 10,000 to 15,000 common anticancer drug doxorubicin molecules in the aqueous compartment and

release into single cell when endocytosized enhancing the therapeutic activity of the drug.[88, 89]

Liposomes that respond to environmental condition like change in pH and temperature have been introduced. Especially as endovacuolar environment is acidic pH senstitive liposomes have greater advantage over others.[90-92] Magnetic liposomes are other types of liposomes, which are in experimental stage.[93, 94] Liposomes are also used for imaging purpose especially in MRI using paramagnetic materials. Therefore, developing novel paramagnetic liposomes have implication in imaging technology. In this thesis, we have developved several novel metallo-liposomes that may find potential application in some of the above.

Table 1.1 Representative Examples of Liposome Preparations in Clinical Use

No.	**Drug incorporated**	**Commercial name of the formulation**	**Target**
1	Daunorubicin	DaunoXome®	Kaposi's sarcoma
2	Doxorubicin	Mycet®	Breast cancer, combination therapy
3	Amphotericin B	AmBisome®	Systemic fungal infections
4	Cisplatin, Oxaliplatin	Platar	Solid tumors especially testicular
5	Inactivated hepatitis A virus and influenza virus hemaglutinin	Epaxal®	Hepatitis A virus infections (vaccine)
6	Verteporfin drug	Visudyne®	Photodynamic therapy for macular degeneration

The metallo-liposome are also used for gene transfection in eukaryotic cells. (Figure 1.10, structures **1** and **2**). Both complexes were found to transfect HEK293 cells with plasmid DNA pLEGFP-N1 with transfection efficiencies respectively of 37 % and

4 %. However, as expected compounds **3** which is not amphiphilic and doesn't have long lipid chain didn't show any transfection.[161]

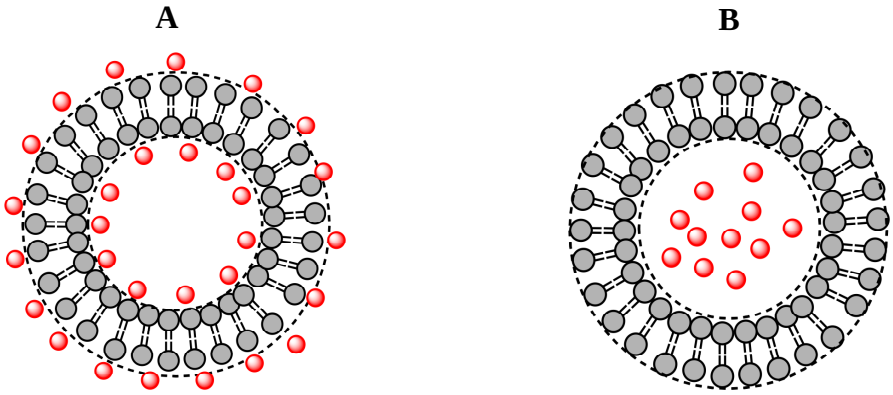

Figure 1.9 Metallo-liposomes with different formulations of heavy metal diagnostic material. Panel A shows metallo-liposome, the membrane doped with metal chelating compounds. Panel B shows Liposome entrapping metal-oxides like iron oxide.

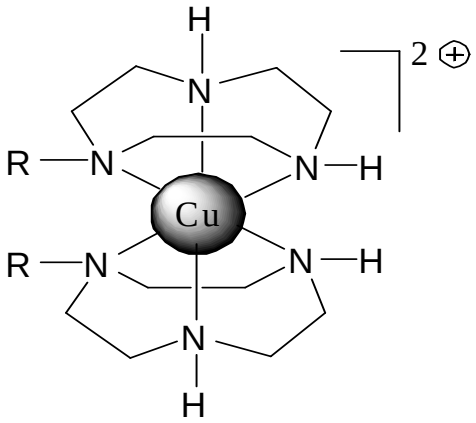

1. R = $C_{12}H_{25}$
2. R = $C_{18}H_{37}$
3. R = H

Figure 1.10 Copper based metal complexes used in liposome preparation.

1.5.3 Advantage of Using Liposomes over other Forms of Delivery Methods

There are several features that make liposome very attractive over other forms of drug delivery methods.[100] Compared to other nanoparticles, which are highly toxic and unstable, liposomes are biocompatible, liposomes can entrap water-soluble (hydrophilic) drugs in their internal aqueous compartment and water insoluble drugs can easily be incorporated into hydrophobic membrane region enabling the delivery of two drugs with opposite solubility (cartoon representation in Figure 1.11, Panel A).[101] Although active research in nanoparticle has yielded several imaging agents like iron oxide nanoparticles and quantum dots they are not biocompatible and often liposomes are used to deliver them.[83, 87] The other greater advantage is that liposomes incorporated cytotoxic agents is protected from inactivating or side effect that arise due to the reaction of drug with blood components if it were not protected.[89, 102] Liposome lends itself to easy modification of size and shape during preparation by adding additives that can modify it. Perhaps the most important aspect of liposome that makes it suitable is that they can easily incorporate targeting agent that selectively bind to tumor cells sparing normal cells. Many cancer cells have over expressed receptors like transferrin, integrins and folates. Therefore, liposomes modified with ligands that bind to these receptors have been used to target tumor cells. [106, 107, 109] Modification of liposome surfaces with polyethylene glycol (PEG) have also enhanced the stability of the liposomes prolonging the residence time in blood during liposome drug delivery (Figure 1.11, Panel B). [87,104-106] Liposomes have the ability to carry several cytotoxic drugs as

well as contrasting agent enabling the following up of drugs and its action on tumor cells in animal tissue. [100]

The other feature of liposomes that make them attractive is the flexibility of modes of introduction into the body in addition to the traditional intravenous administration.[80, 101] Liposomes drug formulation has been administrated orally, an ideal form of introducing drugs, encapsulating various types of therapeutics. For example insulin liposomes has been introduced orally and shown to exert its efficacy in reducing blood glucose level in experimental animals [101] while PEGylated liposome encapsulating ovalbumin was used as oral vaccine.[102] Liposomes containing anticancer drugs like cyclosporine A have been administrated through the lungs as aerosol and proved to be effective.[103]

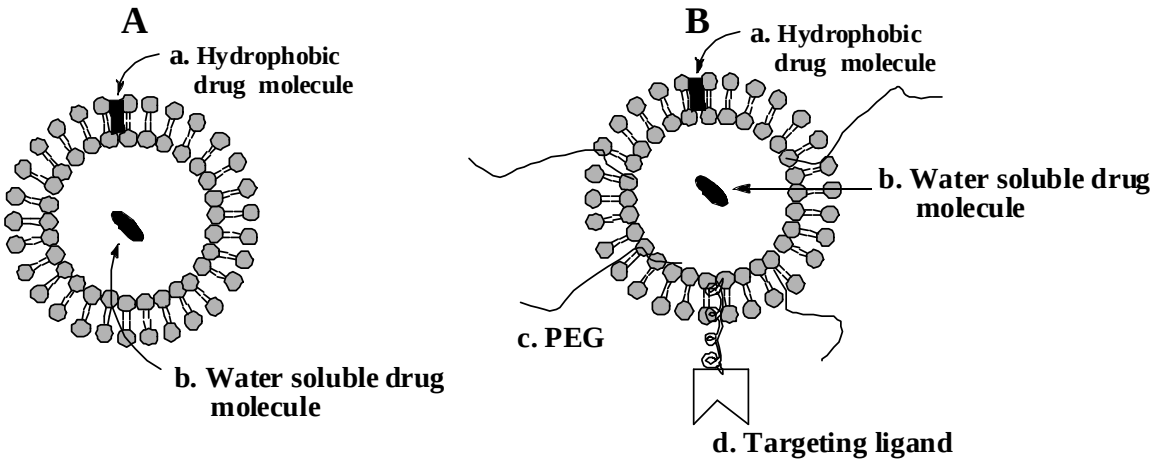

Figure 1.11 Schematic representation of liposome drug formulation (Panel A) and surface modified liposome for stability and targeting (Panel B).

1.5.4 Mechanism of Transfection

Cationic lipid and cationic polymers was first introduced in 1987 as novel transfection vectors of DNA in cultured cells. Cationic lipids rapidly get attention moving to clinical trial in 1993.[50] Cationic lipid/DNA complex and cationic polymer/DNA complex have proved to be an important alternative to viral based transfection agents. They are simple to synthesize and don't triggers immune response like the viral based transfection agents although they suffer from lack of efficiency in transfection. Moreover, the synthetic lipids has a greater capacity to carry large size of DNA as big as 100 kbp has so far been achieved while viral vector has a maximum gene-carrying capacity of 40 kbp.[109, 110] The relatively lower progress in transfection efficiencies using cationic lipids and cationic polymers is because of the fact that little was understood about DNA-lipid or DNA-polymer complexes formation, entry into the cell and transport into the nucleus although some progress has been made recently. Lipoplex is formed by the interaction of positive charge on the cationic lipid and the negative charge on the phosphate backbone of plasmid DNA. [50, 111] The ratio of DNA to lipid, temperature and other environmental factors could determine the efficiency of transfection that could be achieved by the lipoplex. It was found out that lipoplexes with a slight excess of positive charges gives greater transfection efficiency possibly because of positive charge on the complex interact with the negatively charged cell surface allowing ease of interaction.[113, 114] The other possible reason suggested is that depending on the ratio of positive charge on liposome to negative charge on the DNA different sizes of DNA-lipid complexes will form which can greatly affect transfection

efficiency. With just slight excess of positive charge larger aggregates of lipoplexes will form which is believed to have greater transfection efficiency.[112-115] Biophysical characterization of cationic liposome-DNA complex by synchrotron X-ray diffraction has shown that liposome-DNA complexes consists of multilamellar structure (L_{α}^{C}) consisting of DNA monolayers flanked by lipid bilayers as shown (structures in Figure 1.12) under normal condition.[109-110]

To enhance the level of transfection and to bring non-viral delivery system to required efficiency for its application in gene therapy understanding the pathway of uptake of lipoplex into the cell and the delivery of DNA to nucleus, its final destination, is critical.[99, 100] Greater weight of experimental evidence shown by pathway inhibition studies, electron microscopy and immunohistochemistry indicate that lipoplex are taken up by the cell through endocytosis via both clathrin dependent and independent pathways.[99,102] During transfection lipoplex endocytosized is surrounded by endovacuolar membrane in the cytoplasm and its escape from this enclosing condition is crucial for efficient transfection and in avoiding getting chewed by lysosomal enzymes.[99,101] Therefore, the uptake of lipoplexes by cells into the cytoplasmic compartment is necessary but not sufficient for transfection to occur. During the process of transfection, first DNA-lipid complex must be internalized and then DNA dissociated from lipoplex must escape the endosomal membrane into cytoplasm. Once released into cytoplasm the DNA has to navigate its way to nucleus and be able to cross the nuclear membrane for efficient transfection.[114, 115] Several experimental evidence suggest that

endosome has acidic condition or pH which help in transforming the lipoplex from stable lamellar DNA-liposome complex L^c_α to unstable non-lamellar hexagonal-phase structure H^c_{II} (structures in Figure 1.12).[99, 100] This polymorphic transformation of lipoplex helps in dissociation of the DNA from the complex as well as destabilizing the endosomal membrane facilitating the escape of DNA from endosome to cytoplasm. Once released into cytoplasm the plasmid DNA will travel to nucleus and believed to be internalized either by passive transport through nuclear pore or by factors that are able to transport DNA actively across nuclear membrane although latter is the least understood process of transfection process.[99, 114, 115]

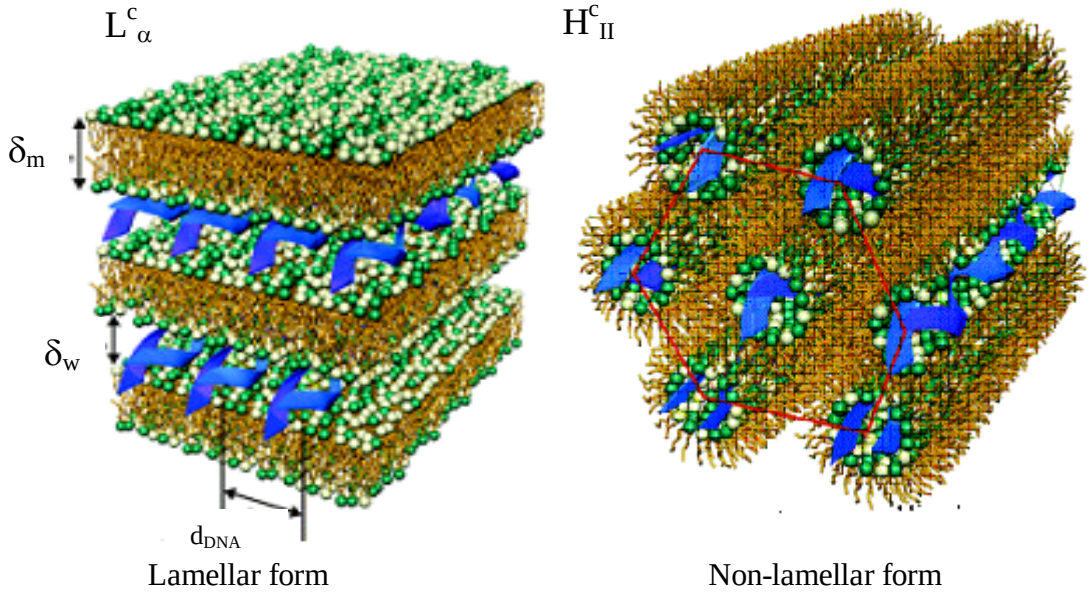

Figure 1.12 Schematic of lamellar (L^c_α) and non-lamellar inverted hexagonal-phase H^c_{II} structures of cationic liposome-DNA complexes (lipoplexes).

CHAPTER II

IRON(III)-SALEN CLEAVES DNA AND CAUSES APOPTOSIS VIA MITOCHONDRIAL PATHWAY

2.1 Introduction

Design and synthesis of small molecules and analyzing their biochemical activities is important for developing novel therapy. Small molecules often have greater advantages over macromolecules in regard to their drug application. Usually they are easy to synthesize, have greater oral bioavailability and easily cross the cell membrane. Understanding the mechanism of action of these biochemically active compounds is crucial for rational drug design with higher efficacy and lower side effects as well as for successful clinical trials. Nucleic acids being the heart of cellular metabolic (replication, transcription and translation) machinery are often the major targets of many drugs. Indeed many of the successful antitumor drugs such as cisplatin, doxorubicin acts via targeting nucleic acids. It is generally believed that DNA/RNA interacting molecules have potential antitumor activities.[42, 43]

Toward the development of novel drugs scientist have designed and developed molecules that may interacts and damage DNA/RNA.[144] The class of molecules that cleaves DNA are called chemical nuclease. Metal-complexes of salen [N,N′-bis(salicylidene)ethylenediamine] (structure **4** in Scheme 2.1) is one such class of well studied chemical nucleases.[116, 117]Over the last several decades the interaction of

metallo-salens with DNA has been thoroughly investigated. For example Mn(III)-salen has been shown to damage DNA in presence of magnesium monoperoxyphthalate with AT-rich sequence preferences while nickel salen showed preference for GC sequence.[47] In order to overcomes the water solubility, salen ligands have been modified that showed enhanced solubility and reactivities. Depending on the metal center and substituents metallo-salen complexes showed varying degrees of activities. Most of the metallo-salens were found to cleave DNA by oxidative reaction producing free radicals in the presence of reducing agents. Their sequence specificity has been found to depend on the nature of central atom and the ligand used. Complexes lacking sequence specificity like cobalt salen have been tethered to drugs like distamycin and ellipticine that binds to DNA in a predictable manner.[37, 48] Therefore, metallo-salen complexes that are able to interact with nucleic acids mimicking natural nucleases will have great potential as anticancer agent, for manipulation of genes and as structural probe for protein-DNA interaction.[42, 44]

Although, many metallo-salen derivatives have been developed and their DNA damaging properties have been studied, most of these investigations have not explored the biochemical actions of these metallo-salens in live cells and *in vivo*. In this chapter we describe the *in vitro* DNA cleavage properties of Fe(III)-salen, mechanism of DNA cleavage and its effect on *in vitro* transcription reaction. We found that Fe(III)-salen produces free radicals under reducing environment and cleaves DNA *in vitro* and inhibits eukaryotic *in vitro* transcription. Moreover, we have investigated the cytotoxic

effects of Fe(III)-salen on cultured human cells and demonstrated that Fe(III)-salen affects cell viability, induce nuclear fragmentation and apoptosis in human cells.

2.2 Results and Discussion

2.2.1 Synthesis of Fe(III)-Salen

Initially, we have chosen to study the DNA cleavage and biochemical activities of Fe(III)-salen complex (structure **4** in Scheme 2.1). We synthesized and characterized the Fe(III)-salen as described previously [124, 125] In brief, salen ligand was synthesized by mixing 2 equivalent of salicylaldehyde with one equivalent of ethylenediamine in methanol that resulted in a yellow precipitate of the salen. The ligand was characterized by ^{1}H and ^{13}C NMR. Fe(III)-salen complex was synthesized by mixing equivalent amount of salen and anhydrous ferric chloride in methanol that resulted in dark brown colored reaction product. The product was precipitated and recrystallized from acetone. The metal-complex Fe (III)-salen.Cl was confirmed by elemental analysis.

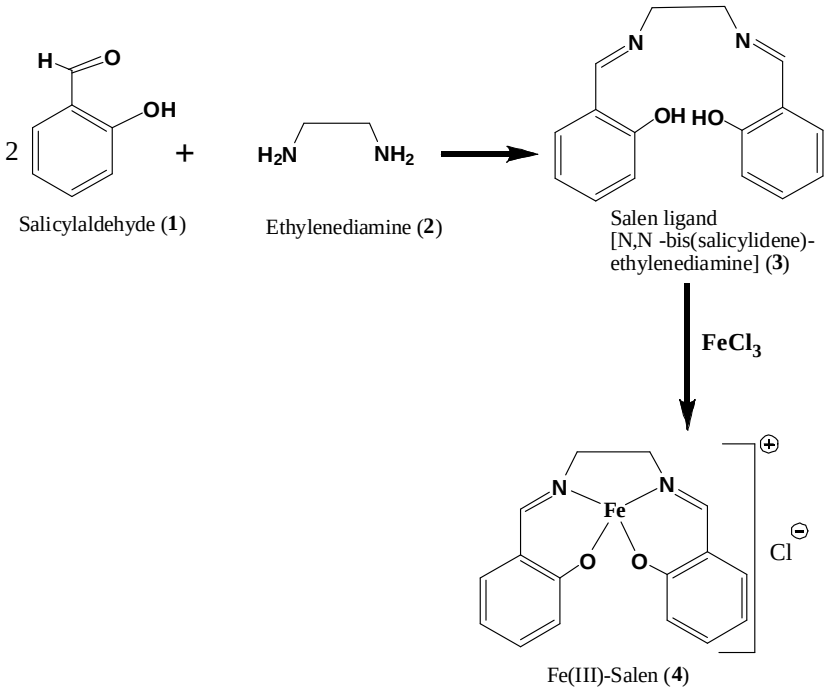

Scheme 2.1 Synthetic route for Fe(III)-salen.

2.2.2 In Vitro DNA Cleavage Assay

In order to investigate the DNA interaction profiles of Fe(III)-salen (**4**), we initially analyzed its ability to cleave DNA in the presence of a reducing agent dithiothreitol. Typically metal complexes when incubated with the supercoiled plasmid DNA, cleavage occur producing linear and nicked forms; the latter is shown in Figure 2.1.

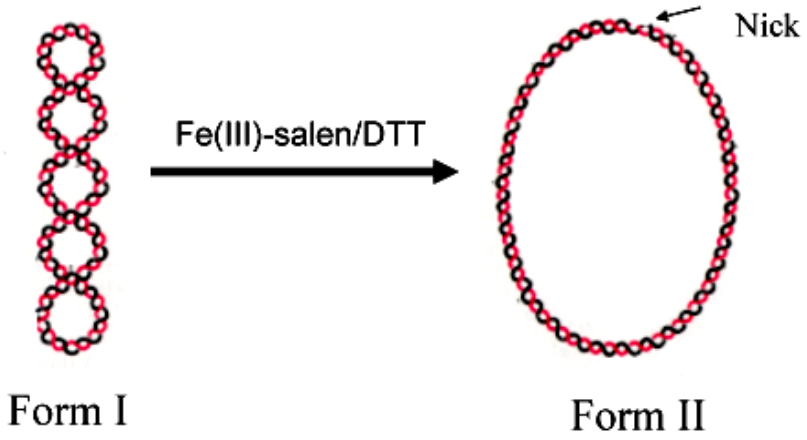

Figure 2.1 Supercoiled form (Form I) and nicked form (Form II) of plasmid DNA.

We incubated supercoiled plasmid DNA, pML20-47 (0.5 μg) with various concentrations of the metal complex in the presence and absence of reducing agent dithiothreitol (DTT, 1 mM), at 37 °C for 1 hr. The products were analyzed on 0.8 % agarose gel electrophoresis, stained with ethidium bromide and visualized under UV light using AlphaImager and the DNA cleavage product was quantified by densitometry. Interestingly, Fe(III)-salen cleaved DNA efficiently at concentration as low as 1 μM in the presence of DTT as evidenced by the conversion of the supercoiled form of the DNA to the nicked circle form (Lane 3, Figure 2.2). Comparison of densitometry result of nicked form (Table 2.1 Lanes 3, 4 and 6) indicates that DNA cleavage at 10 μM is about 1.3 times higher than cleavage observed at 1 μM while cleavage at 100 μM is also about 1.6 times that of cleavage observed at 1 μM. However, no significant DNA cleavage was observed by either of the Fe(III)-salen in the absence of DTT (Lane 7, Figure 2.2) or DTT alone (Lane 2, Figure 2.2) suggesting DTT

dependent productions of reactive species from Fe(III)-salen that cleaved DNA. This experiment demonstrate that Fe(III)-salen damage DNA under reducing environment.

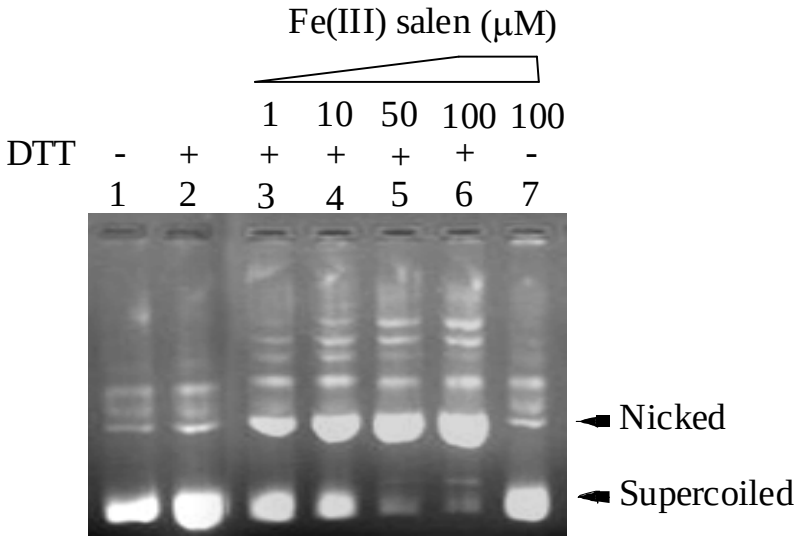

Figure 2.2 Plasmid DNA pML20-47 was incubated with Fe(III)-salen in the presence and absence of DTT for 1 hr at 37 ˚C. Photograph of an ethidium bromide stained agarose gel taken under UV light. Lane 1 DNA alone, Lane 2 DTT and DNA, Lanes 3, 4, 5, 6 with 1 μM, 10 μM, 50 μM, 100 μM Fe(III)-salen in the presence of 1 mM DTT. Lane 7 is DNA and 100 μM Fe(III)-salen without DTT.

Table 2.1 Summary of Relative DNA Cleavage Shown in Figure 2.3 as Quantified by Densitometry

Lane	Fe(III)-salen in μM	DTT (mM)	Relative DNA amount as calculated from densitometry measurement	
			Nicked %	Supercoiled %
1	0	0	25	75
2	0	1	24	76
3	1	1	53	47
4	10	1	65	35
5	50	1	70	30
6	100	1	84	16
7	100	0	24	76

2.2.3 DNA Cleavage Inhibition Assay

DNA cleavage by metal complexes could arise by production of free radicals or by simple hydrolysis as a result of chelation of the metal to DNA making it susceptible to nucleophilic attack by water molecule.[118] In our experiment since Fe(III)-salen cleaves DNA only in the presence of reducing agent we anticipated that Fe(III)-salen mediated DNA cleavage involved free radicals.

In order to test our hypothesis and to investigate the mechanism and species involved in the observed DNA damage caused by Fe(III)-salen we used free radical scavenger dimethyl sulfoxide (DMSO) as previously was suggested.[129] Supercoiled plasmid DNA, pML20-47, was initially incubated with 100 μM Fe(III)-salen in the presence of increasing concentrations of DMSO (0.1, 1 and 5%, v/v) for 5 min at room temperature and then reactions were initiated by the addition of 1 mM DTT followed by further incubation for 1 hr at 37 °C. Lane 1 is DNA alone, Lane 2 is DNA and DTT, Lane 3 is DMSO, DNA and DTT as a control. As expected, the cleavage was inhibited by 5% DMSO (compare Lanes 4, 5, 6 with Lane 7, Figure 2.3). Our data suggest that Fe(III)-salen and DTT generated free radicals that damaged DNA.

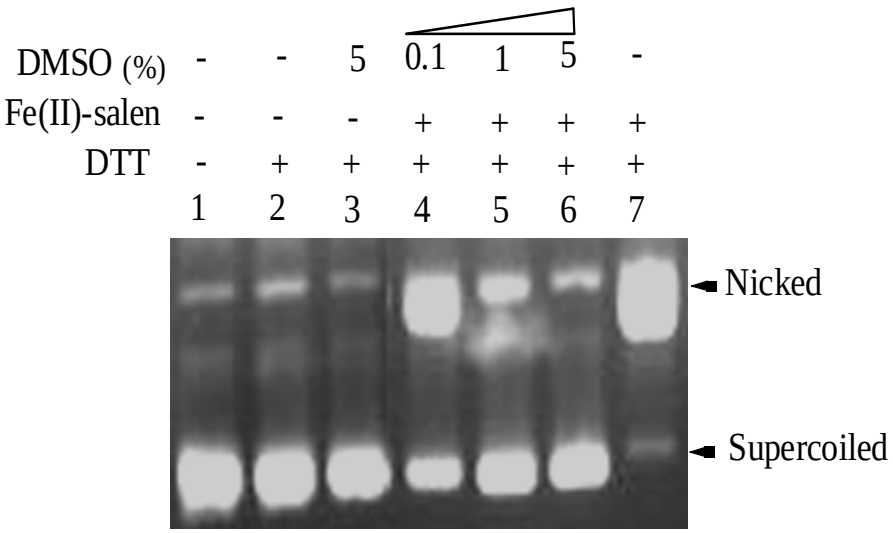

Figure 2.3 DNA cleavage inhibitions by DMSO. Supercoiled plasmid DNA were initially incubated with varying concentrations of DMSO and then subjected to DNA cleavage reaction by Fe(III)-salen and 1 mM DTT. The products were analyzed by 0.8% agarose gel and visualized by ethidium bromide staining. Lane 1 is DNA alone, Lane 2 is DNA and 1mM DTT, Lane 3 is DNA, DTT and 5% (v/v) DMSO. Lanes 4, 5 and 6 are DNA cleavage inhibition with 0.1%, 1% and 5% DMSO respectively in the presence of 100 μM Fe(III)-salen and 1 mM DTT. Lane 7 is DNA in the presence of 1 mM DTT and 100 μM Fe(III)-salen.

2.2.4 DNA Cleavage Sequence Specificity Assay

It is widely known that depending on the central metal complexes and ligand used, the binding of these complexes to DNA is different.[130] Some metal complexes of salen derivative of manganese was found to bind to DNA in a sequence specific manner while others are not able to discriminate between the base sequences in the DNA and therefore cleave DNA randomly.[144] In order to determine the specificities of DNA damage produced by Fe(III)-salen, we generated a 200 bp DNA fragment, which was derived from plasmid DNA pML20-47 and ^{32}P-labeled at its 5′-ends. The radio-labeled DNA fragment was incubated with increasing concentrations of Fe(III)-salen (1μM, 10

μM, 50 μM and 100 μM) in the presence and absence of 1 mM DTT at 37 °C for 1 h. To obtain the resolution of the DNA cleavage pattern at the nucleotide sequence level, the DNA cleavage products were analyzed by high resolution denaturing sequencing gel followed by autoradiography.[130] As expected, neither Fe(III)-salen nor DTT alone could cleave DNA (Lanes 7 and 2, respectively, Figure 2.4) and it is the same as control (Lane 1). However, Fe(III)-salen cleaved DNA in the presence of DTT in a sequence neutral fashion suggesting the involvement of highly reactive radical species that cleaved DNA and doesn't show any base preferences (Lanes 3, 4, 5, and 6, Figure 2.4).

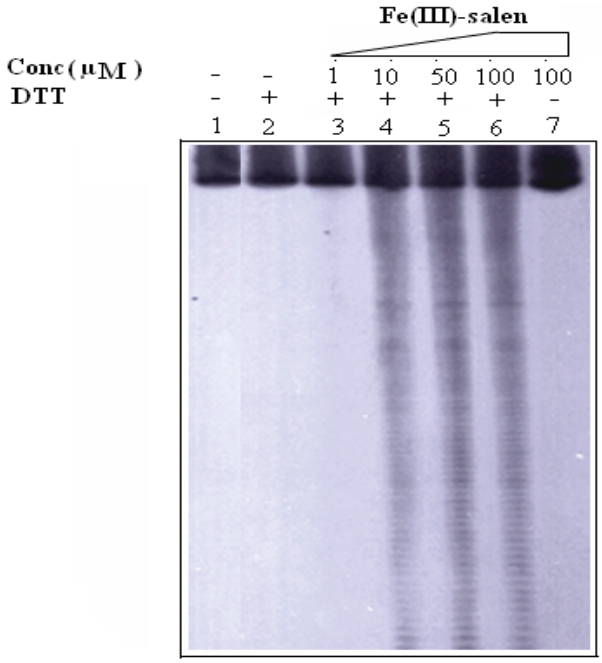

Figure 2.4 Fe(III)-salen damage DNA in a sequence neutral fashion. A $^{\alpha\text{-}32}$P end-labeled 200 bp long DNA fragment was incubated with varying concentrations of Fe(III)-salen in the presence and absence of DTT (1 mM) at 37 °C for 1 hr. The products were analyzed on high resolution sequencing gel and autoradiography. Lane 1 is DNA alone, Lane 2 is DNA and 1 mM DTT. Lanes 3, 4, 5, and 6 are DNA, 1 mM DTT and 1 μM, 10 μM, 50 μM and 100 μM Fe(III)-salen respectively. Lane 7 is in the absence of DTT.

Based on our observations, quenching experiment by DMSO and sequence specificity studies we propose that the free radical involved in DNA cleavage is most likely hydroxyl radical. The redox reaction and the process of generation of DNA damaging agent, hydroxyl radical is depicted in Scheme 2.2. First Fe^{3+} is reduced to Fe^{2+} by DTT and in the process DTT is oxidized to its corresponding heterocyclic six membered molecules with sulfur-sulfur bond. Fe^{2+} produced in turn will reduce atmospheric oxygen in the presence of protons to hydroxyl radical and hydroxyl anion. The hydroxyl radical produced will ultimately interact with DNA and initiate DNA cleavage reaction observed.

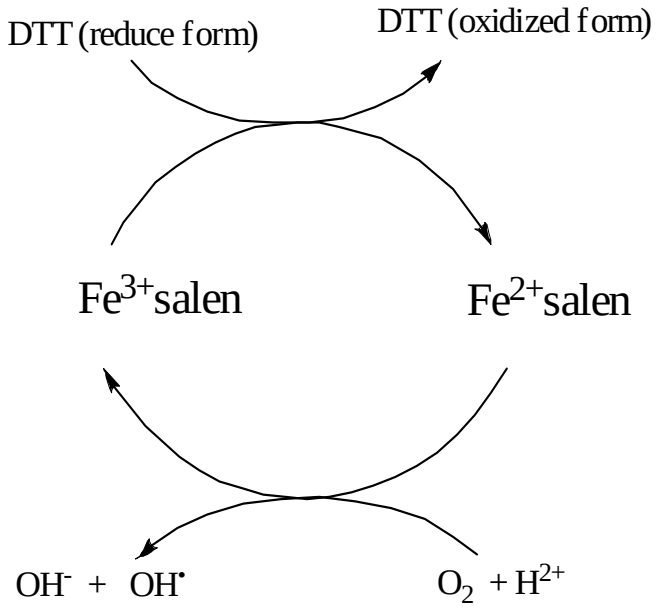

Scheme 2.2 Redox reactions that generate DNA damaging hydroxyl radical. First Fe^{3+} is converted to Fe^{2+} form, which reduced oxygen and two protons into hydroxide anion and hydroxide radical. The hydroxy radical produced is responsible for DNA damage observed.

2.2.5 In Vitro Transcription Assay

Transcription, the process of copying genetic information from DNA into mRNA is an important cellular event and highly regulated. Many human illnesses are associated with the misregulation of transcription leading to defective mRNA synthesis. For, example mutation in the general transcription factor TFIIH is associated with xeroderma pigmentosum.[131] Likewise, p53, well known tumor suppressor gene, is a transcriptional factor that is responsible for DNA repair and apoptosis. About 60 % of human cancers are characterized by misregulation of p53 gene.[4] Natural transcription factors bind to DNA and recruits several factors like chromatin modifying agents, activators and other transcriptional factors. Several transcription factors have two modules, the first is DNA binding domain and the other is transactivation domain where they bind with other proteins. The DNA binding domains have predictable structure and work on few structural themes while the protein-protein interactions are diverse making regulation at DNA of DNA-TF interaction by small molecules more attractive. Several groups have sought small molecules that bind to DNA and modulate transcriptional process as activator or repressor.[132, 133]

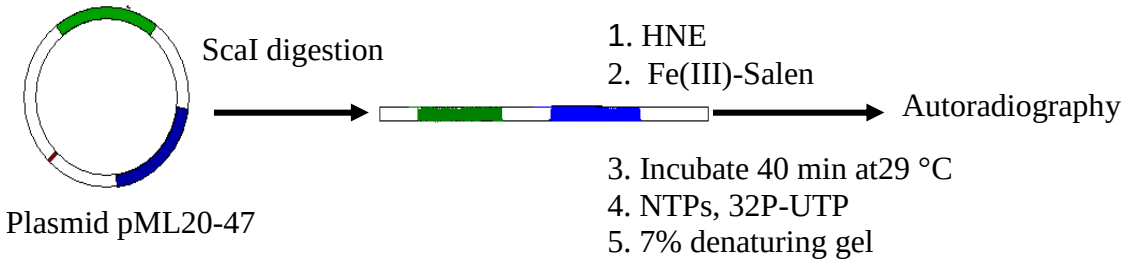

Scheme 2.3 Eukaryotic transcription on naked DNA template. First plasmid DNA pML20-47 was linearized with ScaI digestion. The transcription reaction was initiated with HNE (HeLa cell nuclear extract) and NTPs, ^{32}P-UTP in the presence or absence of metal complex.

To evaluate the effect of Fe(III)-salen on transcription we took plasmid DNA pML20-47 which has Adenovirus Major Late Promoter (AdMLP) and linearized it with ScaI restriction endonuclease as shown in the Scheme 2.3. The Linearized DNA (0.2 μg) was incubated with HeLa cell nuclear extract as a source of transcription factors in transcription buffer in the presence of Fe(III)-salen at 29 °C for 40 minutes. Then NTPs mix with [α^{32}P]-UTP was added to the mixture and it was further incubated for additional 40 minutes at 29 °C and about 1000 bp transcript is expected to form. Finally the reaction was stopped by adding 180 μL of stop buffer (20 mM EDTA pH 8, 0.25 mg/ml glycogen, 0.2 M NaCl, 1% SDS) followed by ethanol precipitation and phenol/chloroform extraction. The isolated transcript was run on 7 % acrylamide-8 M urea denaturing gel with TBE (Tris-Boric acid EDTA) buffer and exposed to x-ray film over night. The film was developed and its autoradiogram is shown in Figure 2.5. Lane 1 is a negative control where all the components required for transcription were added except the DNA template. Lane 2 is positive control with all the mixture required for eukaryotic transcription but in the absence of the metal complex. Lanes 3, 4 and 5 are transcription in the presence of increasing amount of the metal complex 1 μM, 10 μM, and 50 μM respectively. It is clearly seen from autoradiograph that Fe(III)-salen concentration of 10 μM and 50 μM completely inhibited the transcription reaction while at 1 μM it has no visible effect. Although Fe(III)-salen is shown to cleave DNA its ability to inhibit transcription may not solely attributed to DNA cleavage as the reaction mixture is highly rich in glycerol, which quenches the free radical reaction. Rather the

inhibitory effect could be due to but may not be limited to combinations of factors like DNA cleavage, the binding of the metal complex to the DNA, which in turn prevent the binding of transcription factors to the template as well as the binding of the metal complex to the transcription factors. However, further study is required to elucidate the exact mechanism of *in vitro* transcription inhibition.

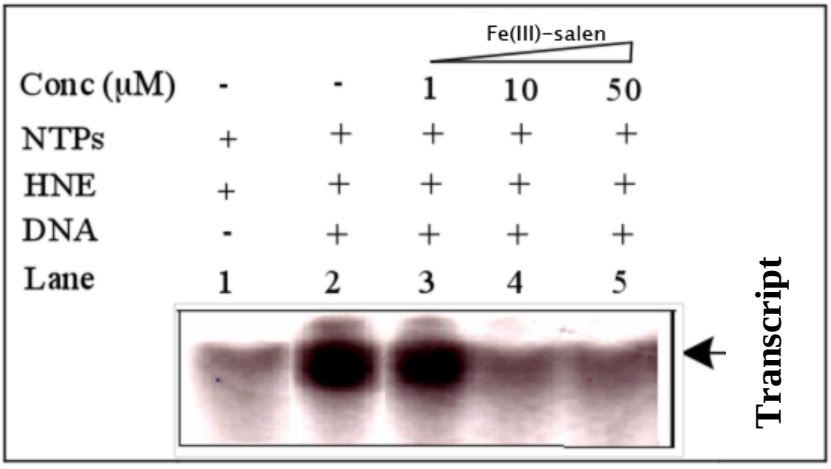

Figure 2.5 Transcription assay on naked DNA. Plasmid DNA pML20-47 was linearized with ScaI restriction endonuclease and 0.2 μg was incubated with HeLa cell nuclear extract at 29 °C for 40 minutes. Then NTPs mix with [α^{32}P]-UTP was added to the mixture and it was further incubated for additional 40 minutes at 29 °C in the presence and absence of Fe(III)-salen Lane 1 is a negative control where all the components required for transcription were added except the DNA template. Lane 2 is positive control with all the mixture required for eukaryotic transcription but in the absence of the metal complex. Lane 3, 4 and 5 are transcription in the presence of increasing amount of the metal complex 1, 10, and 50 μM respectively. The transcript was analyzed on 7 % acrylamide-8 M urea denaturing gel followed by autoradiography.

2.2.6 Cytotoxicity Assay for Fe(III)-Salen in HEK293 Cells

In order to determine the effects of Fe(III)-salen cytotoxicities, we measure the IC_{50} values toward a cultured human cell lines HEK293. IC_{50} is defined as the half maximal or 50 % inhibitory concentration of a substance.[134] We have used MTT assay which is widely used for the determination of IC_{50} values. Notably, MTT is a yellow color dye that gets reduced to purple colored formazan. Viable cells convert yellow colored MTT into violate colored formazan but dead cells are not able to do that. [139]

In brief, 10,000 HEK293 cells were seeded into 96 wells microtiter plate and cells were allowed to attach for 24 hrs. Serial dilutions of Fe(III)-salen was made and added into each of 8 replicate wells and incubated for 96 hrs. Then MTT was added into each well and cells were incubated further for 2 hrs, medium was discarded, 100 µL of DMSO was added into each well and the plate was shacked for additional 2 hrs to lyze the cells. The absorbance of DMSO-cell lysates were measured at 570 nm. The IC_{50} of Fe(III)-salen on HEK293 cells were determined to be 2.0 µM. This shows that Fe(III)salen dramatically affect cell viability and it is potent inhibitor of cell growth and proliferation.[134]

2.2.7 Fe(III)-Salen Mediated Apoptosis

Apoptosis is an important biological event that regulates a variety of physiological process like developmental process and aging. During embryogenesis it helps in the sculpture of body morphology like digit formation. In adult it removes warn out cells, microbially infected cells, and also help to keep the total number of cells

nearly constant. When the usual function of apoptotic process could not take place cell proliferation will by far exceeds cell attrition leading to cancer and other disease related to uncontrolled cell division. Anticancer drugs are known to act on the apoptotic pathways and cause cell death.[66] Therefore, one of the assays that could be done to evaluate the potential of small compounds as anticancer agent is by evaluating whether it can cause apoptosis or not by examining the morphology of nucleus.[135]

To examine the biological effects of Fe(III)-salen, we performed apoptosis assay on cultured human cells. We treated HEK293 cells with varying concentrations of Fe(III)-salen and incubated for 24 hrs. Cells were stained with a dye DAPI (4',6-diamidino-2-phenylindole) and visualized under fluorescent microscope. It is a DNA binding dye with excitation at 358 nm and emission at 461 nm that has been used extensively by others for staining cell nucleus.[135] Interestingly, the effect of Fe(III)-salen treated cells is evident even at 10 μM concentration as shown in Figure 2.6 Panel B compared to control cells in Panel A. While the cells nuclei are smooth and intact in control cells there is significant nuclear fragmentation and condensation for cells treated with Fe(III)-salen and the effect is sever for cells treated with 50 μM (Panel C) and 100 μM (Panel D). Our results here shows that Fe(III)-salen induces apoptosis in HEK293 cells as evidenced by the nuclear fragmentation and condensation which is one of the hallmark of the apoptotic process.

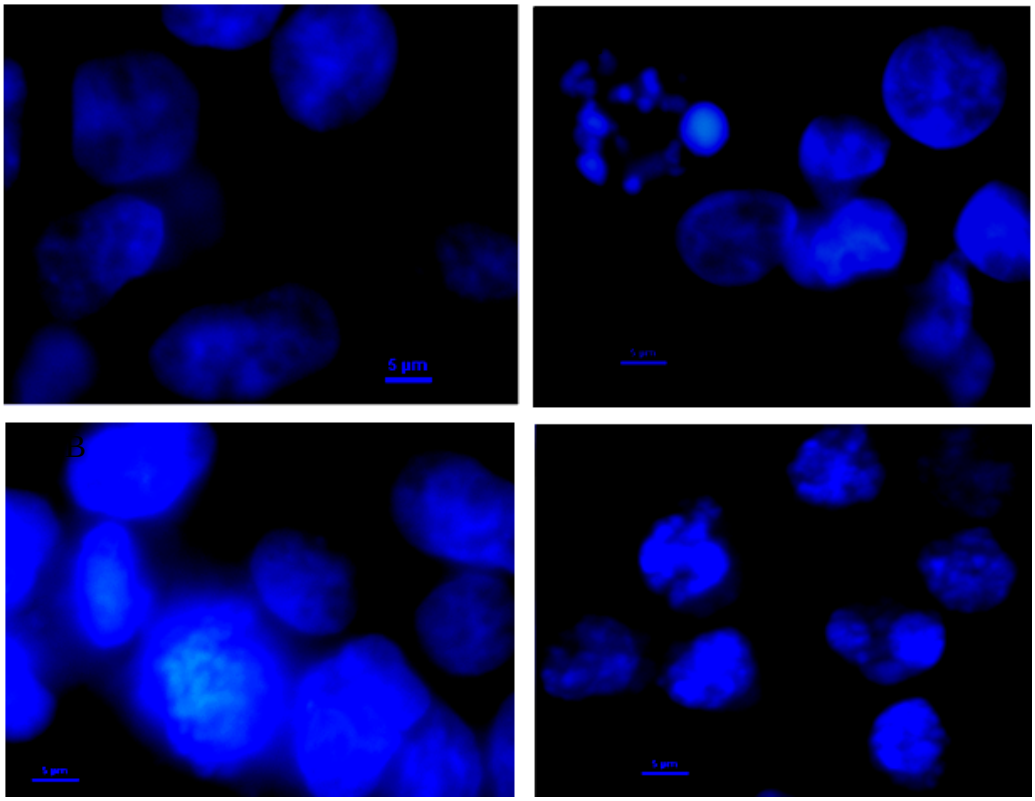

Figure 2.6 Fe(III)-salen induces apoptosis in human cell. HEK293 cells were incubated with 10 µM (Panel B), 50 µM (Panel C) and 100 µM (Panel D) Fe(III)-salen for 24 hrs and stained with DAPI and visualized under fluorescence microscope. Panel A shows untreated control cells. The nuclear fragmentation as well as the condensation of the nucleus shown in Panels B, C and D indicate that cells are undergoing apoptotic cell death.

2.2.8 Mechanism of Apoptosis

To understand the pathway by which Fe(III)-salen induced apoptosis in HEK293 cell line, we performed immunostaining with anti-cytochrome c antibody labeled with fluorescent dye FITC (Fluorescein isothiocyanate**)** before and after treatment with 100 µM Fe(III)-salen at different time points. The immuno-stained cells were visualized under fluorescent microscope (Figure 2.7 Panels A, B and C). The corresponding cell

nucleus was visualized by DAPI staining (Figure 2.7 Panels A′, B′ and C′). It is well established that cytochrome c which is normally present only inside the mitochondria, translocate to cytosol during apoptotic process that involve changes in mitochondrial membrane potential and leads to caspase 9 activation.[120] As shown in Figure 2.7, prior to the treatment of the Fe(III)-salen, cytochrome c is localized inside the mitochondria and clearly seen as speckles (Figure 2.7 Panel A). However, after 8 hrs of incubation with 100 μM Fe(III)-salen, cytochrome c started to diffuse into the cytosol (Figure 2.7 Panel B). Upon longer incubation (12 hrs), more cytochrome c is released and translocated to the cytosol as evidenced by the increase in intensity of staining (Figure 2.7 Panel C). The release of cytochrome c from the mitochondria strongly suggested that Fe(III)-salen induced apoptosis in HEK293 cells via mitochondrial pathway. The release of cytochrome c from mitochondria to cytosol was confirmed by isolating and analyzing the sub-cellular fractions from cultured cells. Using a reported procedure[120] we fractionated cytosolic extracts and mitochondrial pellet from both Fe(III)-salen treated and untreated HEK293 cells. We analyzed the cytosolic fractions by Western blotting using anti-cytochrome c antibody. We observed that cytochrome c is absent in cytosolic fraction of untreated cells (Figure 2.8 Lane 1) while it is present in Fe(III)-salen treated cytosolic fractions (Lanes 2 and 3, Figure 2.8). Anti-actin antibody was used as control for equal protein loading. These data further demonstrated that Fe(III)-salen induced the translocation of cytochrome c from the mitochondria to the cytosol and hence supported our findings that Fe(III)-salen induces apoptosis via mitochondrial pathway.

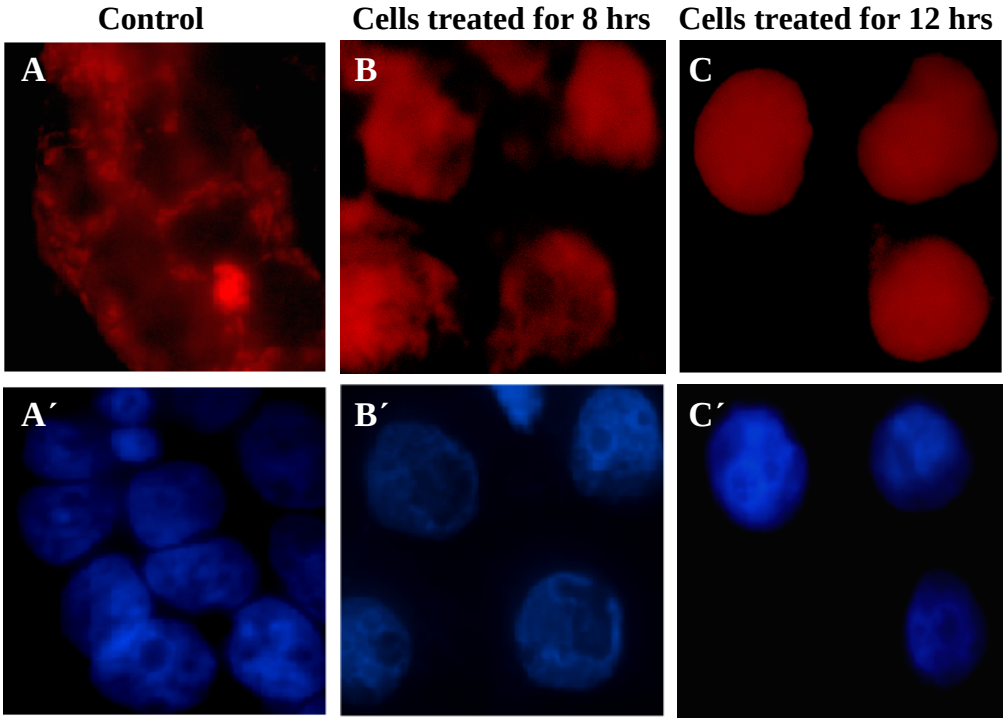

Figure 2.7 Immuno-localization of cytochrome c before and after treatment with Fe(III)-salen. Fe(III)-salen causes translocation of cytochrome c from mitochondria to cytosol. HEK293 cells were incubated with 100 µM of Fe(III)-salen for 8 hr (Panel B) and 12 hr (Panel C) and then stained with anti-cytochrome c. Afterwards, cell were stained with secondary antibody attached to FITC followed by DAPI staining and visualized under fluorescence microscope. Panel A is similar staining for control cells. Panels A′, B′ and C′ are DAPI staining to visualize the nucleus. It is clearly seen that the cytochrome c release from mitochondrial to cytosolic area increased with time of incubation.

Furthermore, the release of cytochrome c from mitochondria is accompanied by activation of caspase enzymes. When cytochrome c binds to Apaf-1 (apoptosis activating factor-1) complexed with caspase 9 the latter gets activated. Once caspase 9 is activated it in turn activates caspase 3, which leads to activation of CAD (Caspase Activated DNase). CAD can inter nucleus and cause the degradation of genomic DNA

into roughly 200 bp. This cleavage of DNA causes nuclear condensation observed by DAPI staining. Moreover, the activation of caspase 3 leads to degradation of cellular structural proteins causing cell shrinkage and membrane blebbing.[121]

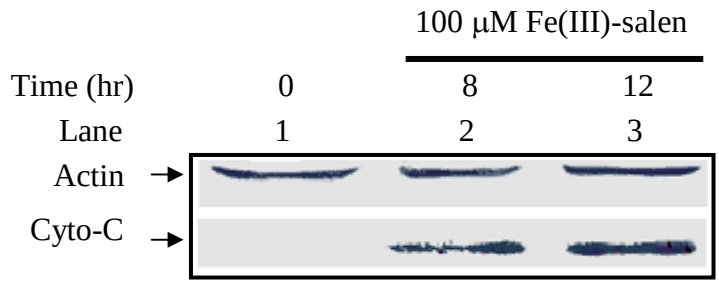

Figure 2.8 Immunoblotting assay for cytochrome c (Cyto-c) release from mitochondria. HEK293 cells control and treated with 100 μM Fe(III)-salen were fractionated to obtain cytosolic extracts and mitochondrial pellet as described previously and were analyzed by Western blot with anti-cytochrome c antibody. Anti-actin antibody was used to show equal protein loading. Lane 1 is for control cells, Lane 2 is for cells treated for 8 hrs and Lane 3 is for cells treated for 12 hrs.

To further examine the death pathways triggered by Fe(III)-salen we have done caspase 9 assay. The Caspase-Glo® 9 assay kit (Promega part number TB333) provides luminogenic caspase 9 substrate, cell lyses buffer and luciferase enzyme. The caspase 9 substrate is small peptide made of leucine-glutamate-histindine-aspartate (LEHD) attached through carboxyl group to the amino unit of aminoluciferin. When LEHD-aminoluciferin is intact luciferase enzyme cannot act on its substrate aminoluciferin and luminescence will not be produced. However, when caspase 9 is activated by cytochrome c in apoptotic cells it removes LEHD protecting group from aminoluciferin making it available for luciferase enzyme which generates luminescence that could be detected.[119]

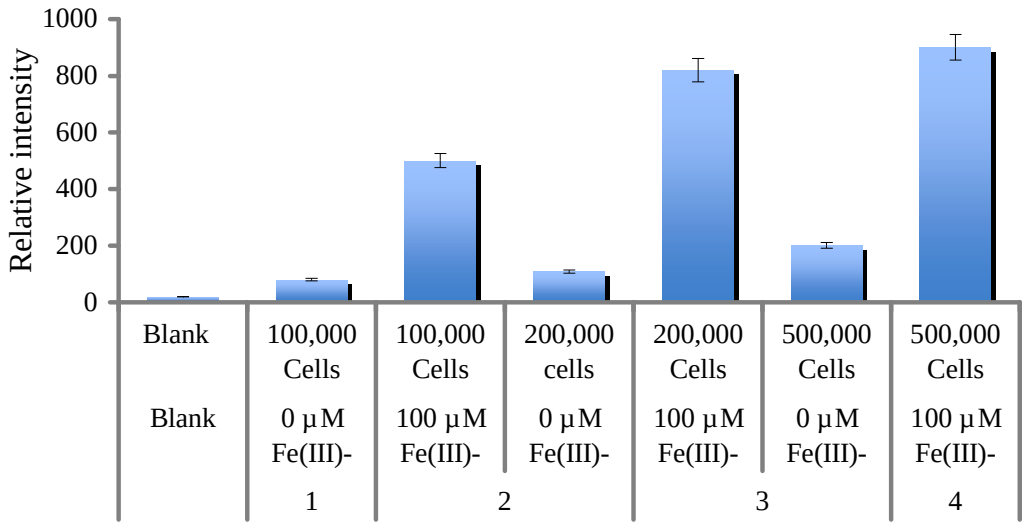

Figure 2.9 Caspase 9 assay. Number 1 is blank reagent and medium without cells. Bars 2-4 are untreated and 100 µM Fe(III)-salen treated cells for 12 hrs. Caspase activity is enhanced upon treatment with Fe(III)-salen compared to untreated cells and increases with the number of cells.

We have investigation the caspase 9 activation for HEK293 cells treated with 100 µM Fe(III)-salen for 12 hrs and compared that with untreated control cells. As shown in the bar graph in Figure 2.9 the first bar shows blank (Caspase-Glo® 9 reagent and cell culture medium without cells) the second, third and fourth bars shows treated and corresponding amount of cells not treated. As it is clear compared to control the treated cells show higher caspase 9 activity and the activity is even greater with the number of cells as expected. This data further substantiate that Fe(III)-salen causes apoptosis via mitochondrial pathway.

2.3 Summary and Conclusions

In spite of great potential of chemists to obtain large varieties of synthetic and natural products, the success rate in drug discovery is very slow partly due to limitations in detail biological evaluation of these molecules. Therefore, understanding biochemical effects of new and known molecules and screening them is very crucial in drug discovery and in developing biological probes. Herein, we have studied interaction of water soluble Fe(III)-salen with nucleic acids and analyzed its biochemical effects on human cell. Our studies demonstrated that Fe(III)-salen efficiently cleaves DNA in the presence of a reducing agent DTT. Furthermore, high resolution analysis of the DNA cleavage products showed that Fe(III)-salen cleaves DNA in a sequence neutral fashion. This sequence neutral DNA cleavage pattern indicates that the reaction is mediated via involvement of highly reactive radical species. The involvement of free radical is further supported by our observation that DMSO, a free radical quencher, inhibited the efficiency of DNA cleavage.

The DNA cleavage via free radical chemistry is not unique to metallo-salens or metal complexes but rather many antibiotics, redox-active enzymes, oxygen metabolites, and molecule ionized by high-energy radiation share similar mechanism. Similar to Fenton chemistry these complexes were found to produce hydroxyl radical that abstract hydrogen from sugar group of nucleic acid backbone. Mechanistic studies showed that compounds that generate hydroxyl radical abstract protons from sugar moiety in the order of H-5′>H-4′>H-2′≈H-3′>H-1′.[118] However, both the nitrogenous bases in nucleic acid and phosphate groups are amenable to free radical attack by

hydroxyl radical although most likely the attack on the sugar leads to rearrangement that ends up in strand break.[118]

Our results also demonstrated that Fe(III)-salen not only damages DNA *in vitro* and inhibits *in vitro* transcription reaction, but also showed significant biochemical effect on cultured human cells. Upon treatment with Fe(III)-salen, HEK293 human cells underwent morphological changes, nuclear condensation and fragmentation which are typical features of apoptotic cell death.[63-65] Importantly, these apoptotic features were observed at concentration as low as 10 μM of Fe(III)-salen and were enhanced at higher concentrations. Moreover, treatment with Fe(III)-salen has also resulted in translocation of cytochrome c from mitochondria to cytosol. The release of cytochrome c from the mitochondria to cytosol have been shown to follow the changes in mitochondrial membrane potential that results from agents triggering apoptosis through caspase 9 activation. Cytochrome c once released to the cytosol, are known to bind to a cytosolic protein Apaf-1 and forms apoptosome complex that activates caspase-9 which in turn activates downstream executioners.[120]

Our staining data using antibody against cytochrome c labeled with fluorescent dye showed its presence in cytosol further supported by protein subcellular fractionation coupled to caspase 9 assay confirms that Fe(III)-salen cause apoptosis through mitochondrial pathway by releasing cytochrome c from mitochondria to cytosol. However the exact molecular species that trigger apoptosis under cellular context is not clear. Our *in vitro* DNA cleavage studies demonstrated that Fe(III)-salen is capable of generating free radicals in the presence of reducing agents. Notably, human cells have

relatively high concentration of glutathione, a strong thiol based reducing agent, that may help to generate hydroxyl radical from Fe(III)-salen that may cause apoptosis. Cytotoxicity measurements in HEK293 cells showed that Fe(III)-salen is a potent compound for inducing cell death with IC_{50} in the range of 2 μM. Our results demonstrate that Fe(III)-salen damages DNA *in vitro* under reducing environment and induces apoptosis in human cells via mitochondrial pathway.[139]

2.4 Materials and Methods

2.4.1 General

All reagents were purchased from Sigma–Aldrich unless otherwise stated. DMSO-d_6 (deuterated dimethyl sulfoxide) was purchased from Cambridge Isotope Laboratories. Tissue culture supplies, DMEM (Dulbecco's Modified Eagle's Medium), FBS (Fetal Bovine Serum), penicillin and streptomycin were purchased from Sigma–Aldrich. Ferric chloride (anhydrous) was purchased from Spectrum Chemical Manufacturing Corporation. Anti-cytochrome c (monoclonal) antibody and rhodamine conjugated goat anti-mouse secondary antibodies, rabbit polyclonal anti-histone H3 K4Me3, H3K9Me2 and anti-acetyl lysine H4 were obtained from Upstate. DAPI (4′,6-diamidino-2-phenylindole) and anti-actin (monoclonal) were obtained from Chemicon. All enzymes and nucleotide triphosphates (dNTPs) and Caspase-Glo® 9 reagent kit were purchased from Promega Corporation. [α-^{32}P]-dATP and [α-^{32}P]-UTP was obtained from GE HealthCare. MTT (3-(4,5-dimethylthiazolyl-2)-2,5-diphenyltetrazolium bromide) was obtained from Tokyo Chemical Industry Co.

HEK293 cell line was obtained from ATCC (American Type Culture Collection).

Monolayer of human embryonic kidney cells (HEK293) were grown and maintained in DMEM that was supplemented with heat inactivated fetal bovine serum (FBS, 10%) and L-glutamine (1%). Penicillin/streptomycin (0.1%) were also included in the medium.[140, 141] Cells were cultured and maintained in humidified incubator with 5% CO2 in air at 37 °C. Cells were grown on cover slip for microscopy experiments. Cells were grown on 96 well microtiter plates for cytotoxicity measurements.

2.4.2 Physical Measurements

Both proton and carbon NMR spectra was recorded on a JEOL 300 MHz spectrometer using DMSO-d_6 as solvent and its residual solvent peak as internal standard. Agarose gel photograph was taken by AlphaImager with multiImage^{TM} light cabinet, Alpha innotech corporation. Infrared spectra were recorded using BRUKER VECTOR 22 spectrometer. Elemental analysis was done using Perkin-Elmer model 2400 CHN analyzer. Beckman LS-230 liquid scintillation counter was used to determine the probe concentration. IC_{50} measurement was taken by microplate reader ELx800. Cells stained with DAPI and anti-cytochrome c antibody were visualization under Nikon fluorescent microscope, ECLIPSE TE2000-U fitted with photometric camera (Cool SNAP Turbo 1394). Caspase assay was done using PerkinElmer spectrophotometer.

2.4.3 Synthesis

Fe(III)-salen (Scheme 2.1, structure **4**) was synthesized and characterized as described previously.[124, 125] In brief, salen ligand was synthesized by mixing two equivalents of salicylaldehyde (**1**) and one equivalent of ethylenediamine (**2**) in methanol at room temperature that resulted in yellow precipitate of salen (**3**). The usual yield obtained was 90%. ^{1}H NMR (DMSO-d_6, δ): 8.36 (s, 2H), 7.41 (dd, J_1=7.79, J_2=1.83, 2H), 7.31 (dt, J_1=8.71, J_2=1.83, 2H), 6.86 (m, 4H), 3.92 (t, J=6.44, 4H). ^{13}C NMR (δ, 40 MHz, DMSO-d_6): 168, 162, 134, 132, 128, 127, 59. IR (KBr, cm^{-1}): 3100, 2900, 1700, 1590, 1500, 1430, 1290, 1200, 1150, 1100, 1050, 1030, 990, 860, 760, 650, 530. Vis: [λ_{max}, nm ($\varepsilon = 4.46x10^3$ $M^{-1}cm^{-1}$)]: 247.00, 315.00, 398.00.

The precipitate was filtered and washed with cold methanol. The salen ligand was mixed with equivalent amount of anhydrous ferric chloride in methanol and heated to 60 °C with continuous stirring for 2 hrs. This resulted in a dark brown solution that was cooled down to room temperature. The metal complex was precipitated by adding diethyl ether into the reaction mixture. The product was isolated, recrystallized from acetone and characterized as [Fe(III)-salen]Cl. IR (KBr, cm^{-1}): 3500, 2900, 1700, 1550, 1460, 1450, 1390, 1300, 1270, 1250, 1160, 1150, 900, 770, 760, 610, 600, 595. UV-Vis: [λ_{max}, nm ($\varepsilon = 7.5x10^3$ $M^{-1}cm^{-1}$)]: 497, 368, 316 and 258. CHN analysis: calculated for [$C_{16}H_{14}ClFeN_2O_2$]; C 53.74 %, H 3.95 %, N 7.83 %; Found, C 53.32 %, H 3.96 %, N 7.81 %.

2.4.4 DNA Cleavage and DMSO Inhibition

Supercoiled plasmid DNA, pML20-47, was grown in *Escherichia coli* and purified as described previously.[142] The plasmid (0.5 µg per reaction) was mixed with various concentrations of Fe(III)-salen in the presence and absence of reducing agent dithiothreitol (DTT) in buffer containing 20 mM Tris–HCl (pH 7.4), 10 mM NaCl and 1 mM EDTA. The reaction mixtures were incubated at 37 °C for 1 hr and then analyzed by 0.8% agarose gel electrophoresis and detected with ethidium bromide staining. DNA cleavage inhibition experiments were carried out under the same condition as cleavage reaction in the presence of increasing amount of dimethyl sulfoxide (DMSO).

2.4.5 Sequence Specificity Assay

Plasmid DNA pML20-47 (5 µg) was linearized by EcoRI digestion in buffer H (pH 7.5 90 mM Tris-HCl 10mM $MgCl_2$ 50 mM NaCl at 37 ˚C for 2.5 hrs with final reaction volume of 30 µL. The enzyme digested DNA was analyzed on 0.8% agarose gel stained with ethidium bromide. After digestion was confirmed the mixture was directly heated on heating block at 65 ˚C to inactivate the enzyme. *In situ* the plasmid DNA was end-radio-labeled with [α-^{32}P]-dATP using Klenow DNA polymerase. Klenow reaction was initiated in the presence of 1µL (5 units) of the enzyme, 6 mM of each of dGTP, dCTP, dTTP and 30 µCi of [α-^{32}P]-dATP. The reaction was incubated at 30 ˚C for 30 minutes followed by heating the mixture at 75 ˚C for 10 minutes to inactivate the enzyme. The end labeled DNA, again *in situ* digested with XbaI by adding 5 units of enzyme and incubating at 37 ˚C for 1.5 hr followed by heat inactivation at 75 ˚C for 10 minutes. Digestion with XbaI yielded a mixture of 200 bp

and 3500 bp long DNA fragments. After the digestion the products were separated on a 6% non-denaturing PAGE (polyacrylamide gel electrophoresis). The gel was exposed to x-ray film and luminescent marker overnight at -80 ˚C. The 200 bp long radiolabeled DNA fragment was excised from the gel, eluted with buffer (10 mM Tris–HCl, 200 mM NaCl and 1 mM EDTA) by shaking overnight at room temperature, ethanol precipitated by adding final concentration of 0.33 M NaOAc salt (3.33 M stock) and 3 volume of ethanol. The mixture was kept at -20 ˚C for 30 minutes followed by centrifugation at 4 ˚C with speed of 13,000 rpm for 30 minutes. The pellet was resuspended in 25 µL TE buffer (10 mM Tris–HCl, 1 mM EDTA, pH 7.5).

DNA cleavage reactions were carried out by incubating the 200 bp long [α^{32}P] -end labeled DNA fragment (100,000 counts per reaction, counted by Beckman LS-230 Liquid scintillation counter, using BCS-NA biodegradable counting scintillant non-aqueous) with varying concentrations of the Fe(III)-salen in the absence and presence of 1 mM DTT in 20 µL final volume TE buffer at 37 °C for 1 hr. At the end of the reaction the mixture was filled with deionized sterile water to 200 µL final volume. Then 200 µL of phenol/chloroform solution was added and the mixture mixed vigorously by vortexing. It was centrifuged at room temperature at about 13,000 rpm. The top aqueous layer was separated and 3 volume of pure ethanol and 0.33 M final concentration of NaOAc were added. The mixture was incubated at -20 overnight to precipitate the linearized DNA followed by centrifugation at 13,000 rpm for 20 min. The supernatant was discarded and precipitated DNA was resuspended in denaturing formamide dye (80% formamide, 10 mM NaOH, 10 mM EDTA, 0.1% xylene cyanol FF and 0.1%

bromothymol blue) and electrophoresed on a denaturing 7% polyacrylamide gel containing 8 M urea and subjected to autoradiography.[130]

2.4.6 Transcription Assay

Plasmid DNA pML20-47 (6 µg) was linearized by incubating 1.57 µL of 3.8 µg/µL DNA with ScaI restriction endonuclease in Buffer J (10 mM Tris-HCl, 7 mM $MgCl_2$, 50 mM KCl 1mM DTT at 37 ˚C and pH 7.5 with final volume of 30 µL for 2.5 hrs (ScaI cuts 1009 bp down stream of transcription start site). At the end of the reaction the reaction mixture was filled with deionized sterile water to 200 µL final volume followed by phenol/chloroform extraction and ethanol precipitation as described in the previous section. The supernatant was discarded and precipitated DNA was washed with 75% ethanol and air dried. The DNA pellet was resuspended in TE buffer and its concentration and purity determined using UV-visible spectroscopy at 260 nm and 280 nm.

Transcription initiation complex (PIC) reactions were started by incubating at 29 ˚C for 40 minutes, 0.2 µg DNA template, 1µM, 10 µM, 50 µM Fe(III)-salen and 120 µg of HeLa cell nuclear extract in transcription buffer (13 mM HEPES, 5.2 mM $MgCl_2$, 2% polyethylene glycol, 500 ng of poly[dG-dC], 45 µg of bovine serum albumin (BSA) 10 mM dithiothreitol, 10 mM $[NH4]_2SO_4$, 0.12 mM phenylmethylsulfonyl fluoride (PMSF), 0.06 mM EDTA with 60 mM KCl). Then the transcription reaction, mRNA synthesis, was initiated by adding 0.6 mM of each of NTPs (ATP, GTP, CTP) and 3.3 µM UTP and 0.5 µL [α-^{32}P]-UTP and further incubating the reaction for another 40 minutes at 29 ˚C. The reaction was stopped by adding 180 µL of transcription stop

buffer (20 mM EDTA pH 8, 0.25 mg/ml glycogen, 0.2 M NaCl, 1% SDS). The reaction mixtures were subjected to phenol/chloroform extraction and ethanol precipitation as described above. The mRNA pellet was resuspended in formamide buffer and electrophoresed using denaturing 7 % SDS-PAGE 8 M urea gel. The gel was exposed to x-ray film overnight at -80 ˚C and developed.[143]

2.4.7 Caspase Assay

First the caspase buffer and caspase 9 substrate was brought to room temperature and then the two were mixed forming complete assay reagent and 60 µM of 26S proteasome inhibitor, MG-132, was added (Promega part# TB333). HEK293 cells grown as described earlier and treated with 100 µM of Fe(III)-salen for 12 hrs was collected and counted by hemocytometer. Into each microcentrifuge tube 200 µL of 100, 000; 200,000 and 500,000 cells suspended in the medium treated and untreated were seeded. Then, 200 µL of Caspase 9 reagent was added into each of the microcentrifuge tubes containing the cells. The caspase 9 reagent and cell suspension mixture was mixed by shaking for 2 minutes, followed by incubation for 1 hr at room temperature. At the end of 1 hr caspase 9-cell suspensions luminescence was measure by spectrophotometer in bioluminescence mode

2.4.8 Cytotoxicity in HEK293 Cells

The cytotoxicity of Fe(III)-salen was evaluated by using MTT (3-(4, 5-dimethylthiazolyl-2)-2, 5-diphenyltetrazolium bromide) assay as described previously[134]. About 10,000 cells (HEK293) in 160 µL of DMEM were seeded into 88 wells of 96 well microtiter plate. In parallel, 160 µL of DMEM were added into 8

control wells. Cell were allowed to attach for 24 h and then 40 μL aliquots of Fe(III)-salen solution (in PBS concentration ranging from 1.5 nM to 25,000 nM) were added to 8 replicate wells to asses IC_{50} of the metal-complex, defined as the concentration at which formazan was reduced by 50%. After 96 hrs of incubation with the Fe(III)-salen, 20 μL of MTT (5 mg/mL stock in PBS) was added into each wells and incubated for additional 2 hrs. The plates were centrifuged at 1000 rpm for 5 min. The medium was discarded and cells were lysed in 100 μL of DMSO by shaking at room temperature for 2 hrs. The absorbance of the lysate was measured at 570 nm.

2.4.9 Apoptosis Assay by DAPI

DAPI staining was carried out as described previously[144] with some modifications as follows. HEK293 cells were first grown to 80% confluence on cover slips followed by incubation with varying concentrations (10 μM, 50 μM and 100 μM) of Fe(III)-salen for 24 hrs. Control (untreated) and Fe(III)-salen treated cells were gently washed twice with cold PBS (phosphate buffered saline: 137 mM NaCl, 2.7 mM KCl, 10 mM Na_2HPO_4, 1.76 mM KH_2PO_4, pH 7.4) and then were fixed with 4% paraformaldehyde in PBS for 15 minutes on ice. Cells were washed three times with PBS, permeabilized with 0.2% Triton X-100 in PBS for 5 min and washed three times with cold PBS followed by incubation with DAPI (5 μg per slide) at 37 °C for 1 hr. DAPI stained cells were washed three times with cold PBS, mounted on microscope slide with mounting media (Vectashield H-1000) and visualized under fluorescent microscope.

2.4.10 Immunocytochemical Assay

The localization of cytochrome c in the sub-cellular compartment was determined by immunostaining as described previously.[120] HEK293 cells were grown on cover slips to 80% confluence and then treated with 100 μM Fe(III)-salen for varying time periods. After washing twice with cold PBS, cells were fixed in 4% paraformaldehyde in PBS on ice for 25 min and then permeabilized using 0.2% Triton X-100 in PBS on ice. Cells were blocked with 10% goat serum at room temperature for 1 hr followed by incubation with anti-cytochrome c antibody at room temperature for additional 1 hr. Cells were washed three times with cold PBS and exposed to rhodamine conjugated goat anti-mouse secondary antibody for 40 min followed by washing with cold PBS. At the end, cells were stained with DAPI, washed again for three times with cold PBS and mounted on cover slip and photographed by fluorescent microscope.

2.4.11 Subcellular Fractionations

HEK293 cells were grown on 10 cm tissue culture plates to 80% confluence (~$2x10^6$ cells), and then treated with100 μM Fe(III)-salen. Control (untreated) and Fe(III)-salen treated cells were harvested separately and washed with cold PBS. Then cells were resuspended in 300 μL of cold mitochondrial buffer (68 mM sucrose, 200 mM mannitol, 50 mM KCl, 1 mM ethyleneglycol-bis[β-aminoethylether]-N,N′ -teraacetic acid, and 1 mM DTT) in the presence of 1x complete protease inhibitor cocktail (Boehringer Mannheim) on ice. The resuspended cells were homogenized by passing several times through a 25-guage needle. The cell lysate was centrifuged at 4 °C at 800 g for 35 min. The supernatant obtained was further centrifuged at 14,000 g at 4

°C for 10 min. The resulting supernatant is the cytosolic fraction and was separated from mitochondrial pellet. For Western blot analysis, 25 µg of protein (cytosolic fraction) was electrophoresed on a 12% SDS-PAGE, transferred to a nitrocellulose membrane (Protran BA85, Whatman) and then probed with anti-cytochrome c and anti-actin antibodies. The Western blot was developed by using alkaline phosphatase method.[120]

CHAPTER III

EFFECTS OF SUBSTITUENTS AND LIPOPHILICITY ON *IN VITRO* DNA CLEAVAGE ACTIVITIES AND CYTOTOXICITIES OF IRON(III)-SALEN DERIVATIVES

3.1 Introduction

The structure of the compound imparts unique electronic, steric and hydrophobic properties that determine its physiochemical characteristics. The structure activity relationship has been exploited in physical organic chemistry, medicinal chemistry and pharmaceutical industries to predict reactivity and properties of molecules and to develop more efficient drugs. Environmental scientists have predicted the toxicity, bioaccumulation etc. in living organisms by using structure-activity relationship paradigm *in silico* minimizing *in vivo* and *in vitro* testing.[145, 146] The history of structure-activity relationship studies goes more than a century ago when Richet showed the inverse relationship between cytotoxicities of simple organic molecules and their water solubilities.[145, 151] Later, Meyer and Overton independently reported that the olive oil-water partition coefficient of some organic compounds parallel their narcotic effects.[147-150] Since then several computer models and equations have been developed and many substituents effects have been quantified enabling the predictions of cytotoxicity of compounds *in silico.*[147] Small functional groups on the compound could drastically affect its physical properties (polarity , hydrophilicity and lipophilicity etc) as well as chemical reactivities. Lipophilicity is defined as the tendency of compounds

to transfer from an aqueous phase to an organic phase. It is a property that has major effect on absorption, biodistribution, metabolism, excretion, toxicity or pharmacological properties of compounds. Lipophilicity of a molecule could also be affected by shape (length and width) and functional groups. [147-149]

The commonly used method in predicting the toxicity of compound is by determining its octanol/water partitioning coefficient (P), which is directly related to its lipophilicity.[146] It is rapid and efficient way for initial compound evaluation and it is given as the ratio of concentrations of a given compound in octanol and water, conveniently expressed as log P. Log P = log ([octanol-phase])/[aqueous-phase]. [148] As shown in Figure 3.1 partition coefficient of the compound in octanol-water system can be related to the bio-uptake and bioaccumulation of the compounds. At an optimum range of logP value of about two the concentration of compounds corresponds to its accumulation in living cells and hence often related to toxicity.[145, 150-152]

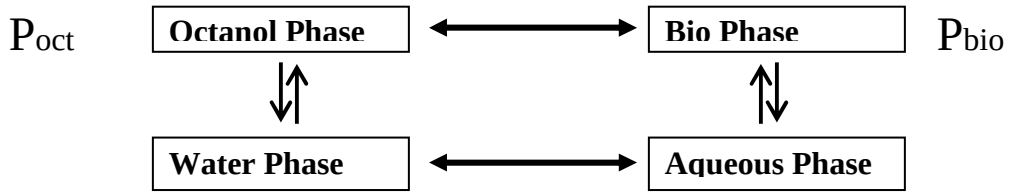

Figure 3.1 The partition of compounds in octanol phase reflects partition in biophase at optimum concentration.[146]

In order to explore the structure activity relationship, we synthesized two sets of Fe(III)-salen derivatives. In the first set (compds. **1-9**), we analyzed the effects of different substituents (hydroxy and methoxy) as well as the aromatic functionalities in the salen moiety. In the second set, we varied the lipophilicity of the salen moiety by introducing different long hydrocarbon chain (such carbons chain C8 to C18, compds. **16**, n=6-16). We have analyzed their DNA cleavage properties (compounds **1-9**) and cytotoxicities toward cultured human cells (MCF7 or HEK293). Analysis of the hydroxy and methoxy substituted Fe(III)-salen derivatives (compounds **1-9**) demonstrated that various derivatives of Fe(III)-salen complexes showed cytotoxicity toward MCF7 cells with IC_{50} values in micromolar range and interestingly, the DNA cleavage potentials of these complexes are not essential for their cytotoxicity. From the analysis of the lipophilic Fe(III)-salen complexes (compds. **16**, n=6-16) demonstrated that cytotoxicity increases upon increase in lipophilicity upto certain extent (data not shown, unpublished observation, carried out by Ansari and Mandal). However, if the chain length (lipophilicity) is increased further (such as compounds **16**, n=6-18), the cytotoxicity is decreased (results discussed herein).

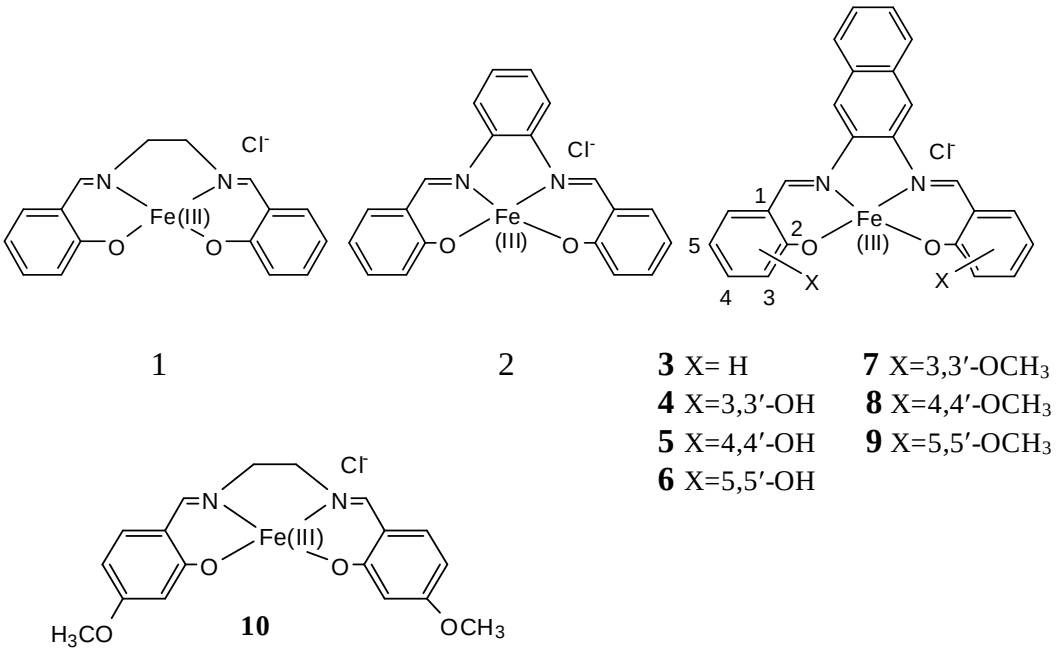

1 2

3 X= H
4 X=3,3′-OH
5 X=4,4′-OH
6 X=5,5′-OH
7 X=3,3′-OCH_3
8 X=4,4′-OCH_3
9 X=5,5′-OCH_3

10

Figure 3.2 Structures of Fe(III)-salen derivatives.

3.2 Results and Discussion

3.2.1 Synthesis of Fe(III)-Salphen and Fe(III)-Salnaphen Derivatives

The synthesis of the parent unmodified Fe(III)-salen (compd. **1**) is described in chapter II.[36] The synthesis and characterization of the hydroxy and methoxy substituted Fe(III)-salen complexes (compds **2-10**) were carried out by James D. Grant (Dr. Mandal lab) and recently published (Organic and Biomolecular Chemistry 2008). (Appendix Manuscript 1).

3.2.2 Synthesis of 4,4′-DialkoxyFe(III)-Salen Lipid Derivatives

The synthesis of the long chain derivatives of Fe(III)-salen complexes are shown in Scheme 3.1. The synthesis was carried out by first synthesizing 4-alkoxy-2-hyroxybenzaldehyde (**13,** Scheme 3.1,) using the corresponding bromoalkanes; 1-bromooctane (**12**, n=6), 1-bromodecane (**12**, n=8), 1-bromododecane (**12**, n=10), 1-bromotetradecane (**12**, n=12), 1-bromohexadecane (**12**, n=14), and 1-bromo-octadecane (**12**, n=16), and 2,4-dihydroxybenzaldehyde (**11**). The synthesis was performed by refluxing the mixture of equivalent amounts of the 2, 4-dihydroxybenzaldehyde and the bromoalkane in the presence of anhydrous potassium bicarbonate in dry acetone and purification was done by column chromatography. The products 2-hydroxy-4octyloxybenzaldehyde (**13**, n=6) and 2-hydroxy-4-decyloxybenzaldehyde (**13**, n=8) were liquids at room temperature. However, 2-hydroxy-(4-dodecyloxy)benzaldehyde (**13**, n=10),2-hydroxy-(4-tetradecyloxy)benzaldehy-de (**13**, n=12), 2-hydroxy-(4-hexadecyloxy)-benzaldehyde (**13**, n=14) and 2-hydroxy-(4-octadecyloxy)benzaldehyde (**13**, n=16) are white powder. The corresponding salen ligands of these long chain contaning aldehydes (**15**, n=6, 8, 10, 12, 14 and 16) were made by mixing two equivalents of corresponding aldehydes (**13**) with one quivalent of ethylenediamine (**14**) in methanol or methanol-THF mixture. All afforded yellowish products of the schiffs bases that are solid at room temperature. Subsequently their iron-metal complexes (**16**) were made in acetone by mixing equivalent amounts of the schiffs bases with the

anhydrous ferric chloride in acetone that resulted in deep brown complexes. The products were filtered and recrystallized from acetone-hexane.

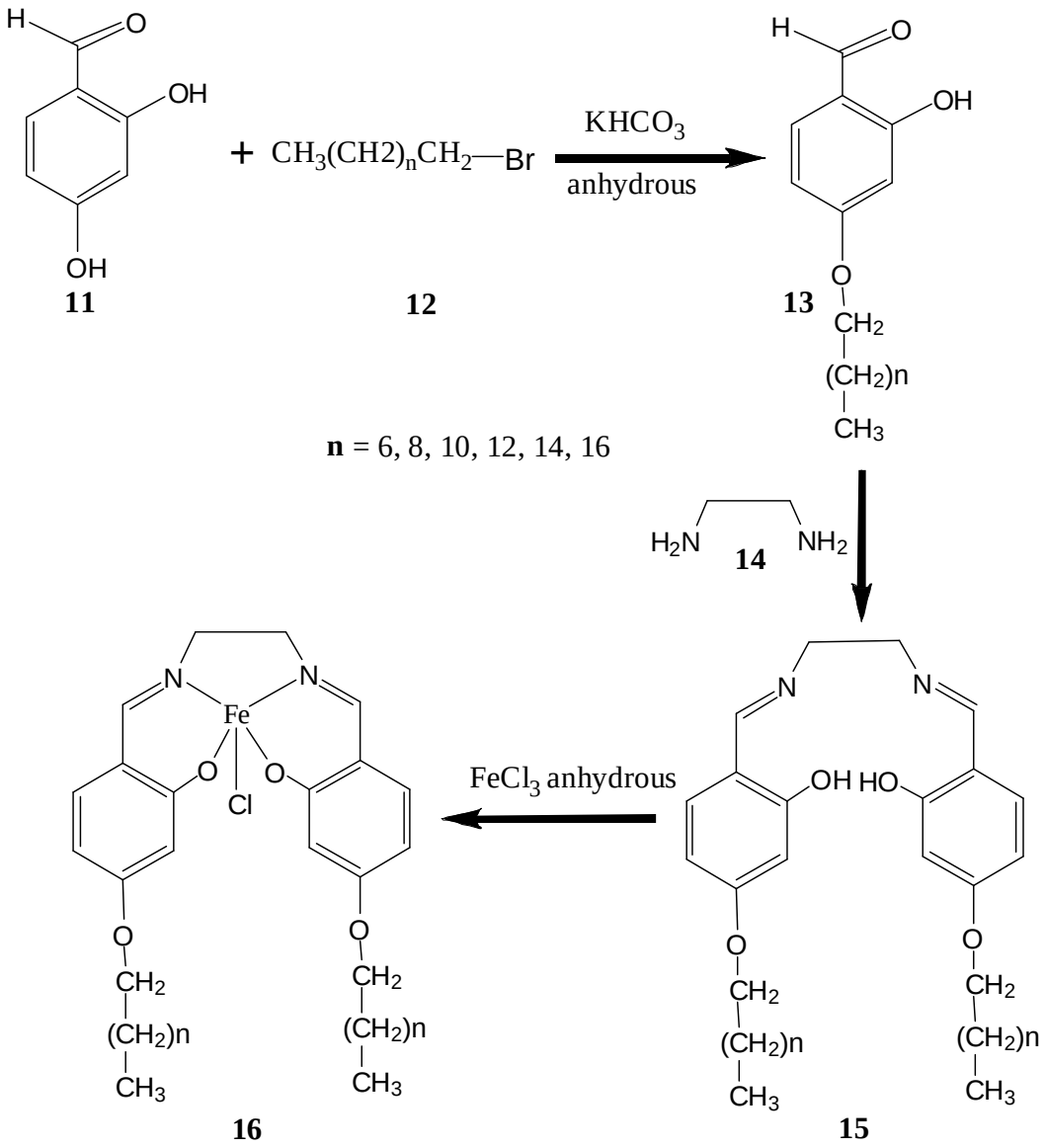

Scheme 3.1 Synthetic route of 4,4´-dialkoxy Fe(III)-salens.

3.2.3 Effect of Bridging Groups on In Vitro DNA Cleavage Activities

It was amply demonstrated that substituents groups play significant role in either enhancing or diminishing the activities of compounds..[145,153,154] Prior getting into the substituent effects analysis we examine if different bridging group in the salen moiety has any effect on their DNA cleavage properties and cytotoxic activities. Initially, we analyzed the DNA cleavage activities of parent Fe(III)-salens (**1**), Fe(III)-salphen (**2**), and Fe(III)-salnaphen (**3**). We incubated supercoiled plasmid DNA pML20-47 with 10 μM and 50 μM of the respective complexes in the presence and absence of DTT (1 mM) at 37 °C for 1 hr. The DNA cleavage product was resolved by 0.8 % agarose gel,stained with ethidium bromide and visualized under UV. The DNA cleavage profile for parents compounds Fe(III)-salen, Fe(III)-salphen, and Fe(III)-salnaphen is shown in (Figure 3.3 Panel A) along with quantification of respective DNA cleavage product by ImageQuant v2005 (Figure 3.3 Panel B). Lane 1 is DNA alone, Lane 2 is DNA and DTT, Lanes 3 and 4 are 10 μM, 50 μM Fe(III)-salen in the presence of 1 mM DTT respectively. Lanes 6 and 7 are 10 μM, 50 μM Fe(III)-salphen in the presence of 1 mM DTT respectively. Lanes 9 and 10 are 10 μM, 50 μM Fe(III)-salnaphen in the presence of 1 mM DTT respectively. Lanes 5, 8 and 11 are 50 μM of the respective metal complexes in the absence of DTT. Our result demonstrates that the DNA cleavage efficiency is decreased as bridging group is changed from ethylenediamine, *ortho*-phenylene diamine to 2,3-naphalene diamine.

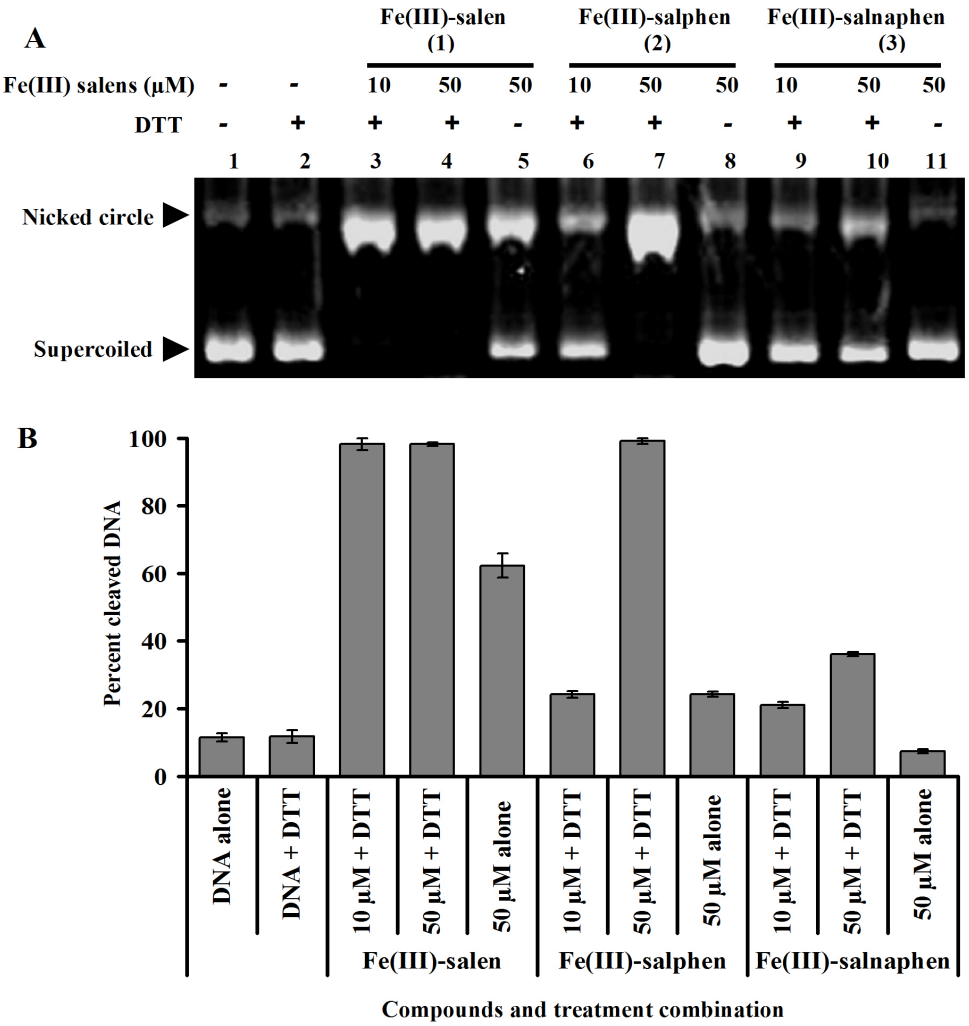

Figure 3.3 Panel A is DNA cleavage profile of Fe(III)-salen (**1**), Fe(III)-salphen (**2**) and Fe(III)-salnaphen (**3**) resolved by 0.8 % agarose gel stained with ethidium bromide and photographed under UV with AlphaImager. The cleavage is done by incubating 0.5 μg DNA with respective metal complexes in the presence and absence of 1 mM DTT at 37 °C for 1 hr. Lane 1 is DNA alone, Lane 2 is DNA and DTT. Lane 3 and 4 are 10 μM and 50 μM Fe(III)-salen in the presence of 1 mM DTT respectivley. Lanes 5 is 50 μM Fe(III) in the absence of DTT. Likewise, Lanes 6 and 7 are 10 μM and 50 μM Fe(III)-salphen in the presence of 1 mM DTT. Lane 8 is Fe(III)-salphen in the absence of DTT. Lanes 8 and 10 are 10 μM and 50 μM Fe(III)-salnaphen in the presence of 1 mM DTT while Lane 11 is 50 μM of the metal complex in the absence of DTT. Panel B is percent DNA cleavage as quantified by ImageQuant for each of the corresponding Lanes.

3.2.4 *Effect of Substituents and Bridging Groups on Cell Viability. (These experiments were carried out by Drs Ansari and Mandal, Org. and Biomolecular Chemistry, 2008)*

After investigating the DNA cleavage profile of Fe(III)-salen based complexes we wanted to investigate if their DNA cleavage efficiency correlates with cytotoxicity in cultured human cells. We incubated MCF7 cells with varying concentrations of each of the Fe(III)-salen, Fe(III)-salphen and Fe(III)-salnaphen for 96 hrs and subjected to MTT assay as described previously. [134] The percent of viable cells relative to control were plotted against concentration of the complexes to obtain IC_{50} values (Table 3.1).

Table 3.1 IC_{50} Values of Fe(III)-Salen Derivatives Towards MCF7 Cell. The Number in Parenthesis Indicates the Standards Error of the Means (SEM). This IC_{50} Values are Determined by Dr. Ansari

Compounds	IC_{50} (μM) on MCF7
1	22 (± 0.7)
2	1.3 (± 0.1)
3	0.5 (± 0.02)
4	0.2 (± 0.06)
5	>100
6	>100
7	1.5 (± 0.2)
8	0.5 (± 0.03)
9	1.3 (± 0.07)

The IC_{50} values for parent Fe(III)-salen (**1**), Fe(III)-salphen (**2**) and Fe(III)-salnaphen (**3**) were determined to be 22, 1.3 and 0.5 μM respectively which suggest that the change in the bridging group from ethylene diamine to 2,3-diamino naphthalene significantly increased the toxicity of the compounds although Fe(III)-

salnaphen have shown the least DNA cleavage ability.

As Fe(III)-salnaphen showed the highest cytotoxicity, we examined the cytoxicity and DNA cleavage properties of different hydroxy and methoxy derivatives of Fe(III)-salnaphen. First we examined DNA cleavage activities of these complexes as previous described. we hypothesized that the DNA cleavage profile of hydroxy and methoxy drivartives of Fe(III)-salnaphen (compnds **4-9**) will be different in a manner dependent on substituent position and type. Our DNA cleavage assay result showed that compared to methoxy derivatives (**7-9**) the hydroxy derivatives have shown better DNA cleaving propertie. Figure 3.4 Panel A, Lanes 1 and 2 are control. Lanes 3, 4 and 6,7 and 9,10 and 12, 13 are respectively 10 μM and 50 μM Fe(III)-salenaphen (**3**), 3,3-dihydroxy Fe(III)-salnaphen (**4**), 4,4′-dihydroxy Fe(III)-salnaphen (**5**) and 5,5′-dihydroxy Fe(III)-salnaphen (**6**) in the presence of 1 mM DTT. Lanes 5, 8, 11 and 14 are 50 μM of espective complexes with DNA in the absence of DTT. Panel B, Lanes 1, 2 and 4, 5 and 7, 8 are respectively 10 μM and 50 μM 3,3-dimethoxy Fe(III)-salnaphen (**7**), 4,4′-dimethoxy Fe(III)-salnaphen (**8**) and 5,5′-methoxy Fe(III)-salnaphen (**9**)in the presence of 1 mM DTT. Lanes 3, 6 and 9 are the corresponding metal complexes in the absence of DTT. Next, as we have undertaken for the parent compounds we incubated MCF-7 cells with these complexes and determined their IC_{50} values as described in previous section. In agreement with our ealier result the less DNA cleavage efficient 3,3′-dihydroxy Fe(III)-salnaphen (**4**) showed significant toxicity

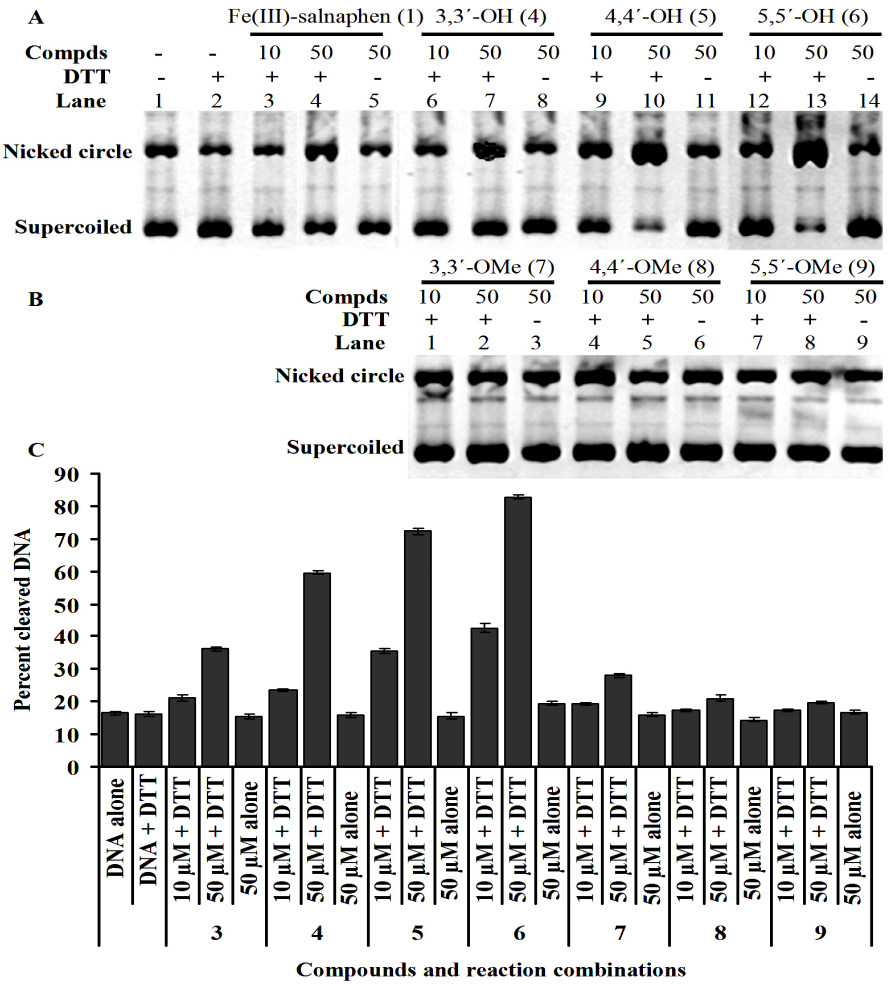

Figure 3.4 DNA cleavage profile of derivatives of Fe(III)-salnaphen. Panel A is for parent and hydroxy derivatives, Panel B is for methoxy derivatives as resolved by 0.8 % agarose gel stained with ethidium bromide and photographed under UV with AlphImager (Negative image). Panel C is percent DNA yield.Panel A, Lanes 1 and 2 are control. Lanes 3, 4 and 6,7 and 9,10 and 12, 13 are respectively 10 μM and 50 μM Fe(III)-salenaphen, 3,3′-dihydroxy Fe(III)-salnaphen (**4**), 4,4′-dihydroxy Fe(III)-salnaphen (**5**) and 5,5′-dihydroxy Fe(III)-salnaphen (**6**) in the presence of 1 mM DTT. Lanes 5, 8, 11 and 14 are 50 μM of respective complexes in the absence of DTT. Panel B, Lanes 1, 2 and 4, 5 and 7, 8 are respectively 10 μM and 50 μM 3,3′-dimethoxy Fe(III)-salnaphen (**7**), 4,4′-dimethxoy Fe(III)-salnaphen (**8**) and 5,5′-methoxy Fe(III)-salnaphen (**9**)in the presence of 1 mM DTT. Lanes 3, 6 and 9 are the corresponding metal complexes in the absence of DTT.

with IC_{50} value of of 0.2 μM (Table 3.1) while 4,4′-dihydroxy Fe(III)-salnaphen (**5**) and 5,5′-dihydroxy Fe(III)-salnaphen (**6**) were found to be non-toxic with large IC_{50} value. Our finding demonestrated that changing just the position of substituition could have drastic effect on the efficacy of the compounds toward cultured human cells. Moreover, all the methoxy compounds which are not efficient in their DNA cleavage activities, 3,3′-dimethoxy Fe(III)-salnaphen (**7**), 4,4′-dimethoxy Fe(III)-salnaphen (**8**), 5,5′-dimethoxy Fe(III)-salnaphen (**9**) were shown to have significant toxicity toward MCF-7 cells as demonestrated by their small IC_{50} values 1.5 μM, 0.5 μM and 1.3 μM (Table 3.1) respectively. Our comparative study of DNA cleavage versus cytotoxicity on human cells showed that the ability of the Fe(III)-salen derivatives to cleave DNA does not correlate with their cytotoxicy observed on cultured human cells.

3.2.5 Effect of Carbon Chain Length on Cell Viability

Herein, we investigated the effect of 4,4′-dialkoxy Fe(III)-salen metal complexes on HEK293 cells as a function of the size of alkoxy groups. We anticipate that these metal complexes will have different cytotoxicity profiles although their metal centers are the same. It is known that the cytotoxicities of compounds in the cellular context are greatly affected not only by the chemical reactivity of the compounds but also in the ability of the compounds to cross the cell membrane.[155]

We have undertaken comparative studies of cytotoxicities of 4,4′-dimethoxy Fe (III)-salen (**10**), 4,4′-dioctyloxy Fe(III)-salen (**16**, n=6), 4,4′-didecyloxy Fe(III)-salen

(**16**, n=8), 4,4′-didodecyloxy Fe(III)-salen (**16**, n=10), 4,4´-ditetradecyloxy Fe(III)-salen (**16**, n=12), 4,4′-dihexadecyloxy Fe(III)-salen (**16**, n=14) and 4,4′-dioctadecyloxy Fe(III)-salen (**16**, n=16) complexes by determining the IC_{50} values of the compounds in HEK293 cells. Our results as described in Table 3.2 showed that the cytotoxicities of the compounds sharply decreased as a function of increase in carbon chain length for the compounds used in our studies. 4,4´-dimethoxy Fe(III)-salen complex was the most cytotoxic with IC_{50} value of 0.5 μM which was followed by 4,4′-dioctyloxy Fe(III)-salen and 4,4′-didecyloxy Fe(III)-salen having IC50 values of 2.7 and 62 μM respectively. The compounds with longer side chains (compounds **16**, n=10, 12, 14, and 16) were not cytotoxic towards HEK293 cells. The lack of cytotoxic activity of long chain metal complexes as shown by their high IC_{50} values is less likely because of the difference in their chemical activity or reactivity with their cellular targets as they all have identical active metal centers. However, any difference their cytotoxicity may be attributed to the molecular size of the compounds and their ability to partition between aqueous layer and cellular membrane. In general highly hydrophilic compounds are less permeable across cell membrane though they are highly water soluble both in intracellular and extracellular fluids. On the other hand, highly hydrophobic compounds interact with cell membrane better but they are poorly soluble in water and often aggregate.[152] The metallo-lipids in our study also have tendency to form aggregate structure in water which could partly explain why 4,4´-dimethoxy Fe(III)-salen was highly toxic while compounds with long chain were not cytotoxic towards HEK293 cells.

Table 3.2 Cytotoxicities of 4,4′-Dialkoxy Fe(III)-Salen

	Metal complex	IC50 values in HEK293 (μM)
1	Methoxy	0.5
2	n=6	2.7
3	n=8	62
4	n=10	>100
5	n=12	>100
6	n=14	>100
7	n=16	>100

3.2.6 Apoptosis Assay via DAPI Staining for 4,4′-Dialkoxy Fe(III)-Salens

In order to further investigate the effects of these compounds HEK293 cells were incubated with 100 μM of 4,4′-dialkoxy Fe(III)-salen complexes for 24 hrs. Cells grown on cover slips were then stained with DAPI and visualized under fluorescent microscope. Figure 3.5 shows the DAPI staining for nucleus of HEK293 cells untreated and treated with the corresponding metal complexes. As cells treated with 4,4′-dimethoxy Fe(III)-salen (**10**) (Panel B) and 4,4′-dioctyloxy Fe(III)-salen (**16**, n=6) (Panel C) showed significant nuclear fragmentation compared to either control cells (Panel A) or cells treated with 4,4′-didecyloxy Fe(III)-salen (**16**, n=8) (Panel D). However, treatment of the cells with compounds having longer side chains for example 4,4′-dodecyloxy Fe(III)-salen (**16**, n=10, Panel E), 4,4′-ditetradecyloxy Fe(III)-salen (**16**, n=12, Panel F), 4,4′-dihexadecyloxy Fe(III)-salen (**16**, n=14, Panel G) and 4,4′-dioctadecyloxy Fe(III)-salen (**16**, n=16, Panel H) resulted in partial cell cycle arrest instead of nuclear fragmentation. These results demonstrated that 4, 4′-dialkoxy Fe(III)-salens with shorter side chain induce nuclear condensation, fragemnation and

possibly apoptosis in HEK293 cells. However, the increase in side chain length decreases the cytotoxic activities and no nuclear fragmentation was observed.

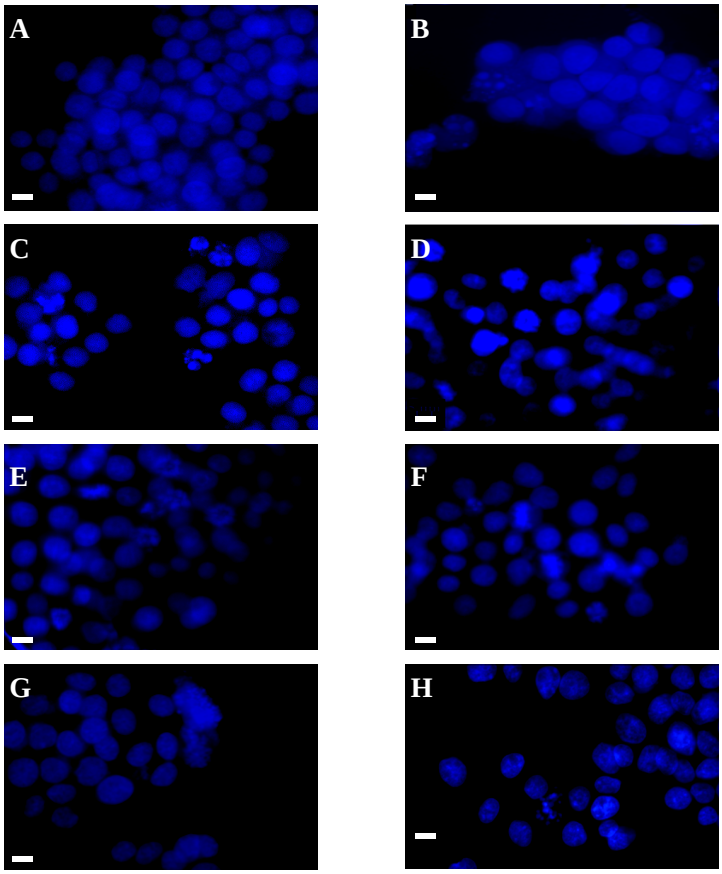

Figure 3.5 Nuclear fragmentation assay by DAPI staining for metallo-salen based lipids. DAPI staining for control cells (Panel A) and cells treated with 100 µM concentration 4,4´-dimethoxy Fe(III)-salen (Panel B), 4,4´-dioctyloxy Fe(III)-salen (**16**, n=6, Panel C), 4,4′-didecyloxy Fe(III)-salen (**16**, n=8, Panel D), 4,4′- didodecyl oxy Fe(III)-salen (**16**, n=10, Panel E), 4,4′-ditetradecyloxy Fe(III)-salen (**16**, n=12, Panel F), 4,4′-dihexadecyloxy Fe(III)-salen (**16**, n=14, Panel G) and 4,4′-dioctadecyloxy Fe(III)- salen (**16**, n=16, Panel H). Bar is 5 µM.

3.2.7 TUNEL Assay

To further confirm the 4,4′-dialkoxy Fe(III)-salens induced apoptosis, we analyzed DNA fragmentation of HEK293 cells by using TUNEL assay. In brief, monolayer of HEK293 cells were grown to 80 % confluence on microscope slide and treated with 50 µM 4,4´-dimethoxy Fe(III)-salen (**10**), 4,4´-dioctyloxy Fe(III)-salen (**16**, n=6), 4,4´-didecyloxy Fe(III)-salen (**16**, n=8), 4,4´-didodecyloxy Fe(III)salen (**16**, n=10), 4,4´-ditetradecyloxy Fe(III)-salen (**16**, n=12), 4,4´-dihexadecyloxy Fe(III)-salen (**16**, n=14), 4,4´-dioctadecyloxy Fe(III)-salen (**16**, n=16). After 24 hrs of treatment cells were washed and then subjected to terminal end labeling (TUNEL) of DNA using fluorescent dUTP. The cells were also stained with propidium iodide (PI) as a counter staining dye that intercalates DNA. The cell membrane of viable cell is impermeable to PI while dead cell membrane allows it to pass through freely. After staining, cells were photographic with fluorescent microscope using FITC (Figure 3.6 and 3.7 Panels, A, B, C, D, E, F, G and H) and TRITC (Figure 3.6 and 3.7 Panels, A´, B´, C´, D´, E´, F´, G´ and H´) filters. The two corresponding channels FITC and TRITC for both control and treated cells with each of the compounds were mixed (Figure 3.6 and 3.7 Panels A´´, B´´, C´´, D´´, E´´ F´´, G´´ and H´´). Cells undergoing apoptosis will incorporate fluorescein-dUTP label and PI intercalates their DNA while viable cells don't incorporate significant amount of fluorescein-dUTP and PI. In mixed channels apoptosis cells will look yellow and the intensity corresponds to the degree of incorporation while viable cells don't appear yellow. Significant number of cells in Figure 3.6 Panels B´´ and C´´ looks yellow but as carbon chain increases the number of

apoptotic cells decrease in agreement with our DAPI staining assay and IC_{50} values given in previous sections.

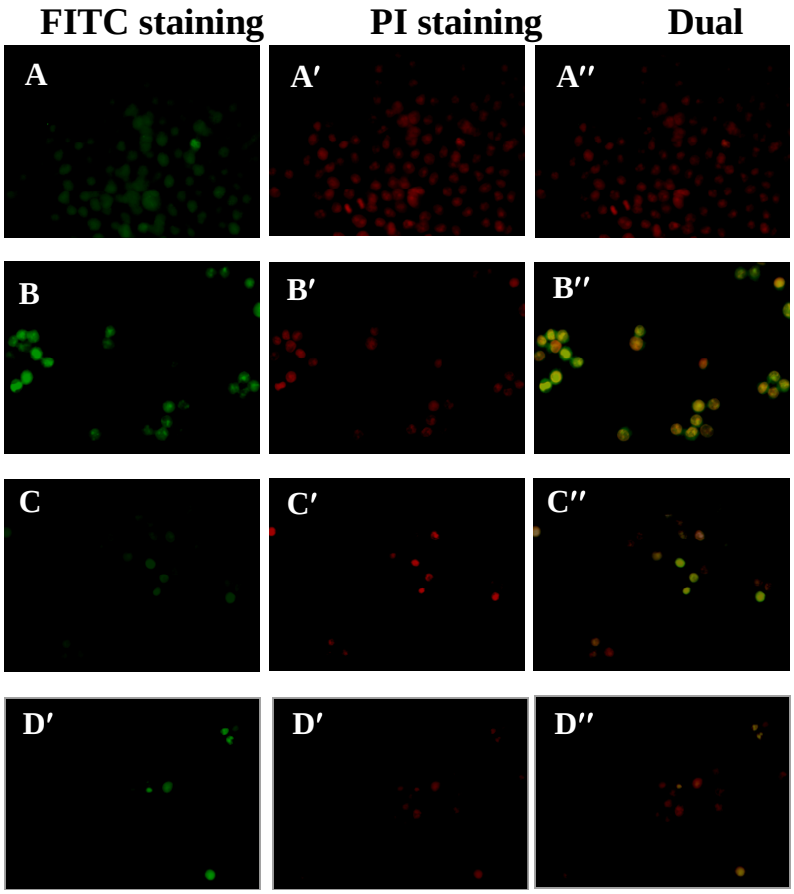

Figure 3.6 TUNEL assay for control cells (Panel A) and for cells treated for 24 hrs with 50 µM concentrations of 4,4′-dimethoxy Fe(III)-salen (**10**, Panel B), 4,4′-dioctyloxy Fe(III)-salen (**16**, n=6, Panel C), 4,4′-didecyloxy Fe(III)-salen (**16**, n=8, Panel D). Apoptotic cells appear yellow in dual channel.

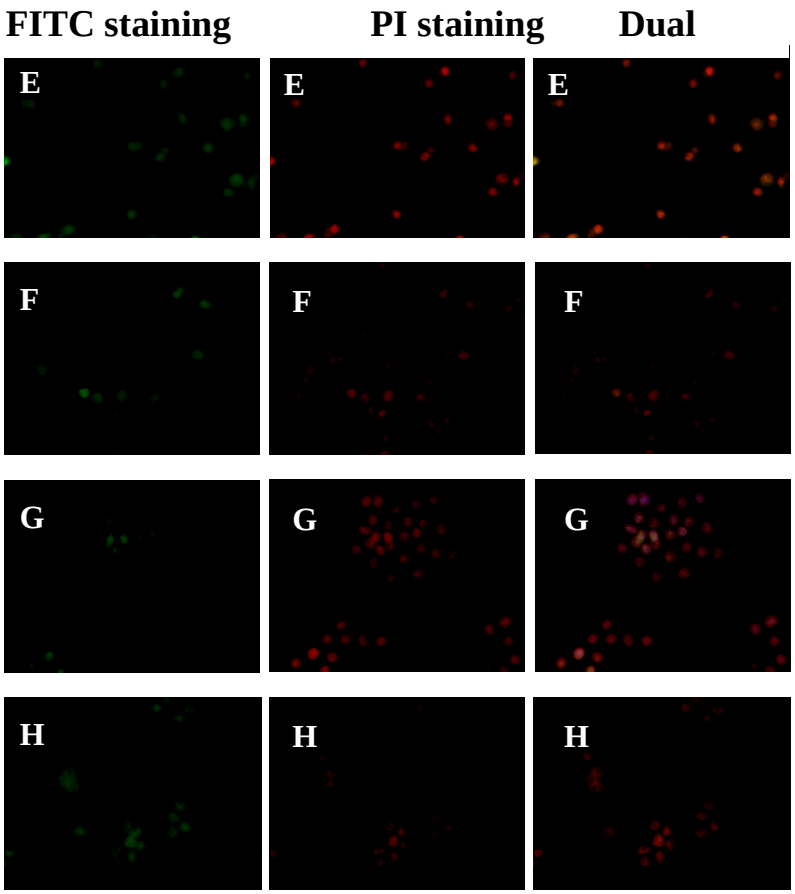

Figure 3.7 TUNEL assay for HEK293 cells treated with 4,4′- didodecyloxy Fe(III)-salen (**16**, n=10, Panel E), 4,4′-ditetradecyloxy Fe(III)-salen (**16**, n=12, Panel F), 4,4′-dihexadecyloxy Fe(III)-salen (**16**, n=14, G) and 4,4′-dioctadecyloxy Fe(III)-salen (**16**, n=16, Panel H). In dual channel apoptotic cells appear yellow while non-apoptotic cells looks red. Control cells are shown in Figure 3.6 Panel A.

3.2.8 Determining Octanol-Water Partition Coefficient for 4,4′-Dialkoxy Fe(III)-Salen Derivatives

In order to investigate the relative solubilities of 4, 4′-dialkoxy Fe(III)-salen derivatives we have determined the partition coefficient ($P_{o/w}$) of these compounds in octanol-water system. It is known that compounds that have optimum partition coefficient will in general show greater cytotoxicity than compounds with either very

low or very high values provided that all other factors remain the same.[148] Here in partition coefficients were determined by determining the concentration of the compounds after they partition in the two phases (octanol-water system). First equivalent amount of octanol and water was mixed and equilibrated. Then compounds were mixed with pre-equilibrated octanol-water mixture followed by shaking for 48 hrs with occasional agitation. Then the mixture was allowed to settle for 24 hrs. Each phase was carefully separated and centrifuged at 14,000 rpm for 10 minutes and further separated. The concentration in octanol phase was determined and the partition coefficients were calculated by taking the ratio of concentrations in octanol phase to that of aqueous phase and LogP was determined (Table 3.3).[152] As shown in Table 3.3 the log partition coefficient value (LogP) of these compounds increases with increasing carbon number as expected with 4,4′-dimethoxyFe(III)-salen logP of 1.93 close to the optimum value while 4,4′-dioctadecyloxy Fe(III)-salen having the highest value of 3.2 in the series.

Studies show that optimum LogP value for bioavailability of the compounds is about two and the cytotoxicity of the compounds decreases sharply when either the values are less or greater than that.[148] Our LogP value determined for 4,4′-dimethoxy Fe(III)-salen falls close to two which is an optimum value while for 4,4′-dioctadecyloxy Fe(III)-salen it is far from optimum value. As expected the general trend as seen in Table 3.3 is as carbon number increases the LogP value gets higher and this could probably be one reason for the decline in observed toxicity for higher carbon containing compounds.

Table 3.3 Octanol-Water Partition Coefficient for 4,4′-Dialkoxy Fe(III)-Salens

	Compound	Poct/water	logP
1	Fe(III)-salen	65.0	1.81
2	4,4′-dimethoxyF(III)-salen	85.9	1.93
3	4,4′-dioctyloxyFe(III)-salen	405.7	2.61
4	4,4′-didecyloxyFe(III)-salen	719.9	2.85
5	4,4′-didodecyloxyFe(III)-salen	976.2	2.98
6	4,4′-ditetradecyloxyFe(III)-salen	1057.2	3.02
7	4,4′-dihexadecyloxyFe(III)-salen	1250.5	3.09
8	4,4′-dioctadecyloxyFe(III)-salen	1599.9	3.20

3.3 Summary and Conclusions

Understanding the correlation between the DNA damagae potential of small molecules with their biochemical and apoptotic activities is important for designing novel anti-tumour agents. Herein, we synthesized several Fe(III)-salen complexes (compds. **1**-**9**) with varying substituents and bridging spacers, analyzed their DNA cleavage properties *in vitro* and cytotoxicity in cultures human cells.

The comparison of the IC_{50} values for the unmodified Fe(III)-salen, Fe(III)-salphen and Fe(III)-salnaphen complexes ($IC_{50s:}$ 22, 1.3 and 0.5 μM for compds. **1, 2** and **3** respectively towards MCF7 cells), indicated that the increase in aromatic functionality in the diimino bridges of Fe(III)-salen complexes increases their cytotoxicities. Analysis of cytotxicities of the hydroxy and methoxy substitueted Fe(III)-salnaphen complexes (compds. **4**-**9**) demonstrated that the position and the nature of substituents play critical role in determining their cytotoxic efficiencies. For example, 3,3′-dihydroxy substitueted Fe(III)-salnaphen (**4**) was highly effective in inducing cell death (IC_{50}.0.2 μM), whereas 4,4′- and 5,5′-dihydroxy Fe(III)-

salnaphen complexes (**5** and **6**) were almost inactive toward MCF-7 cells. However, all three corresponding methoxy substituted Fe(III)-salnaphen derivatives (compds. **7-9**) showed effective cytotoxicity towards MCF7 cells ($IC_{50s:}$ 1.5, 0.5 and 1.3 μM respectively).

The comparison of the *in vitro* DNA cleavage activities of different Fe(III)-salen complexes (compds. **1-9**) with their cytotoxicities were most intriguing. For example, the trend in DNA cleavage efficiencies is that it decreased from Fe(III)-salen to Fe(III)-salphen and Fe(III)-salnaphen complexes (compds. **1-3**), while their cytotxicities toward MCF-7 cells were increased in a reciprocal manner (IC_{50} values decreased). The similar results were observed for various hydroxy and methoxy substitueted Fe(III)-salenaphen complexes (compds. **4**-**9**). The lower the DNA cleavage potential of Fe(III)-salen derivative, the higher is their cytotoxicities (lower IC_{50} values). These results indicate that the *in vitr*o DNA cleavage activities are not essential for the apoptotic efficiencies of Fe(III)-salen complexes in cultured human cells. Instead, less DNA cleavage active Fe(III)-salen derivative induced more efficient apoptosis.

We have also evaluated series of long carbon chain alkoxy substituents Fe(III)-salens (**16**, n=6-16) at the *para* position and studied the effects of these substituents on cell viability by determining IC_{50} values, DNA fragmentation and apoptosis by TUNEL assay. Our results demonstrated that maximum toxicity is achieved when the substituent is methoxy group and the efficacy of the compounds declined with increase in carbon chain length. Evaluation of the partition coefficient of the compounds in octanol-water

phase demonstrated that the higher efficacy of 4,4´-dimethoxyFe(III)-salen. This is most likely due to its optimum logP partitioning value. The cell membrane is hydrophobic while intracellular and extracellular fluid is largely made of aqueous condition. Compounds that are highly hydrophobic have difficulty of solubility in the extracellular and intracellular aqueous conditions although it has higher ability to cross the cell membrane. On the other hand compounds that are highly soluble in water or aqueous system are polar and have difficulty crossing the hydrophobic cellular membrane. Those compounds that partition well in both water and octanol have an advantage of easy solubility in extracellular and intercellular aqueous conditions as well as ability to cross the cell membrane.[148] In general provided other factors the same compounds with log partition coefficient of around 2 have been found to have maximum cytotoxicity.[147-149] The observed higher cytotoxicity of 4,4′-dimethoxy Fe(III)-salen could be attributed to this phenomenon. Moreover, in addition to partition coefficient the other factors that could contribute to the lack of toxicity of higher carbon containing lipids is that they can easily self assemble into liposome which is less toxic compared to the individual lipid molecules.

3.4 Materials and Methods

3.4.1 General

The reagents used for the experiments, 1-bromooctane, 1-bromodecane, 1-bromododecane, 1-bromotetradecane, 1-bromohexadecane, 1-bromooctadecane were purchased from Sigma–Aldrich. Deuterated chloroform $CDCl_3$ was purchased from Cambridge Isotope Laboratories. HEK293 cells were cultured and maintained in DMEM that was supplemented with FBS, L-glutamine (1 %), penicillin/streptomycin (0.1 %) as described in Chapter II section 2.4.1.

3.4.2 Physical measurements

Both proton and carbon NMR spectra were recorded on either JEOL 300 MHz or 500 MHz spectrometer using $CDCl_3$ as solvent and its residual solvent peak as internal standard. FTIR and elemental analysis was done as described in Chapter II section 2.4.2. UV-Visible spectra were recorded on JASCO 550 spectrometer. Mass spectra (ESI-MS) were recorded on LCQ Deca XP Thermo Finnigan. TUNEL assay was analyzed with Nikon fluorescence microscope.

3.4.3 Synthesis

Synthesis of 4-octyloxy salicylaldehyde (13, n=6): A mixture of 2,4-dihydroxybenzaldehyde (0.69 g, 5.0 mM), 1-bromooctane (0.92 g, 4.8 mM) and two equivalents of anhydrous $KHCO_3$ (1.0 g, 10 mM) in dry acetone was refluxed for 16 hrs. The solvent was removed from the crude reaction mixture and the products were purified by column chromatography using petroleum ether/ethyl acetate solvent system. The product is yellowish liquid. Yield: 40 %. IR (cm^{-1}): 2950 , 2850, 1650, 1590, 1390,

1350, 1300, 1200, 1100, 800, 650; ^{1}H NMR ($CDCl_3$, δ): 11.49 (s, 1H), 9.7 (s, 1H), 7.4 (d, *J*=4.12, 1H), 6.5 (m, J_1=6.42, J_2=2.29, 1H), 6.4 (d, J_2=2.29, 1H), 3.9 (t, J_1=13.06, J_2=6.64, 2H), 1.7 (m, 2H), 1.5 (m, 2H), 1.14 (m, 3H), 0.87 (m, 8H). ^{13}C ($CDCl_3$, 78 MHz, δ): 194.36, 166.56, 164.62, 135.27, 115.10, 108.86, 101.15, 68.70, 31.86, 29.34, 29.26, 29.00, 26.00, 22.72, 14.15.

Synthesis of 4-decyloxy salicylaldehyde (**13**, n=8)**:** Equivalent amount of 2,4-dihydroxybenzaldehyde was reacted with 1-bormodecane as described above. Yield: 50 %. IR(cm^{-1}): 3050, 2925, 2850, 1680, 1600, 1500, 1200, 1100, 750, 690; ^{1}H NMR ($CDCl_3$): 11.47 (s, 1H), 9.69 (s, 1H), 7.37 (d, *J*=4.5, 1H), 6.49 (dd, J_1=6.4.2, J_2=2.29, 1H), 6.4 (d, *J*=2.29, 1H), 3.98 (m, 2H), 1.8 (m, 2H), 1.4 (m, 2H), 1.2 (m, 12H), 0.87 (m, 3H); ^{13}C NMR ($CDCl_3$, 78 MHz, δ): 194.29, 188.35, 166.54, 165.84, 164.60, 163.44, 135.23, 130.21, 119.03, 115.10, 108.79, 106.31, 101.15, 99.02, 68.66, 68.47, 31.95, 29.59, 29.37, 29.00, 26.03, 25.98, 22.73, 14.14; MS 277, 555 (deprotonated dimer).

4-dodecyloxy salicylaldehyde (13, n=10**):** Equivalent amount of 2,4-dihydroxybenzaldehyde was reacted with 1-bormododecane as described above. Yield: 45 %. mp: 37-39 ˚C. IR(cm^{-1}): 2950, 2050, 1750, 1650, 1500, 1450, 1350, 1300, 1210, 1125, 550. ^{1}H NMR ($CDCl_3$): 11.49 (s, 1H), 9.7 (s, 1H), 7.4 (d, *J*=4.2, 1H), 6.5 (dd, J_1=6.2, J_2=2.29, 1H), 6.4 (d, *J*=2.29, 1H), 3.9 (m, 2H), 1.8 (m, 2H), 1.5 (m, 2H), 1.2 (m, 16H), 0.87 (m, 3H); ^{13}C NMR ($CDCl_3$,78 MHz, δ):194.36, 166.56, 164.62, 135.27, 115.09, 108.87, 101.15, 68.70, 31.99, 29.70, 29.65, 29.61, 29.42, 29.38, 29.00, 22.77, 14.19. MS: 277 (monomer), 555 (dimer). CHN analysis: calculated for $C_{19}H_{30}O_3$, C 74.47 %, H 9.87 %, found C 74.37 %, H 9.71 %.

4-tetradecyloxy salicylaldehyde (13, n=12**):** Equivalent amount of 2,4-dihydroxybenzaldehyde was reacted with 1-bormotetradecane as described above. Yield: 54 %; mp:42-43 ˚C. IR(KBr, cm^{-1}): 2900, 2850, 1680, 1650, 1600, 1580 , 1490, 1450, 1380, 1350, 1300, 1290, 1200, 1100, 1110, 1100, 950, 810, 790, 710, 615. ^{1}H NMR ($CDCl_3$): 11.47 (s, 1H), 9.69 (s, 1H), 7.41 (d, *J*=4.2, 1H), 6.5 (dd, J_1=6.19, J_2=2.29, 1H), 6.4 (d, *J*=2.29, 1H), 3.99 (m, 2H), 1.8 (m, 2H), 1.4 (m, 2H), 1.2 (m, 20H), 0.87 (m, 3H).^{13}C NMR ($CDCl_3$,78 MHz, δ):194.38, 166.56, 164.62, 135.27, 115.08, 108.88, 101.13, 68.70, 32.02, 29.75, 29.67, 29.62, 29.46, 29.40, 26.01, 22.79, 14.22.). CHN analysis: calculated for $C_{21}H_{34}O_3$: C 75.41 %, H, 10.25 %, found C 75.46 %, H 10.12 %.

4-hexadecyloxy salicylaldehyde (13, n=14**):** Equivalent amount of 2,4-dihydroxybenzaldehyde was reacted with 1-bormohexadecane as described above. Yield: 51 %; mp:48-50 ˚C. IR (KBr, cm^{-1}): 2900, 2825, 1740, 1700, 1650, 1625, 1600, 1500, 1490, 1380, 1320, 1300, 1210, 1100, 1150, 1110, 1000, 980, 825, 890, 750, 700, 650, 620, 520. ^{1}H NMR ($CDCl_3$): 11.47 (s, 1H), 9.69 (s, 1H), 7.40 (d, *J*=8.7, 1H), 6.5 (dd, J_1=6.42, J_2=2.29, 1H), 6.4 (d, *J*=2.29, 1H), 3.99 (m, 2H), 1.8 (m, 2H), 1.5 (m, 2H), 1.27 (m, 24H), 0.87 (m, 3H). ^{13}C NMR ($CDCl_3$,77 MHz, δ): 194.39, 166.58, 164.59, 135.25, 115.09, 108.81, 101.14, 68.68, 29.763, 29.6301, 29.60, 29.44, 29.39, 29.00, 22.77, 14.19. CHN analysis: calculated for $C_{23}H_{38}O_3$ C 76.20 %, H 10.56 % found C 76.32 % H 10.71 %.

4-octadecyloxy salicylaldehyde (13, n=16**):** Equivalent amount of 2,4-dihydroxybenzaldehyde was reacted with 1-bormooctadecane as described above.

Yield: 45 %; mp: 60-63 ˚C. IR: (KBr, cm^{-1}): 2900, 2825, 1740, 1700, 1650, 1625, 1600, 1500, 1490, 1380, 1320, 1300, 1210, 1100, 1150, 1110, 1000, 980, 825, 890, 750, 700, 650, 620, 520. ^{1}H NMR ($CDCl_3$): 11.47 (s, 1H), 9.69 (s, 1H), 7.79 (d, J=8.71, 1H), 6.5 (dd, J_1=6.64, J_2=2.06, 1H), 6.4 (d, J=2.29, 1H), 4.00 (m, 2H), 1.8 (m, 2H), 1.5 (m, 2H), 1.30 (m, 28H), 0.87 (m, 3H). ^{13}C NMR ($CDCl_3$, 77 MHz, δ):188.62, 188.53, 165.86, 165.69, 163.46, 130.51, 130.27, 130.16, 119.00, 106.45, 106.26, 88.04, 68.65, 68.51, 68.32, 32.02, 29.79, 29.68, 29.46, 26.14, 22.79, 14.22. CHN analysis: calculated for $C_{25}H_{42}O_3$ C 76.87 %, H 10.84 %, found C, 76.86 %, H 10.79 %.

N,N'-Ethylene-bis(4-octyloxysalicylideneimine) (**15**, n=6)**:** Two equivalents (0.5 g, 1.99 mmol) of 4-octyloxy salicylaldehyde was mixed 1 equivalent of ethylenediamine (0.06g, 0.999 mmol) in methanol. The reaction mixture was stirred at room temperature with occasional heating for 30 minutes that resulted in the yellow precipitate of the corresponding Schiff base. The yellow precipitate was filtered, washed with cold methanol and dried under vacuum. Yield: 85 %; mp: 65-67 ˚C. IR (KBr, cm^{-1}): 2923, 2847, 1590, 1528, 1461, 1385, 1357, 1300, 1223, 1123, 833, 633, 628, 595. ^{1}H NMR ($CDCl_3$, δ): 8.2 (s, 2H), 7.1(d, J=2.22, 2H), 6.3 (m, 4H), 3.9 (m, 4H), 1.7 (m, 4H), 1.3 (m, 16H), 0.8 (m, 6H). ^{13}C NMR ($CDCl_3$, 78 MHz, δ): 165.505, 164.749, 163.191, 132.75, 112.22, 106.99, 101.68, 68.18, 58.91, 31.99, 29.65, 29.44, 29.17, 26.08, 22.77, 14.21. CHN analysis: calculated for $C_{32}H_{48}N_2O_4$, C 73.25 %, H 9.22 %, N 5.34 %, found 73.16 %, 9.32 %, 5.36 %.

N,N'-ethylene-bis(4-decyloxysalicylideneimine) (**15**, n=8)**:** Two equivalents (0.5 g, 1.79 mmol) of 4-decyloxy salicylaldehyde was reacted with 1 equivalent of

ethylenediamine (0.054g, 0.9 mM mmol) in methanol mixture as described. The product (yellow ppt) was filtered, dried and characterized. Yield: 83 %; mp: 70-72 ˚C. IR(KBr, cm^{-1}): 2919, 2850, 1626, 1576, 1522, 1504, 1473, 1430, 1410, 1389, 1300, 1286, 1229, 1173, 1145, 1034, 1018, 970, 853, 827, 796, 757, 720, 630, 580. ^{1}H NMR ($CDCl_3$): ^{1}H NMR ($CDCl_3$,): 8.1 (s, 2H), 7.06 (d, *J*=2.12, 2H), 6.38 (m, 4H), 3.93 (m, 4H), 3.83 (d, *J*=7.13, 4H), 1.75 (m, 4H), 1.42 (m, 4H), 1.26 (m, 24), 0.87 (t, J_1=12.73, J_2=6.54, 6H). ^{13}C NMR ($CDCl_3$,77 MHz, δ): 165.49, 164.68, 163.18, 112.26, 106.97, 101.71, 68.50, 58.94, 31.96, 29.62, 29.42, 29.37, 26.06, 22.74, 14.16. CHN analysis: calculated for $C_{36}H_{56}N_2O_4$, C 74.44 %, H 9.72 %, N 4.82 %, found C 74.32 %, H 9.69 %, N 4.87 %.

N,N'-ethylene-bis(4-dodecyloxy-salicylideneimine) (**15**, n=10): Two equivalents (0.5 g, 1.63 mmol) of 4-dodecyloxy salicylaldehyde was reacted with1 equivalent of ethylenediamine (0.05g, 0.816 mmol) in methanol mixture as described. The product (yellow ppt) was filtered, dried and characterized. Yield: 85 %; mp: 75-76 ˚C. IR(KBr, cm^{-1}): 2920, 2850, 1628, 1573, 1523, 1473, 1410, 1390, 1301, 1286, 1229, 1172, 1145, 1034, 1003, 970, 852, 796, 757, 719, 639, 580. ^{1}H NMR ($CDCl_3$): 8.13 (s, 2H), 7.02 (d, *J*=7.79, 2H), 6.33 (m, 4H), 3.92 (m, 4H), 3.80 (s, 4H), 1.73 (m, 4H), 1.39 (m, 4H), 1.23 (m, 32H), 0.87 (t, J_1=13.75, J_2=6.42, 6H). ^{13}C NMR ($CDCl_3$,77 MHz, δ): 165.43, 164.75, 163.19, 132.86, 112.07, 107.08, 101.78, 68.59, 58.32, 31.96, 29.67, 29.63, 29.60, 29.39, 29.12, 26.03, 22.73, 14.13. CHN analysis: calculated for $C_{40}H_{64}N_2O_4$.0.28 H_2O, C 75.43 %, H 10.13 %, N 4.4 %, found C 75.67 %, H 10.27 %, N 4.12 %,

N,N'-ethylene-bis(4-tetradecyloxy-salicylideneimine) (15, n=12): Two equivalents (0.6 g, 1.79 mmol) of 4-tetradecyloxy salicylaldehyde was reacted with1 equivalent of ethylenediamine (0.054g, 0.897 mmol) in methanol mixture as described. The product (yellow ppt) was filtered, dried and characterized. Yield: 82 %; mp:78-80 ˚C. IR (KBr, cm^{-1}): 2921, 2852, 1629, 1576, 1524, 1474, 1412, 1392, 1303, 1288, 1232, 1173, 1147, 1038, 1014, 972, 854, 797, 759, 721, 641, 582. ^{1}H NMR ($CDCl_3$): 8.18 (s, 2H), 7.07 (d, *J*=8.26, 2H), 6.39 (m, 4H), 3.93 (m, 4H), 3.83 (s, 4H), 1.78 (m, 4H), 1.43 (m, 4H), 1.25(m, 40H), 0.87 (t, J_1=13.75, J_2=6.42, 6H). ^{13}C NMR ($CDCl_3$,77 MHz, δ): 165.50, 164.74, 163.19, 132.75, 112.22, 106.99, 101.68, 68.19, 58.918, 32.024, 29.75, 29.69, 29.46, 29.17, 26.08, 22.79, 14.22. CHN analysis: calculated for $C_{44}H_{72}N_2O_4.0.1H_2O.0.25\ CH_3OH$, C 75.59 %, H 10.75 %, N 3.98 %, found C 75.8 %, H 10.89 %, N 3.73 %.

N,N'-ethylene-bis(4-hexadecyloxy-salicylideneimine) (15, n=14): Two equivalents (0.6 g, 1.66 mmol) of 4-hexadecyloxy salicylaldehyde was reacted with one equivalent of ethylenediamine (0.049g, 0.827 mmol) in methanol mixture as described. The product (yellow ppt) was filtered, dried and characterized. Yield: 75 %; mp: 81-82 ˚C, IR(KBr, cm^{-1}): 2919, 2850, 1628, 1574, 1523, 1472, 1410, 1390, 1300, 1266, 1230, 1171, 1146, 1036, 971, 852, 794, 757, 719, 639, 580, ^{1}H NMR ($CDCl_3$): 8.14 (s, 2H), 7.03 (d, *J*=8.94, 2H), 6.32 (m, 4H), 3.93 (m, 4H), 3.81 (s, 4H), 1.74 (m, 4H), 1.40 (m, 4H), 1.23 (m, 48H), 0.86 (t, J_1=12.75, J_2=6.54, 6H). ^{13}C NMR ($CDCl_3$,78 MHz, δ):165.54, 165.45, 163.45, 132.86, 112.07, 107.08, 101.75, 68.19, 58.41, 32.01, 29.77,

29.67, 29.44, 29.15, 26.06, 22.77, 14.19. CHN analysis: calculated for $C_{48}H_{80}N_2O_4$, C 76.95 %, H 10.76 %, N 3.74 %, found C 76.82 %, H 10.75 %, N 3.82 %.

N,N'-ethylene-bis(4-octadecyloxy-salicylideneimine) (15, n=16): Two equivalents (0.6 g, 1.54 mmol) of 4-octadecyloxysalicylaldehyde was reacted with one equivalent of ethylenediamine (0.046g, 0.768 mmol) in methanol-THF mixture as described. The product (yellow ppt) was filtered, dried and characterized. Yield: 50 %; mp:85-87 ˚C. IR (KBr, cm^{-1}): 2919, 2850, 1629, 1576, 1522, 1505, 1471, 1410, 1389, 1300, 1268, 1230, 1172, 1146, 1034, 852, 817, 719, 639. ^{1}H NMR ($CDCl_3$): 8.17 (d, J=5.96, 2H), 7.05 (d, J=8.94, 2H), 6.37 (m, 4H), 3.93 (m, 4H), 3.82 (d, *J*=7.1, 4H), 1.74 (m, 4H), 1.41 (m, 4H), 1.26 (m, 56H), 0.86 (t, J_1=13.45, J_2=6.24, 6H), ^{13}C NMR ($CDCl_3$,77 MHz, δ). ^{13}C NMR($CDCl_3$,78 MHz, δ):165.47, 165.11, 163.12, 132.75, 111.88, 107.00, 101.72, 68.19, 58.79, 32.00, 29.77, 29.67, 29.43, 29.16, 26.07, 22.76, 14.17. CHN analysis: calculated for $C_{52}H_{88}N_2O_4$, C 77.56 %, H 11.01 %, N 3.48 %, found C 77.6 %, H 11.19 %, N 3.52 %.

Synthesis of Fe(III)-salen lipid derivatives (16, n=6, n=8, n=10, n=12, n=14 and n=16**):** The long chain modified salen derivatives (Schiff bases) were mixed with equivalent amount of anhydrous ferric chloride in acetone and stirred at room temperature for 30 minutes that resulted in dark brown precipitate of the respective metal complexes. The metal-complexes were recrystallized from acetone or acetone-hexane mixture and characterized by IR, mass spectroscopy and elemental analysis.

4, 4′-Dioctyloxy Fe(III)-salen (16, n=6**):** Yield:53 %. IR (KBr cm^{-1}): 2900, 2800, 1610, 1538, 1447, 1379, 1335, 1310, 1200, 1101, 1010, 850, 798, 761, 711, 620, 600, 579;

ESI-MS: 578.20. CHN analysis: calculated for $C_{32}H_{46}ClFeN_2O_4$, 62.59 C %, 7.55 H %, 4.56 N %, found 62.58 C %, 7.53 H %, 4.51 N %.

4,4′-Didecyloxy Fe(III)-salen (16, n=8**):** Yield:50 %. IR (KBr): 2900, 2800, 1600, 1540, 1450, 1390, 1350, 1200, 1110, 1050, 1000, 850, 800, 620, 600; ESI-MS: 634.47. CHN analysis: calculated for $C_{36}H_{54}ClFeN_2O_4$, C 64.52 %, H 8.12 %, N 4.18 %, found C 64.41 %, H 8.05 %, N 4.03 %.

4,4′-Didodecyloxy Fe(III)-salen (16, n=10**):** Yield:42 %. IR (KBr, cm^{-1}): 2910, 2850, 1600, 1500, 1400, 1380, 1340, 1300, 1200, 1100, 1010, 850, 800, 760, 710, 620, 600, 580. ESI-MS: 690.60. CHN analysis calculated for $C_{40}H_{62}Cl_{Fe}N_2O_4.0.6\ H_2O$, C 65.18 %, H 8.64 %, N 3.8 %, Found C 65.16 %, H 8.67 %, N 3.77 %.

4,4′-Ditetradecyloxy Fe(III)-salen (16, n=12**):** Yield:48 %. IR (KBr, cm^{-1}): 2900, 2850, 1680, 1650, 1600, 1508, 1490, 1450, 1380, 1350, 1300, 1290, 1200, 1100, 1110, 1100, 950, 810, 790, 710, 615. ESI-MS: 746.60. CHN analysis: calculated for $C_{40}H_{62}ClFeN_2O_4$, C 67.55 %, H 9.02 %, N 3.58 %, found: C 67.59 %, H 9.1 %, N 3.67 %.

4,4′-Dihexadecyloxy Fe(III)-salen (16, n=14**):** Yield: 35 %, IR (KBr, cm^{-1}): 2900, 2800, 1600, 1500, 1450, 1300, 1325, 1380, 1200, 1110, 1050, 1000, 890, 810, 720. ESI-MS:802.67. CHN analysis calculated for $C_{48}H_{78}ClFeN2O_4.1.6\ H_2O$, C 66.82 %, H 9.43 %, N 3.25 %, found C 66.68 %, H 9.23 %, N 3.31 %.

4,4′-Dioctadecyloxy Fe(III)-salen (16, n=16**):** Yield: 34 %. IR (KBr, cm^{-1}): 2919, 2850, 1628, 1523, 1472, 1410, 1391, 1300, 1230, 1171, 1145, 1034, 852, 795, 757, 718,

634, 580, ESI-MS: 859.93. CHN analysis calculated for $C_{52}H_{86}ClFeN_2O_4$.2.5 H_2O, C 66.47 %, H 9.76 %, N, 2.98 %, found C 63.77 %, H 8.69 %, N 2.80 %.

3.4.4 In vitro DNA Cleavage Assay

Each of the metal Fe(III)-salens derivatives (compounds**, 1-9**) were incubated with plasmid DNA pML20-47 (0.5 µg) in the presence and absence of DTT in TE buffer (20 mM Tris-HCl, pH 7.4, 10 mM NaCl and 1 mM EDTA) at 37 ˚C for 1 hr. The product was analyzed by 0.8 % agarose gel electrophoresis and photographed by AlphaImager.

3.4.5 Apoptosis Assay by DAPI Staining

DAPI staining of the cells were done as described previously in Chapter II. HEK293 cells were grown on microscope slide to 80 % confluence and treated for 24 hrs with 100 µM of 4,4′-dimethoxyFe(III)-salen, 4,4′-dioctyloxy-Fe(III)-salen, 4,4′-didecyloxyFe(III)-salen 4,4′-ditetradecyloxyFe(III)-salen, 4,4′-dihexadecyloxyFe(III)-salen, 4,4′-DioctadecyloxyFe(III)-salen. Treated and untreated cells were washed with PBS (Phosphate Buffered Saline) buffer and fixed with 4 % paraformaldehyde in PBS for 15 minutes followed by permeabilization by 0.2 % Triton X-100 for 5 minutes. Cells were stained with DAPI (5 µg per slide) at 37 °C for 1 hr as described previously and analyzed with fluorescent microscope.

3.4.6 Determining IC_{50} Values of the Metal Complexes

The IC_{50} values of compounds both series of compounds (**1-9**) and (**16,** n=6, n=8, n=10, n=12, n=14, n=16) were determined by using MTT as previously described.[155] About 10,000 MCF-7 (for compnds **1-9**) or HEK293 (for compnds (**16,**

n=6, n=8, n=10, n=12, n=14, n=16) cells were seeded into 96 well microtiter plates with 8 replicate wells. After cells were allowed to attach metal complexes concentration between 1.5 nM to 200 µM prepared by serial dilution were added into each wells. Cells were allowed to incubate for 96 hrs. Then 20 µL of MTT previously dissolved in PBS (5 mg/mL) was added and cells were allowed to incubate further for 2 hrs. The media were discarded and cells were lysed with 100 µL DMSO by shaking on a shaker for 2 hrs and absorbance were measured at 570 nm.

3.4.7 TUNEL Assay

TUNEL DNA fragmentation assay was done as described in ApoAlert DNA fragmentation assay kit user manual (Clontech Cat# 630107). Briefly, HEK293 cells were grown on microscope slide to about 80 % confluence. Cells treated with 50 µM of 4,4′-dimethoxy Fe(III)-salen, 4,4′-dioctyloxy Fe(III)-salen, 4,4′-didecyloxy Fe(III)-salen, 4,4′-didodecyloxy Fe(III)salen, 4,4′-ditetradecyloxy Fe(III)-salen, 4,4′-dihexadecyloxy Fe(III)-salen and 4,4′-Dioctadecyloxy Fe(III)-salen for 24 hrs. Treated and control cells were washed with cold PBS buffer and fixed with 4 % formaldehyde in PBS at 4 ˚C for 25 minutes followed by washing by PBS for 5 minutes at room temperature. Cells were permeabilized by incubating in 0.2 % Triton X-100 in PBS and then washed again with PBS. Cells were covered with 100 µL of equilibrating buffer (200 mM potassium cacodylate, pH 6.6, 25 mM Tris-HCl pH 6.6, 0.2 mM DTT, 0.25 mg/ml bovine serum albumin, 2.5 mM cobalt chloride) for 10 minutes. The buffer was drained and cells were stained with 5 µL of nucleotides mix containing dATP, dGTP, dCTP and dUTP-fluorescein and 1 µL (5 units) of TdT (Terminal deoxynucleotidyl

Transferase) mixed in 45 µL of equilibration buffer. The enzymatic reaction was done in dark for 37 ˚C for 60 minutes. Then the reaction was stopped by using 2x SSC (0.3 M NaCl, 30 mM $Na_3Citrate{\cdot}H_2O$) buffer.[156]

3.4.8 Determining Partition Coefficient

The partition coefficient of the compounds was determined as previously described with some modifications.[145] First the absorbance of known concentrations of the compounds was determined in octanol phase to find the extinction coefficient. Then 1 mM concentration of the respective compounds were dissolved in pre-equilibrated equal volumes of octanol and water mixture by shaking for 48 hrs at room temperature. Then the two phases were allowed to separate by first by centrifugation at 14,000 rpm for 10 minutes and then by standing at room temperature for 24 hours. The two phases were separated by and each was allowed to stand followed by removal of traces of water from octanol phase. The absorbances of the compounds in water and octanol phase were measured for all of the compounds. The partition coefficient for each was determined by dividing the concentration in octanol phase to water phase.

CHAPTER IV

CHARACTERIZATION OF Fe(III)-SALEN BASED LIPOSOMES AND THEIR APPLICATION IN DNA TRANSFECTION IN HUMAN CELLS

4.1 Introduction

Transfection is a process by which an external DNA/RNA molecule is introduced into the eukaryotic cell. This technique has important implications in various aspects of molecular biology and in gene therapy.[50,100,111] For example, in molecular biology experiments small nucleic acid sequences, antisense RNA and siRNA (small interfering RNA) have been introduced into eukaryotic cells for studying metabolic pathways and/or for attenuating the expression of particular gene. On the other hand, it has been used to replace defective genes in clinical setup as gene therapy to cure various genetic disorders. [115]

There are various techniques available to date which are widely used by molecular biologist in delivering therapeutic DNA.[100] For example, disabled viral particles have been used to transfect cells with nucleic acids. However, it was found out that viral particles are unsafe.[159] Dendrimers, nano-paricles, polymers, hydrogels and microparticles[83] have also been used to deliver DNA into the cell. Although, many of these techniques are widely used, they suffer from various limitation such as delivery efficiency, cellular toxicities etc.[99] To overcome these issues, researchers are developing novel DNA delivery vehicles including synthetic cationic liposomes.[160,161]

Cationic lipids (such as like dihexadecyldimethylammonium bromide, DHDAB) are amphiphilic molecules that self assemble in aqueous environment into various structures depending on their molecular structure. Many cationic lipids (including DHDAB) are shown to form membrane like hallow spherical vesicles called liposomes (Figure 4.1). As described in our previous chapter, we have synthesized several Fe(III)-salen lipid complexes with varying long chains (16, n=6, 8, 10, 12, 14 and 16) (structure shown in Figure 4.2). Notably, these lipids similar to DHDAB contain a cationic head group and two long chain lipophilic moieties (Figure 4.3). Therefore these Fe(III)-salen lipophiles are very similar to many synthetic cationic lipids that are known to self assemble into various structure (such as hollow liposome's, nano-tubes, helics etc).[83,99]

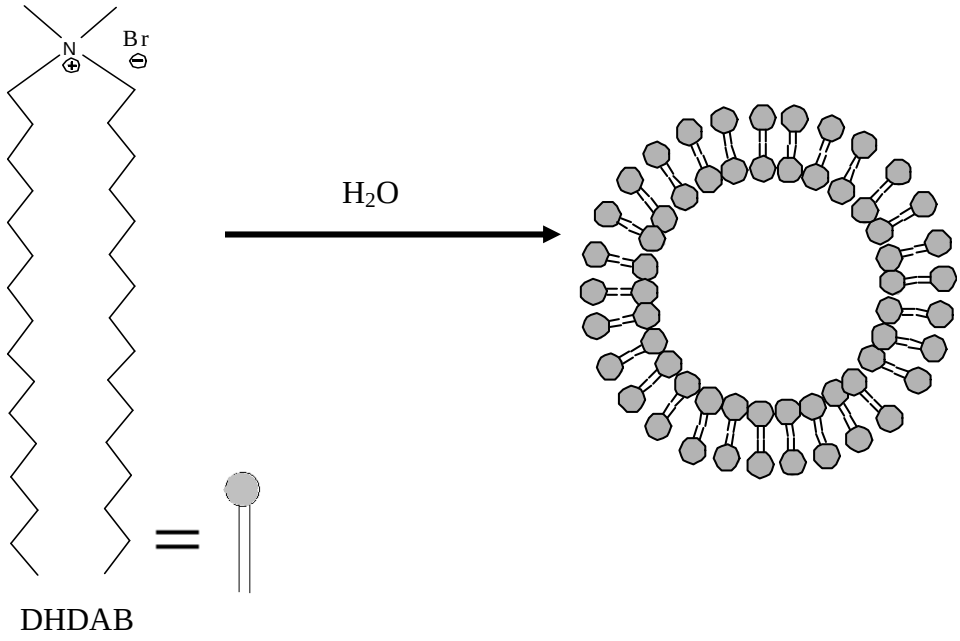

Figure 4.1 Lipid molecule self assemble into liposome in water. (DHDAB = dihexadecyldimethylammonium bromide)

As Fe(III)-salen lipids look very similar to synthetic cationic lipids (Figure 4.3) we investigated their self assembly properties in aqueous environment. Furthermore, as cationic liposomes are shown to be efficient DNA transfection agents, we also investigated the Fe(III)-salen liposome mediated transfection experiments. Our results demonstrated that demonstrated that Fe(III)-salen lipids self assemble into liposomal structures and importantly, some of the Fe(III)-salen liposomes showed efficient transfection abilities in cultured human cells. The synthesis of 4,4′-dialkoxy Fe(III)-salen (structure in Figure 4.2) have been described in chapter III.

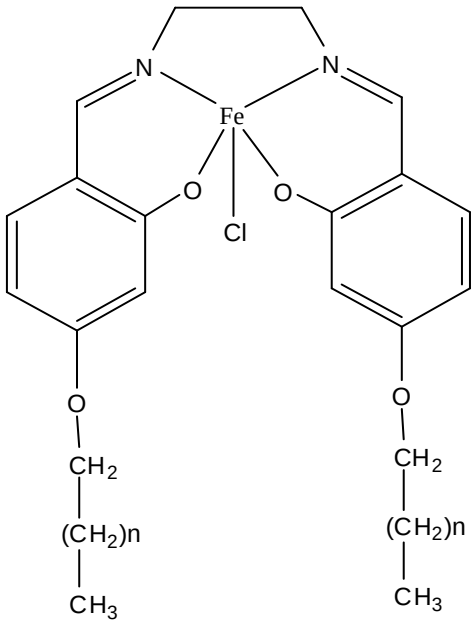

16 **n** = 6, 8, 10, 12, 14, 16

Figure 4.2 Structures of salen based metallo-lipids.

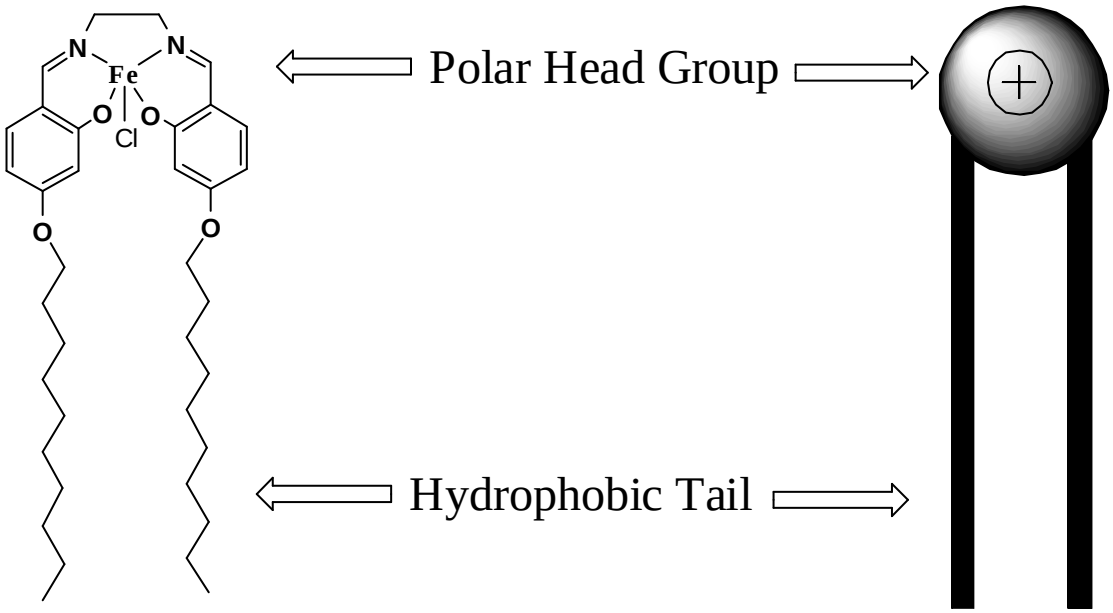

Figure 4.3 Illustration of polar group and hydrophobic groups of metallo-lipid with ten carbon alkoxy group. The central iron metal imparts a polar head group with one positive charge.

4.2 Results and Discussion

4.2.1 Fe(III)-Salen Lipids Self Assembled into Liposomes

It is well known that when cationic amphiphiles are resuspended in aqueous solution, they assemple into various microstructures based on their molecular architectures.[83,99] This self assembly is driven by various factors especially to minimize

the entropically unfavorable interactions between hydrophobic long carbon chains with surrounding water. The bilayer is formed in such a way that the hydrocarbon part of the lipid contact with each other while the polar water soluble head group stays surrounded by water. The geometry of the lipid molecule like hydration shell of its polar group, volume of the lipid molecule will determine if liposome, micelle or other different aggregates will form. [165, 166]

Herein, in order to investigate the self-assembly and transfection abilities of Fe(III)-salen lipids, initially we examined their liposomal assembly properties. The liposomes were synthesized following the previous protocol.[175] In Brief, the metallo-lipids (5 mg, structures shown in Figure 4.2, n=8-16) were dissolved in chloroform in round bottom flask followed by evaporation under stream of air while rotating the flask which yielded thin film on the wall of the flask. The thin film was hydrated with water using heating-cooling followed by sonication that resulted in a slightly cloudy brownish solution of Fe(III)-salen liposomes (self-assemblies).

4.2.2 Determining the Size of Fe(III)-Salen Lipid Self Assemblies with Dynamic Light Scattering

Initially, we examined the size of these Fe(III)-salen self assembled lipid particles using dynamic light scattering (DLS) also known as photon correlation spectroscopy. It is a well used method to measure the size of particles in a solution from few nanometer to micrometer.[167] The principle relies on the fact that when particle is suspended in solvent they experience random Brownian motion. When particles under Brownian motion are illuminated with coherent source of light, laser light of 633 nm in this case the scattering of the light occurs in all direction at a different intensity and

frequency from that of the incident light used. The shift in the frequency observed in scattered light is related to size of the particle causing the scattering, with smaller particle showing greater shift in frequency because of their higher speed compared to larger particles.[167, 168]

Using laser light of 633 nm we have measured hydrodynamic sizes of our self assembled lipids using DLS as previous described. [167, 168] As a positive control the size of standard known particle polystyrene beads was measured to examine if the instrument is properly calibrated. Then, the metallo-liposomes were diluted (100 fold) by dissolving in deionized water.. The size of the liposomes was measured under the same condition as that of the standard (Table 4.1). As seen in Table 1, the sizes of the liposomes vary from 177 nm to 489 nm and varies based on the chain length of the Fe(III)-salen lipids. For example, Fe(III)-salen liposomes with C-10 hydrocarbon chain length (compd., **6**, n=8) has hydrodynamic diameter about 177 nm. The sizes of the particles (iron-salen liposomes) increased with the increase in chain length (Table 1). Notably, we also measure the hydrodynamic size of C-18 chain containing Fe(III)-salen self-aggregates with hydrodynamic size of 489 nm. Based on sizes, the Fe(III)-salen self-aggregates appeared to be in the ranges of liposomal aggregates.

Table 4.1 Sizes of Liposomes Measured by DLS

No.	*Liposome*	*Average Diameter in nm*	*Expected*
1	Polystyrene beads (standard)	207	200 ±7
2	n=8	177.5	
2	n=10	207.9	
3	n=12	224.0	
4	n=14	377.1	
5	n=16	489.0	

4.2.3 Encapsulation of 5(6)-Carboxyfluorescein (5-FC) into the Fe(III)-Salen Liposomes

In order to further characterize the Fe(III)-salen liposomes (hollow vesicles), we tested the dye (5-FC) encapsulation properties for different chain length containing Fe(III)-salen lipids (16, n=8, 10, 12, 14). To study the dye encapsulation properties, we prepared the Fe(III)-salen liposomes in presence of 5-FC and then separated the 5-FC encapsulated liposomes using size exclusion column (Sephadex G-75)[167] and then examined the release of the encapsulated 5-FC using the lyses of the liposomes using 1 % Triton-X100 and monitoring the fluorescence of 5-FC (λ_{ex} at 492 nm and λ_{em} at 517). Notably, the 5-FC dye molecules that are encapsulated inside the liposomes usually have quenched fluorescence. Upon lyses of the liposomes by triton-X100, the 5-FC gets released into the solution and fluorescence is enhanced. Triton X-100 is a nonionic surfactant that is able to destroy the membrane causing leakage of 5(6)-carboxyfluorescein from the liposome core.[167] Our results shown in Figure 4.4 (**16;** Panel A n=8, Panel B n=10, Panel C n=12**,** Panel D n=14) demonstrates that the fluorescence of 5-FC increases with each addition of Triton X-100.

The release of 5-FC upon lysis of the Fe(III)-salen self-assemblies indicated that the assemblies are hollow liposomes with hallow aqueous core that traped 5-FC molecules. However, the C-8 (n=6) containing lipids could not yield any release property as that of other Fe(III)-salen lipids described. This shows that it doesn't form hallow aqueous core as that of other liposomes described.

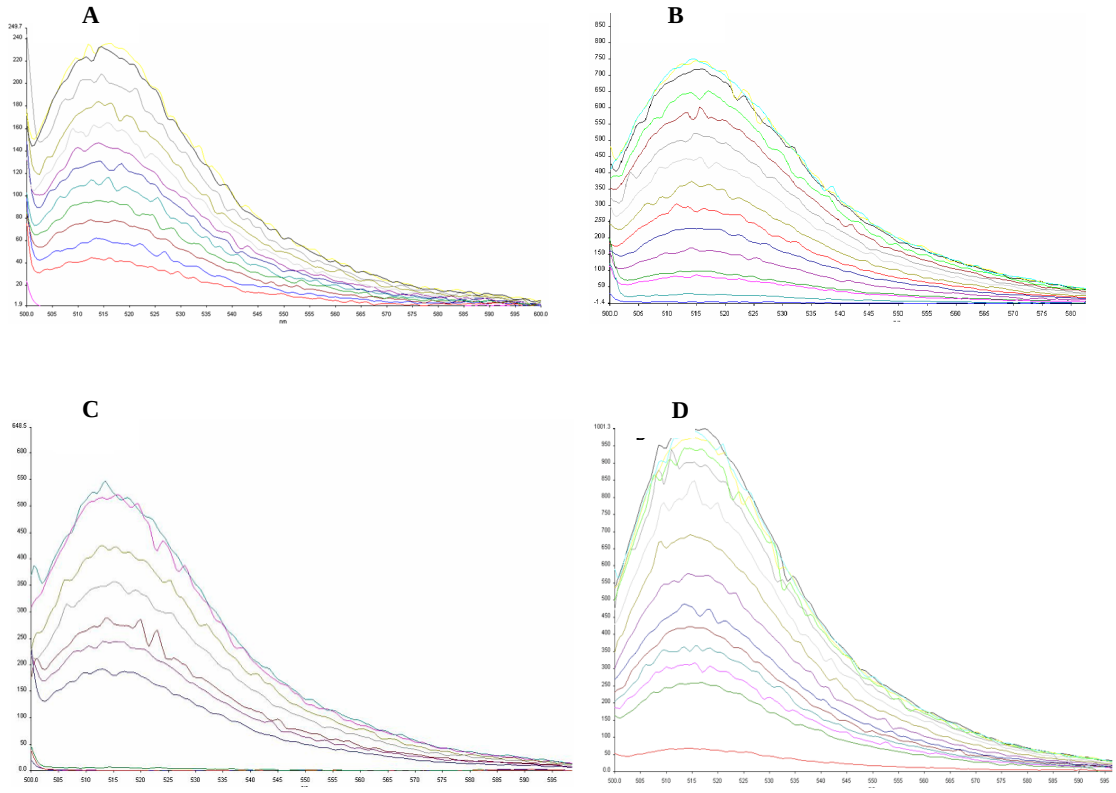

Figure 4.4 Encapsulation of 5(6)-carboxyfluorescein (5-FC) into metallo-liposomes aqueous core and release experiment. The Liposome-5(6)-carboxyfluorescein formulation was purified by fractionation with gel filtration (Sephadex G-75). The 5-FC release from liposome core was triggered by Triton X-100 (1%) sequentially and followed by measuring fluorescence of the dye (λ_{ex} 492 nm, λ_{em} 517 nm). Panel A is for (**16** n=8) metallo liposome, Panel B is for (**16**, n=10), Panel C is for (**16**, n=12) and Panel D is for (**16**, n=14).

4.2.4 SEM (Scanning Electron Microscopy) Measurement of Fe(III)-Salen Liposomes

In order to visualized the morphologies of the Fe(III)-salen self assemblies, we examined the them under scanning electron microscope (SEM). For the SEM studies we, prepared the Fe(III)-salen lipids self-assemblies in deionized water using heating-cooling method followed by sonication as described earlier. [172, 173, 175]

The lipid aggregates were placed on gold plates, lyophilized and examined under SEM. The SEM pictures for different Fe(III)salen self assemblies are shown in Figure 4.5 and 4.6. As seen in Figure 4.5 (Panel A) the lipid aggregates resulting from n=6 (8 carbons) chain containing Fe(III)-salen showed no distinct morphologies. This is probably because when the substituent carbon length is around 8 carbons the lipid will not be long enough to form self assembly bilayer. Interestingly, as the chain length changed from n=6 to n=8 (8 carbons to 10 carbons) we observed distinct spherical morphologies with sizes in the ranges of 100 nm (Figure 4.4 Panel C and C′). The spherical particles were clearer in higher resolution SEM pictures. These results indicates that 10 carbon chain containing Fe(III)-salen lipids formed liposomal aggregates in solution. The features and morphology of the self-assemblies were more distinct with longer chain length Figure 4.5 (Panels D and D′) and Figure 4.6 (Panels E and E′), (Panels F and F′) and (Panels G and G′). The n=12 and and n=14 liposome were the best in appearance. Figure 4.5 shows the SEM micrograph of liposomes, Panel A is micrograph of liposome from commercial lipid dihexadecyl dimethyl ammonium bromide (DHDAB) as positive control.

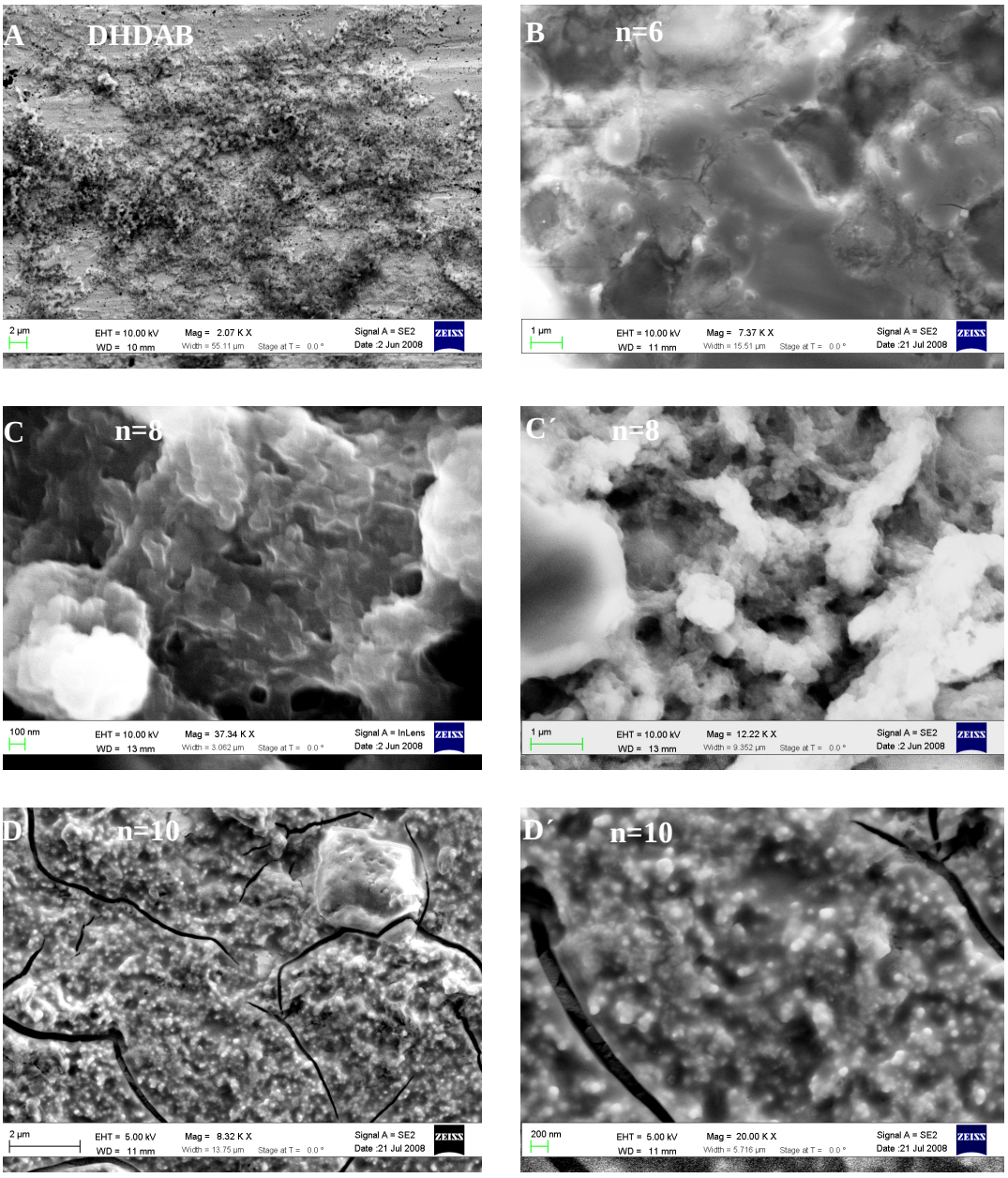

Figure 4.5 Scanning electron microscope (SEM) micrograph of liposome from commercial source, dihexadecyl dimethyl ammonium bromide (DHDAB), micrograph of metallo-lipids n=6, n=8, n=10. Panel A is for DHDAB, Panel B is for n=6 no liposome formation is observed. Panels C and C´ for n=8 metallo-lipid and Panels D and D´ for n=10. Micrograph shows liposome formation as seen as small spherical particles for all except for n=6.

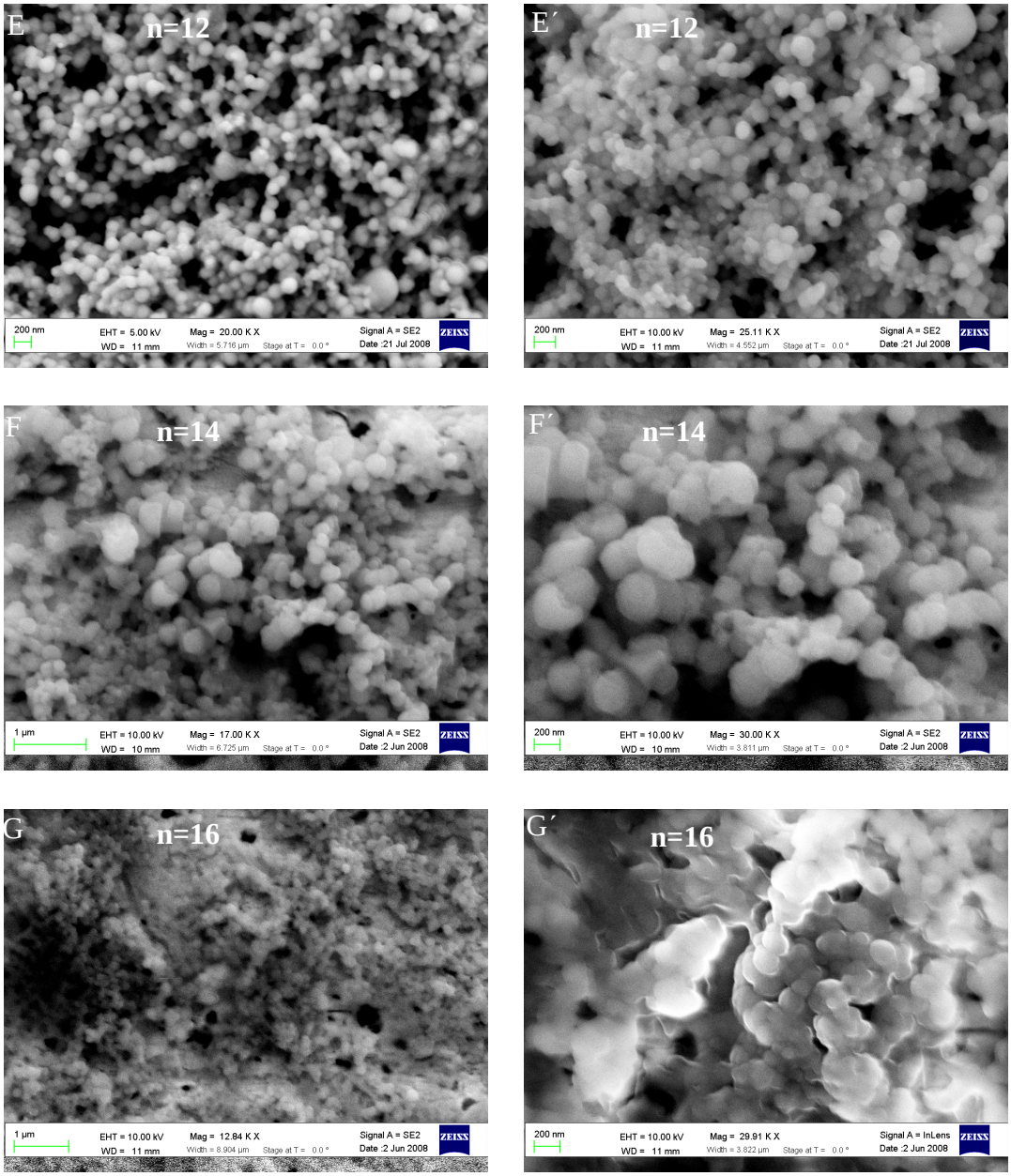

Figure 4.6 Scanning electron microscope micrograph of liposomes made of n=12, n=14 and n=16 metallo-lipids. Panels E and E´ show micrograph for liposome made of n=12, Panels F and F´ for n=14, Panels G and G´ are for n=16. Liposome particles are clearly seen as small spheres.

4.2.5 Characterization of DNA-Liposome Condensate

Cationic lipids are well known for their application in DNA transfection in eukaryotic cells. Notably, due to the presence of cationic Fe(III)-centers at the head group Fe(III)-salen lipids, Fe(III)-salen based liposomes should provide a cationic surface to form complex with negatively charged polymers like DNA. This liposome-DNA complexes may have abilities to transfect DNA in human cells. Herein, in order to explore Fe(III)-salen liposomes mediated DNA transfection in human cells, we initially analyzed their ability to interact and form complexes with DNA.

We used a plasmid DNA, pLEGFP-N1 (6.9 kb retrovirus vector with CMV promoter) that contains a green fluorescence protein (GFP) gene under the CMV promoter and therefore can express GFP proteins in eukaryotic cells.[175] Using pLEGFP-N1 plasmid DNA, we examined the liposome-DNA complexation properties of Fe(III)-salen liposomes. In brief, Fe(III)-salen liposomes (10 µL, 2.98 mM stock) were mixed with varying amounts (0.1, 0.2, 0.3 µg) of plasmid DNA (pLEGFP-N1) in 1XTE buffer, incubated at room temperature for 15 minutes, and then analyzed by 1 % agarose gel electrophoresis. [175] It is expected that excess uncomplexed DNA moves out of the well of the gel while DNA complexed with the liposome will stay in the well.[25, 113]

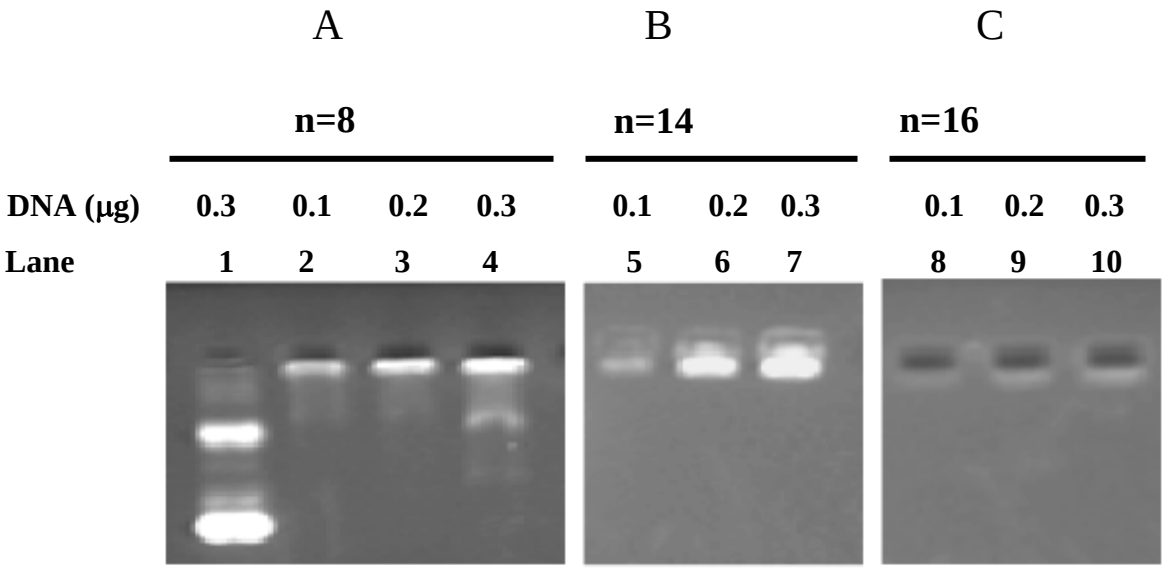

Figure 4.7 Liposome-DNA complex for metallo-liposome n=8, n=14, n=16 and plasmid DNA pLEGFP-N1. The concentration of liposome used is 2.98 mM. Lane 1 is DNA alone, Lanes 2, 5 and 8 are 0.1 μg DNA complexed with liposome for n=8, n=14, n=16 respectively. Lanes 3, 6, and 9 are 0.2 μg DNA complexed with respective liposomes (n=8, n=14 and n=16). Lanes 4, 7 and 10 are 0.3 μg DNA complexed with liposomes (n=8, n=14 and n=16).

As seen in Figure 4.7, Panel A Lane 1 shows control plasmid DNA without liposome and as expected upon electrophoresis the DNA moved out of the well. However, in lanes 2 and 3 (Figure 4.7) which contains increasing amounts of DNA (0.1 and 0.2 μg) in the presence of Fe(III)-salen liposomes (n=8), most DNA did not migrate away from the wells of the gel indicating the efficient complex formation leading to the compaction and neutralization of charge in DNA. Upon addition of larger amounts DNA, the uncomplexed DNA moved out of the well (lane 4, Panel A, Figure 4.7). We also examined the DNA-liposome complexation properties of other Fe(III)-salen liposomes and demonstrated that DNA condensation effects is enhanced as the carbon

chain for the liposome is increased to n=14 and n=16 Lanes 5-10 (panels B and C, Figure 4.7). For n=16 liposome-DNA complex, the DNA condensation is so severe that no DNA is visible (Figure 4.7 Panel C Lanes 8-10). Overall, these results demonstrated that Fe(III)_salen based liposomes complexes with DNA efficiently and these the complexation efficiencies vary with chain length of the liposome.

4.2.6 Transfection of HEK293 Cells with pLEGFP-N1 Plasmid using Liposomes Made of Fe(III)-Salen Lipids

As the Fe(III)-salen liposomes were found to interact and complex with plasmid pLEGFP-N1, we examined their transfection abilities in cultured human cells. We used plasmid pLEGFP-N1 for the transfection experiments, because upon transfection followed by expression of the GFPs, the cell will turn green. The resulting green fluorescent protein gene product expressed will fluoresce at excitation wavelength of 488 nm and emission maxima of 507 nm and can be easily monitored using fluorescence microscope. In order to assess the transfection abilities of the Fe(III)-salen liposomes, we used similar procedure as described previously.[175] In brief, initially, 1 µg of plasmid DNA (pLEGFP-N1) in 100 µL of serum free DMEM media in a micro centrifuge tubes. In parallel, varying concentration Fe(III)-salen liposomes (2 to 6 mM) and MAXifect liposome (System Bioscience, positive control), were dissolved separately in 100 µL of serum free DMEM. Then DNA (in DMEM) was directly added into the liposomes, mixed gently and the liposome-DNA complex was allowed to form for about 20 minutes. Then 200 µL of the media containing liposome-DNA complex was directly added into the HEK 293 cells prepared for the transfection experiments (in

800 µL serum and antibiotic free DMEM). The cells were immediately placed in a tissue culture incubator and grown for about 6 hrs. The media were removed, cells were rinsed once with DMEM media and for fast recovery and growth, cells were incubated with with 1 mL of 2x media with 20 % FBS and 2% L-glutamine and 0.2% Penicillin/streptomycin and grown for 42 hrs. The cells were fixed with 4% paraformaldehyde, permeabilized by 0.2% Triton X-100 and stained with DAPI to visualize the nucleus. The coverslips containing cells were mounted on the slide and visualized under fluorescent microscope for GFP expression using filter set for FITC.

The HEK293 cells that were transfected with pLEGFP-N1 using 1 µL of commercial liposome, MAXifect ((positive control, panel B′), showed many cells that were turned green. The presence of green colored cells indicated the expression of GFT resulted from the transfection of pLEGFP-N1 plasmid. Interestingly, cells that were transfected with Fe(III)-salen liposomes (n=8) [0.5 µL and 1 µL(panel C and D, Figure 4.8) of 2.98 mM stock] also showed many green cloored cells under fluorescence microscope and it was about the similar extent in comparision to the commercial liposome used. An attempt to transfect the cells with either higher or lower concentrations of this metallo-liposome were not successful. Panels A-C Figure 4.8 and Panels D-F Figure 4.9 show cells nuclei stained with DAPI. Panels B′, C′, and D′ show cells in Panel B, C and D (in Figures 4.8 and Figure 4.9) respectively transfected with GFP gene and expressing green fluorescent protein, as indicated by their green appearance. Panels B′′, C′′ and D′′ are overlay of the GFP and DAPI stained nucleus.. Control cells (panel A′, Figure 4.8) and cells that were transfected with Fe(III)-salen

liposomes (n=14 and n=16liposomes Panels E′ and F′,Figure 4.9) did not shown the GFP expressed cells. This results demonstrated that Fe(III)-salen liposome with n=8 chain length is efficient in transfection of pLEGFP-N1 in HEK293 cells.

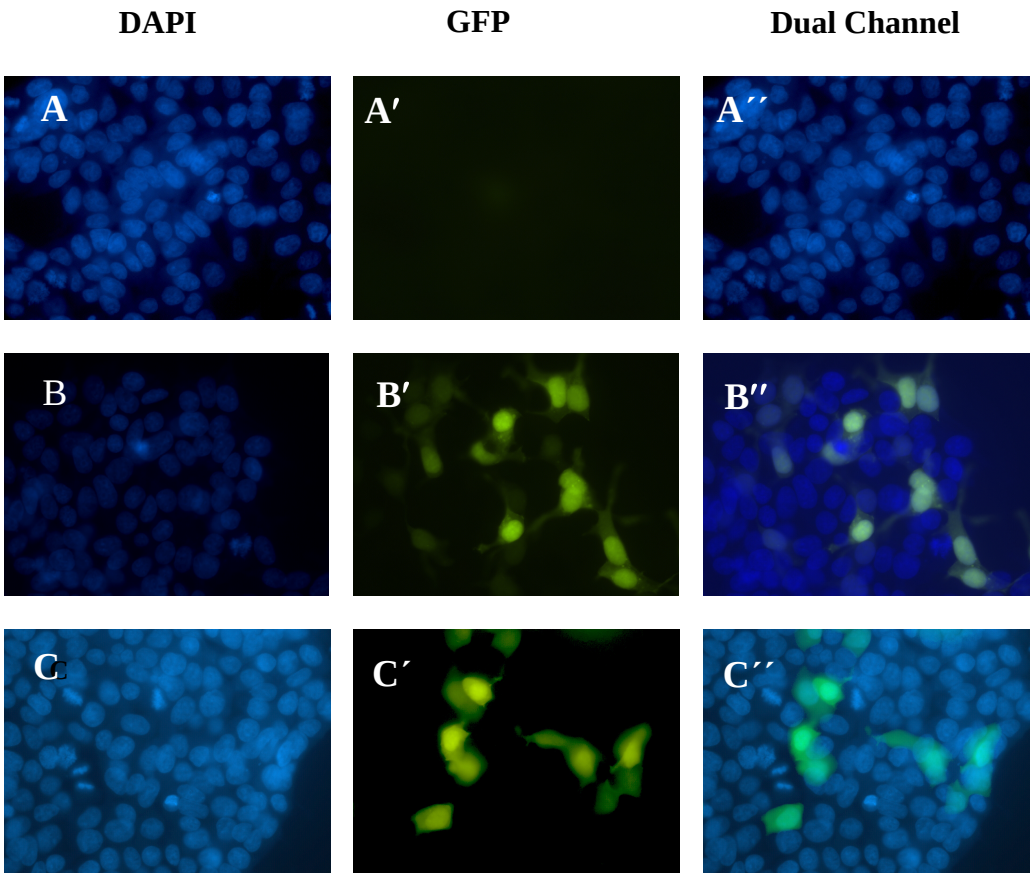

Figure 4.8 Transfection of HEK293 cells with pLEGFP-N1 plasmid containing green fluorescent protein gene using commercial liposome MAXifect as positive control and metallo-liposomes, n=8. Panel A-C show cells nuclei stained with DAPI. Panels B′ and C′, show cells transfected with GFP gene, respectively MAXifect, n=8 metallo-liposome with 1µg DNA, 0.5 µL liposome. No transfection is observed for control cells Panel A. Panels A′′-C′′ are dual channel obtained by overlay of corresponding DAPI and GFP channels.

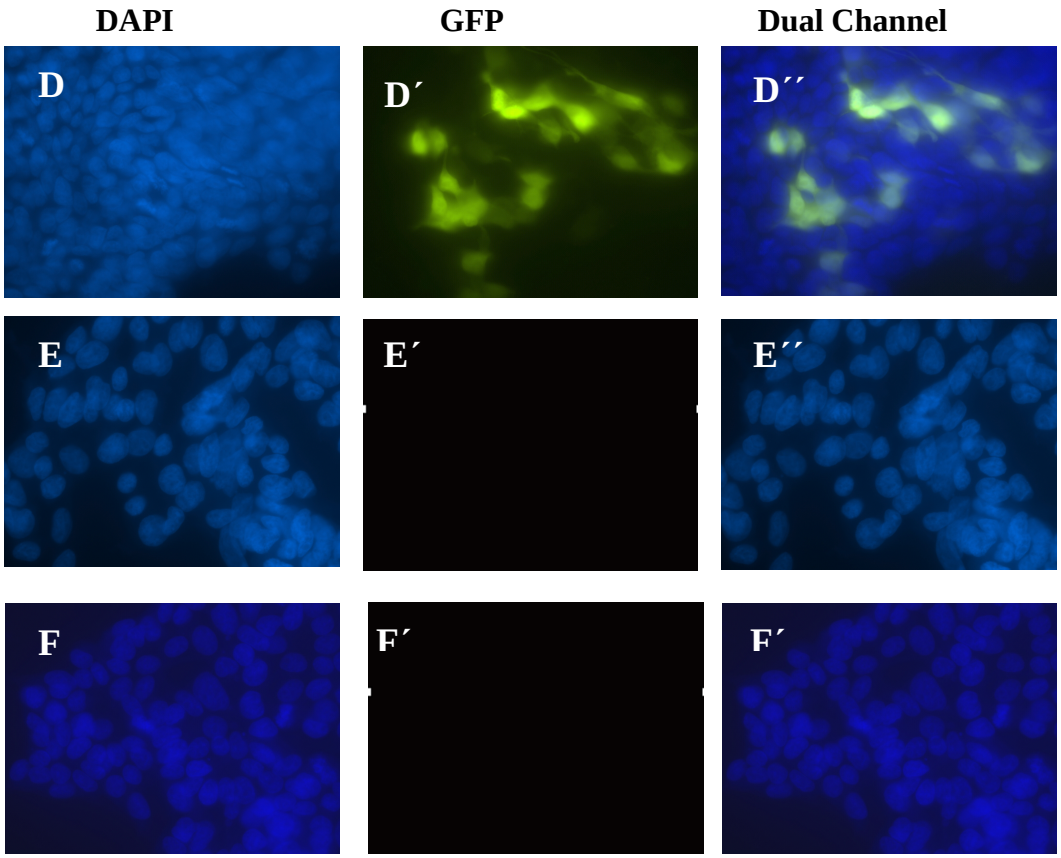

Figure 4.9 Transfection of HEK293 cells with pLEGFP-N1 plasmid containing green fluorescent protein gene using metallo-liposomes n=8, n=14 and n=16. Panels D-F show cells nuclei stained with DAPI. Panel D´ shows cells transfected with GFP gene using 1µg DNA 1 µL liposome made of n=8 metallo-lipid. None of liposomes made from n=14 and n=16 were able to do transfection (Panels E′ and F′) transfection is observed. Panels D´´-F´´ are dual channel obtained by overlay of corresponding DAPI and GFP channels. Control cells are shown in Figure 4.7, Panel A.

4.3 Summary and Conclusions

Herein, we investigated synthesis and characterization of novel metallo-liposomes based on Fe(III)-salen lipids with varying chain length (C8-C18). Our results demonstrated that Fe(III)-salen lipids self-assemble in aqueous solution in liposomes.

Dynamic light scattering experiments demonstrated that Fe(III)-salen lipids with chain length C10 or above formed self-assembled particles with hydrodynamic diameter about 177-489 nm. 5(6)-carboxyfluorescein encapsulation experiments demonstrated that Fe(III)-salen lipids produced hollow liposomes. Scanning electron miscopy demonstrated that Fe(III)-salen liposomes are fairly uniform spherical in size and the quality of liposomes were enhanced with in chain length. Taken together, different physical measurements demonstrated that Fe(III)-salen lipids self-assembles into hollow liposomes in aqueous environment.

We examined the DNA interaction and transfection abilities of these novel Fe(III)-salen liposomes in cultured human cells. Our results demonstrated that each of the Fe(III)-salen liposomes interact with DNA efficiently forming lipid-DNA complex. Most Interestingly, our results demonstrated that Fe(III)-salen liposomes with n=8 is able to transfects DNA into HEK293 cells. Notably, other lipids (n = 10-16) did not show any transfection although the compounds differ only by few carbon numbers.. Similar phenomenon has also been (chapter I Figure 1.10).[161] It was shown that of the three copper complexes studied only complex **1** not complex **3** was able to do transfection while the efficiency of transfection for **3** went down significantly as **R** group increased from 12 to 18. The lack of the transfection ability of the liposomes with longer chain length could be ascribed to an enhanced melting temperature of the liposome which may hinder the phase transition required to release DNA.[110].. Overall, we have synthesized and characterised several novel Fe(III)-lipsomes and demonstrated that some of them are apable of delivering DNA into eukaryotic cells.

4.4 Materials and Methods

4.4.1 General

All tissue culture works and cell growing conditions have already been described in Chapter II under Materials and Methods. 5(6)-carboxyfluorescein was purchased from Sigma–Aldrich. Cells were grown on cover slip for microscopy experiments.

4.4.2 Physical Measurements

Dynamic light scattering (DLS) was recorded using NeHe laser 633 wave length, Brookhaven Instruments, Brookhaven, NY. Scanning electron microscopy was done using ZEISS Supra 55 up Leo Gemini column, with high performance variable pressure FE-SEM, with resolution of 1.0 nm at 15 kV with CCD-camera and IR-illumination. Fluorescence study involving 5(6)-carboxyfluorescein was recorded on PerkinElmer LS 55. Nikon fluorescence microscope was used for GFP expression analysis.

4.4.3 Synthesis of Liposomes

Fe(III)-salen liposomes were prepared using heating cooling method followed by sonication as described earlier. [175] Each of the Fe(III)-salen lipid derivatives (5 mg) was dissolved in chloroform in a 10 mL round bottom flask and slowly evaporated (with rotation) to obtain the thin lipid films. Traces of organic solvent were removed by keeping the thin film-containing flask overnight under vacuum. The lipid film was hydrated with water (final concentration 2.98 mM) followed by heating (60 °C) and

cooling cycles (~ 15 cycles). The liposome suspension was sonicated further (Branson sonicator) for five minutes three times.

4.4.4 Measuring Liposome Size by Dynamic Light Scattering (DLS) Technique

The Fe(III)-salen liposomes (stock 2.98 mM) dispersion obtained was further diluted with deionized water 100 fold. Then 3 mL of the diluted liposome was placed in test tube and mixed by vortexing for 3 minutes. Decaline was used to correct for refraction that arise due to glass used as sample tube for measurement and instrument was calibrated with polystyrene beads 200±7 nm diameter that was similarly diluted in 10 mM KCl solution. Measurement of liposomes size was undertaken by Dynamic Light Scattering *(*DLS) instrument using NeHe laser 633 nm wavelength (Brookhaven Instruments, Brookhaven, NY). using 633 nm laser light.[167, 168]

4.4.5 Encapsulation of Liposomes with 5(6)-Carboxyfluorescein

Thin film of the corresponding metal complexes was formed on the walls of flask as previously described.[167] Residual organic solvent was removed by vacuum and the film was hydrated with PBS. Subsequently, 159 mM stock of 5(6)-carboxyfluorescein dissolved in PBS was added to film being hydrated to make the final concentration of the dye 50 mM. The hydration process was continued for about 30 minutes and then the hydrated film was subjected to heating-cooling cycles followed by low power sonication (three times 5 minutes each time). After sonication was over the sample was allowed to stay for 30 minutes before gel filtration was done.

Slurry of Sephadex G-75 was made in 1x PBS and added to 2/3 volume of column. Then about 250 µL of liposome encapsulated with 5(6)-carboxyfluorescein was

added. Fractionation was done by eluting with PBS and collecting 250 µL of the fractions. Then the turbidity of the fractions was measured by UV-visible and fractions with high liposome content showed higher back scattering. Those fractions that have higher backscattering were taken and further diluted in water. The diluted sample was placed in fluorescent spectrophotometer and spectra were collected with excitation at 492 nm and emissions at 517 nm. Once the background reading was obtained 1% of Triton X-100 was added into the cuvette containing the sample and mixed well. The fluorescence was recorded after each additional Triton X-100 addition and the experiment was stopped when no more change was observed.

4.4.6 Scanning Electron Microscopy (SEM) Sample Preparation and Measurement

To take SEM micrograph, first liposomes were prepared as described in the Section 4.4.3. The prepared liposomes were allowed to anneal for about 30 minutes after three times of 5 minutes sonication. Two gold plated steel sample mounting plates were placed in -80 ˚C to cool it to very low temperature. The lypholizer doesn't have a cooling system and to circumvent this problem the cooled gold plates were placed in drying chamber of lypholizer and liquid nitrogen was poured to cool the system even further. Then 100 µL of each of the liposomes was placed on the gold plates in the chamber and constantly liquid nitrogen was poured to keep it at very low temperature. After all samples have been placed on the plates the chamber was once again splashed with liquid nitrogen and the vacuum was applied slowly to avoid splashing of the sample from the plates and the drying process was done for at least 48 hrs. At the end of 48 hrs of drying the vacuum system was released slowly to avoid the samples flying off

the plates. The plates were carefully placed on ZEISS Supra 55 VP Scanning Electron Microscope, the micrograph was taken shining electron on the sample and detection was achieved by secondary electron detector.[172, 173]

4.4.7 Agarose Gel Electrophoresis of Lipoplex

The optimum Lipid-DNA complex charge ratio was assessed by mixing 0.1, 0.2, 0.3 µg plasmid DNA with 10 µL (1 µM final concentration) of liposomeand incubating for 15 minutes. Once the complex is formed the complex was run on 1% agarose gel electrophoresis at 40 volts and stained with ethidium bromide. The photograph of the gel was taken with AlphaImager.

4.4.8 E. coli Expression and Purification of pLEGFP-N1 Plasmid DNA

E. coli strain, DH5α, competent cells were transformed with plasmid DNA pLEGFP-N1 containing ampicillin selective marker by calcium chloride and heat shock method as described previously.[174] Three different colonies were inoculated into three 5 ml sterile LB (Luria-Bertani) media containing 50 µg/mL ampicillin in a culture test tube. The bacteria were grown overnight at 37 ˚C by agitating at 2.5 rpm. Once the bacteria were grown to the required level 50 µL of the overnight culture was inoculated into 5 mL sterile LB media containing 50 µg/mL of ampicillin. The bacteria were grown for about 12 hrs at 37 ˚C by shaking at 2.5 rpm. Once the bacteria were grown to the required level the culture was centrifugation at 10,000 g for 1 minute to harvest the cells. The media were removed and extraction of the plasmid DNA pLEGF-N1 was done by Omega bio-tek E.Z.N.A endo free plasmid midprep kit (D6915-03). The

concentration and purity of the DNA was determined by UV-visible spectrophotometer at 260/280 nm. The typical yield obtained for the plasmid DNA was about 50 µg.

4.4.9 Transfection of HEK293 Cells with pLEGFP-N1

Microscope slide cover was placed in 35 mm x10 mm tissue culture plate and then kept under UV lamp for at least 2 hrs in a tissue culture sterile laminar flow. Freshly cultured HEK293 cells were seeded into each of the plates and the cells were allowed to attach overnight. DNA-liposome complex for transfection was made by first dissolving 1 µg of plasmid DNA in 100 µL of antibiotic and serum free DMEM media in a microcentrifuge tubes.[175] Similarly, between 2 mM to 6 mM metallo-liposome concentrations and MAXifect liposome (System Bioscience), as positive control was dissolved in 100 µL of antibiotic and serum free media. Then 1 µg of plasmid DNA pLEGFP-N1 that was dissolved in DMEM media was directly added into the liposomes. The liposome-DNA complex was allowed to form for about 20 minutes.

The DMEM media from HEK293 cells that were grown in 35 mm plate was removed and the cells were washed twice by 1 mL serum free and antibiotic free DMEM media. 800 µL of antibiotic free and serum free media was place into each of the plates containing the cells. Then 200 µL of the media containing liposome-DNA complex (lipoplex) was directly added into the cells using 1 mL pipette. The cells were immediately placed in a tissue culture incubator and grown for about 6 hrs. At the end of 6 hrs incubation the media were removed and cells were rinsed once with DMEM media. For fast recovery and growth of cells 1 mL of 2x media with 20 % FBS and 2%

L-glutamine and 0.2% Penicillin/streptomycin were added and the cells were incubated further for about 42 hrs. At the end the cells were washed with PBS and fixed with 4% paraformaldehyde, permeabilized by 0.2% Triton X-100 and stained with DAPI to visualize the nucleus. The slide covers containing cells were mounted on the slide and then visualized under fluorescent microscope for GFP expression using filter set for FITC (Fluorescein isothiocyanate).

APPENDIX A

^{1}H , ^{13}C NMR and IR SPECTRA OF SALEN LIGAND

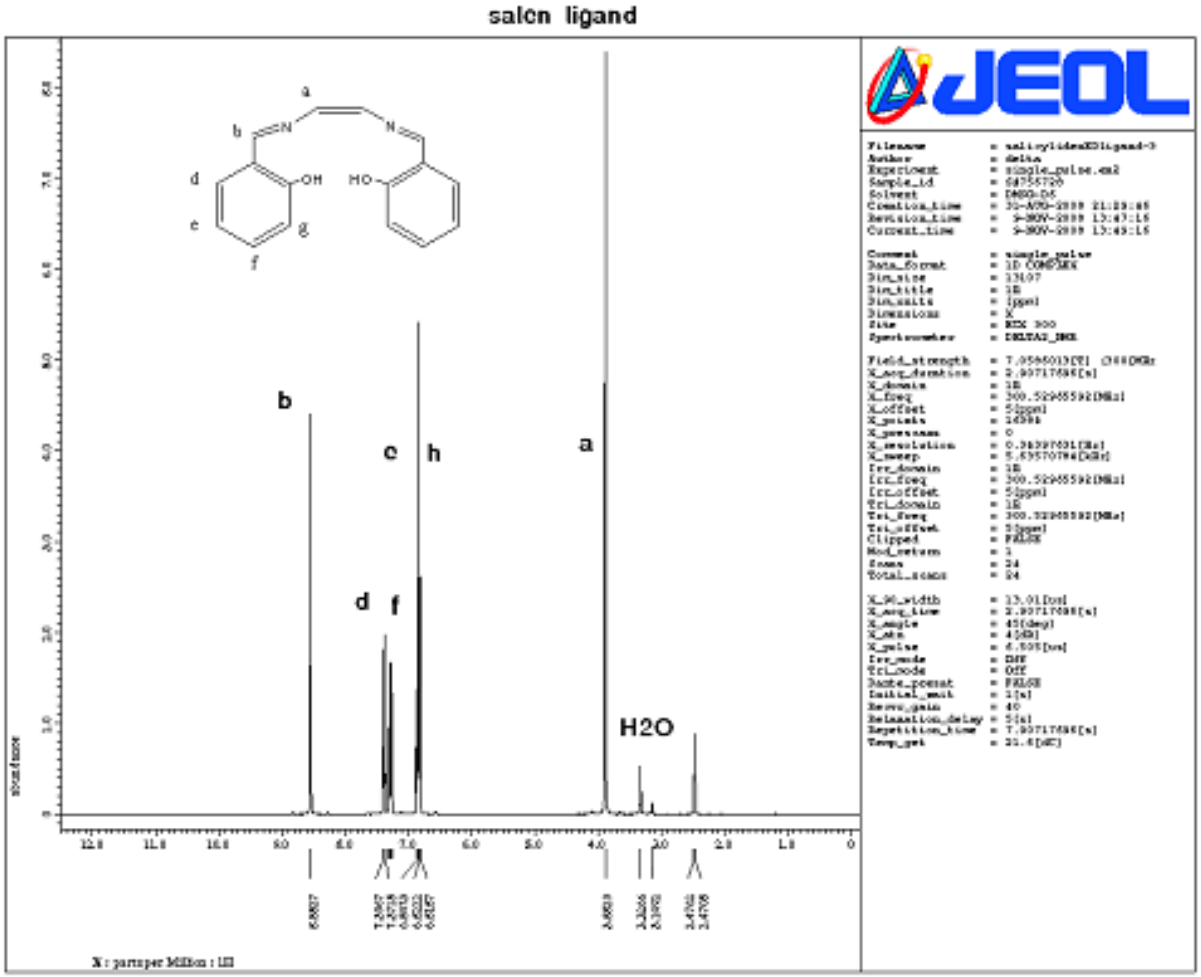

^{1}H NMR of Salcn ligand in DMSO-d6

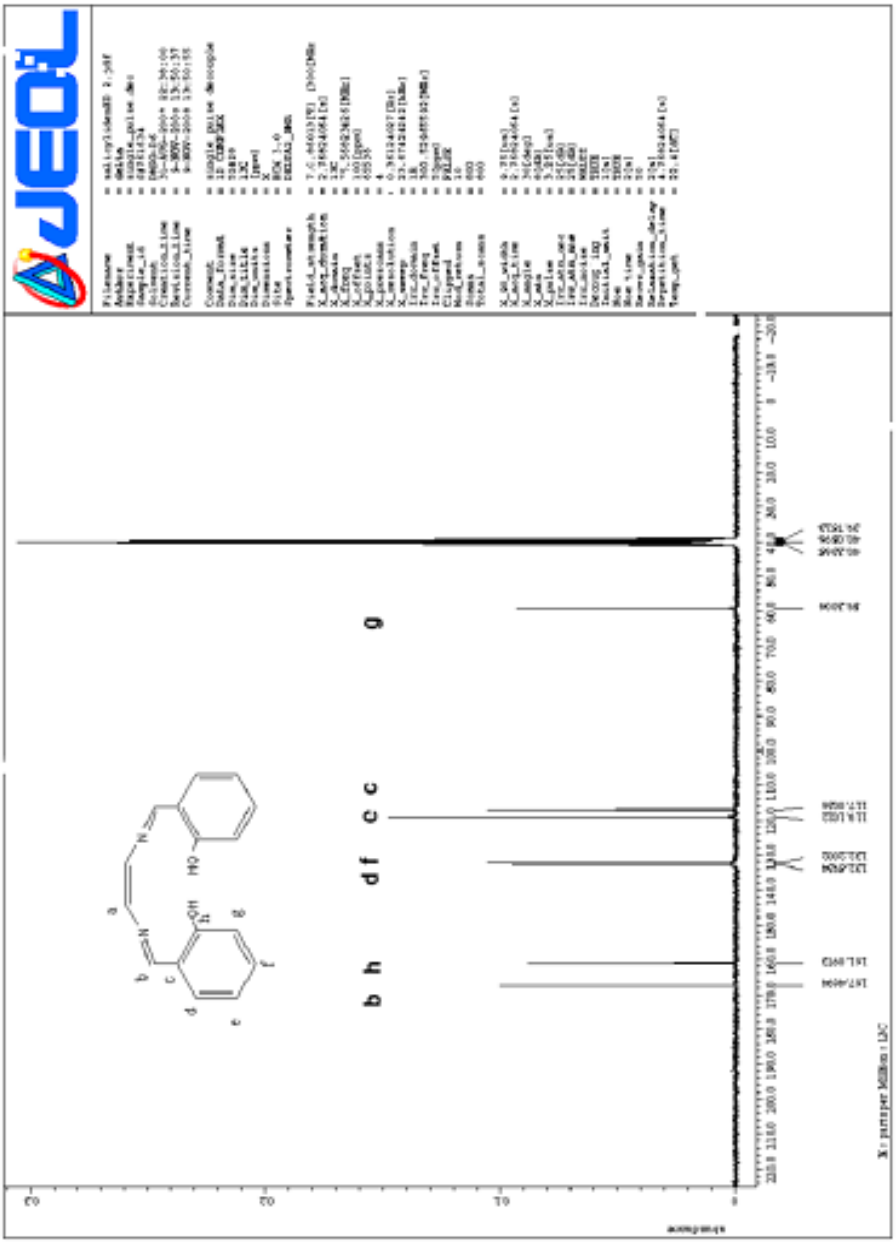

^{13}C NMR spectrum of salen ligand in DMSO-d6

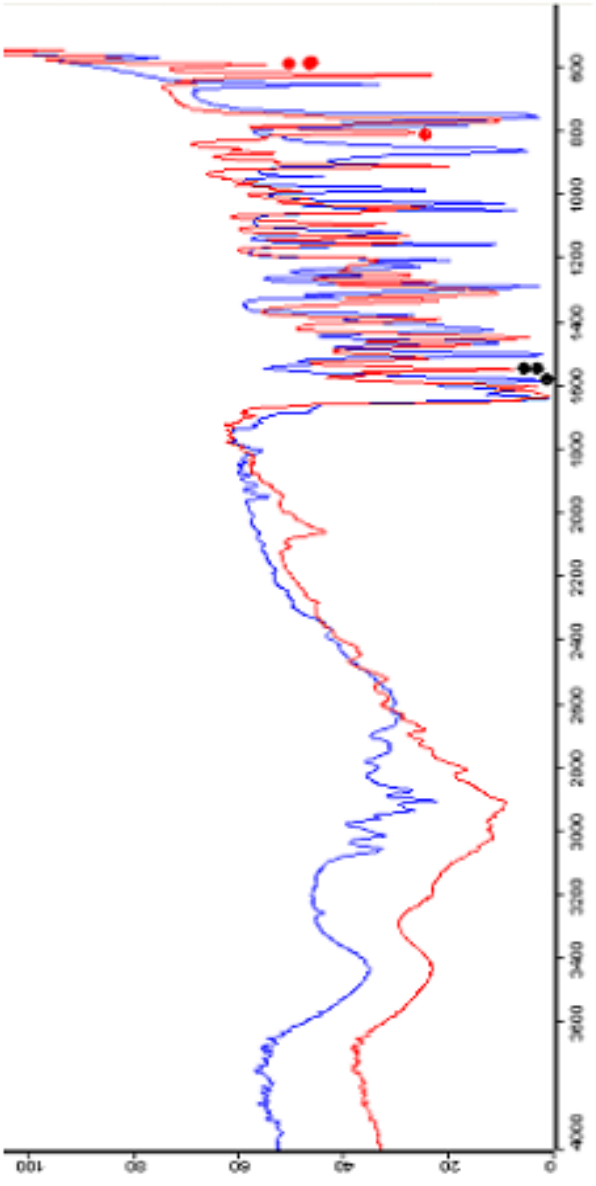

IR spectra of salen ligand (blue) and Fe(III)-salen overlay

APPENDIX B

^{1}H, ^{13}C NMR AND ESI-MS SPECTRA OF n=8 ALDEHYDE

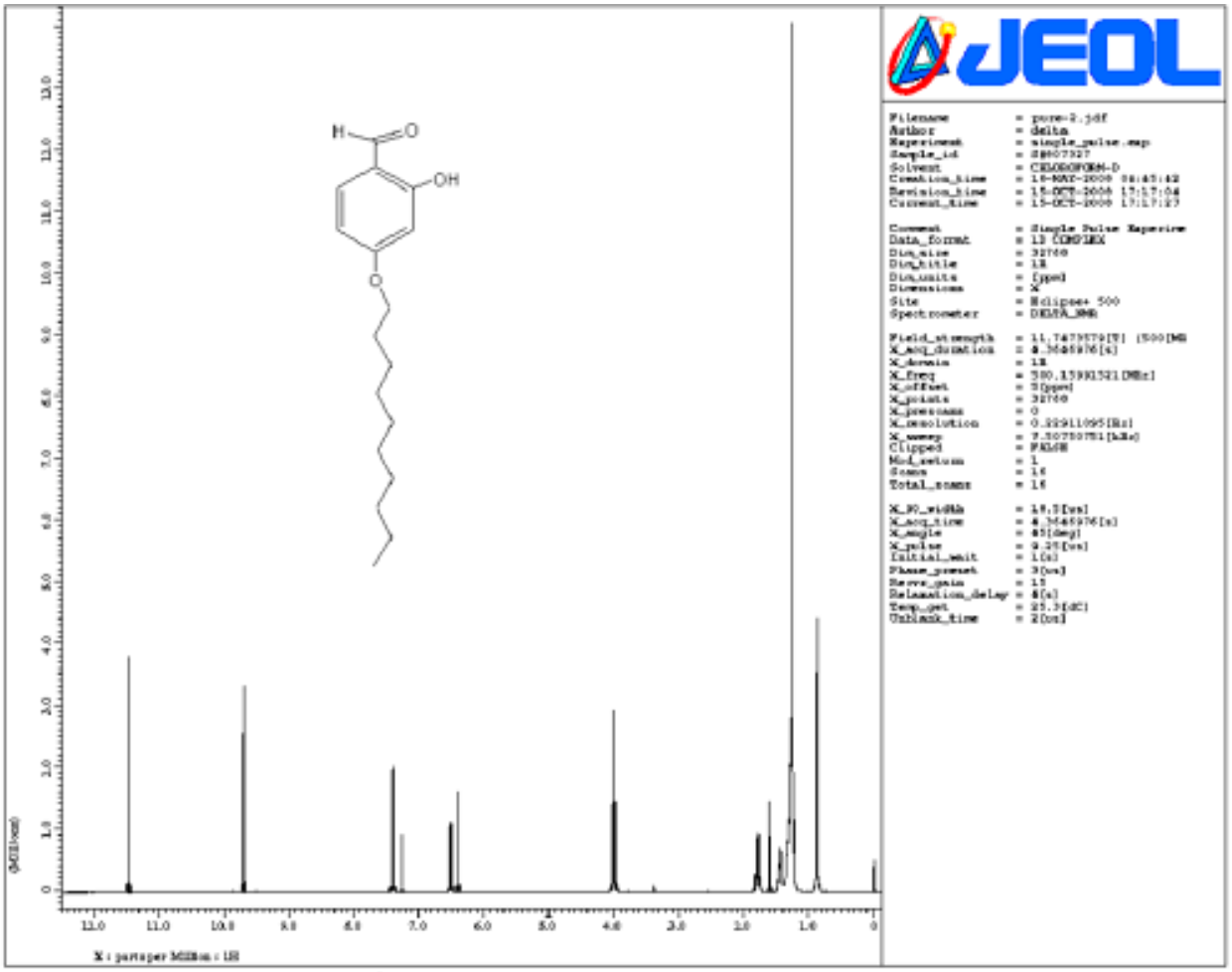

^{1}H NMR spectrum of n= 8 aldehyde in chloroform-D

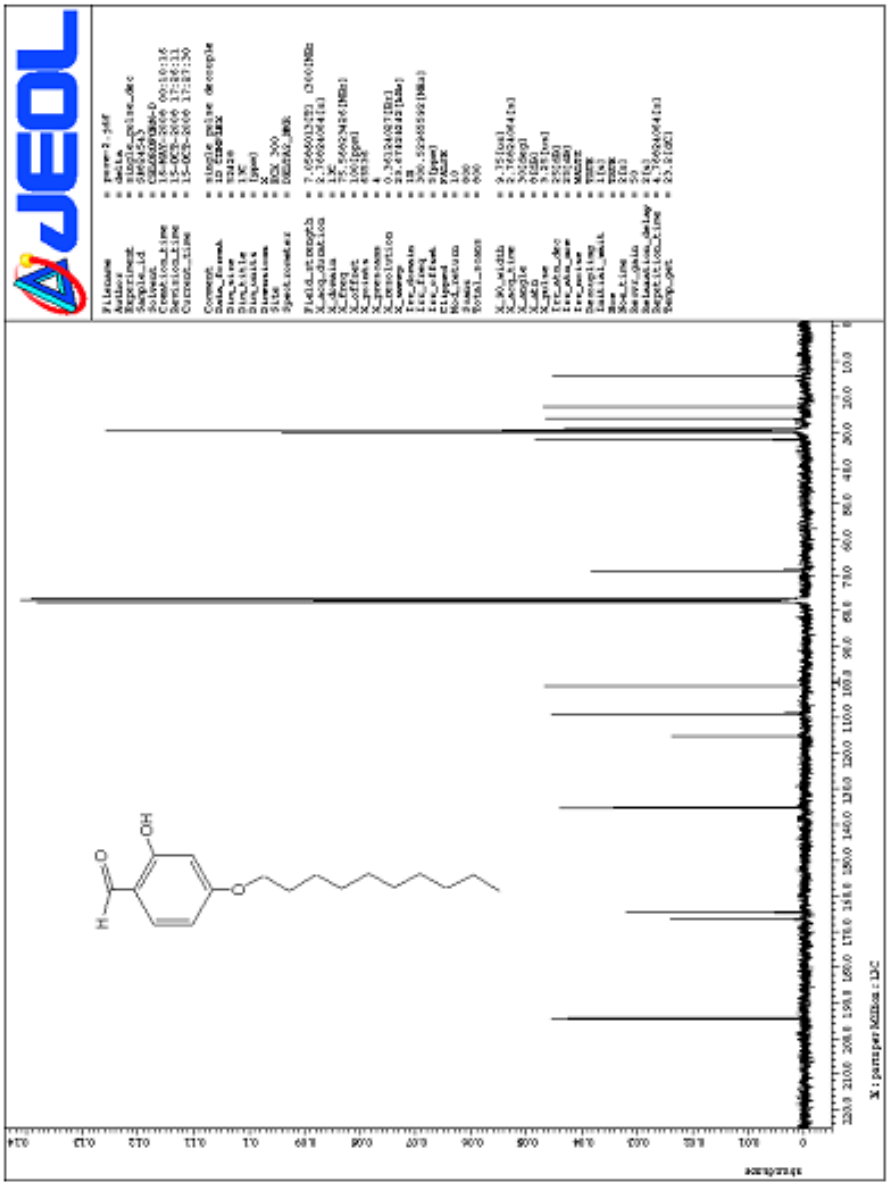

13C NMR spectrum of n=8 aldchydc in chloroform-D

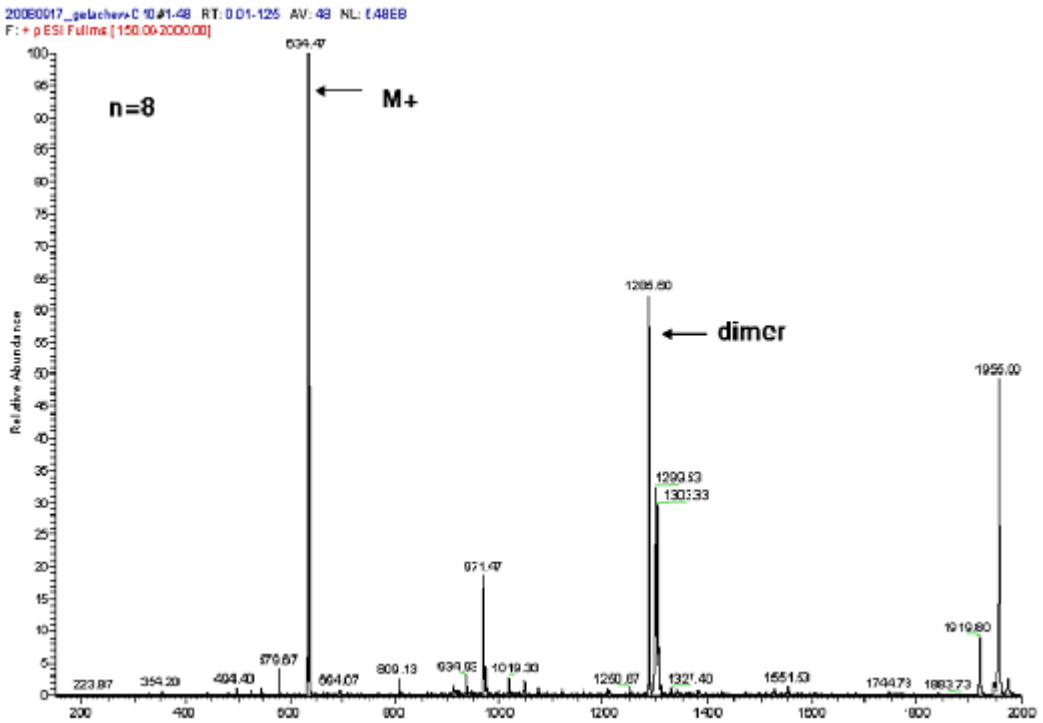

ESI-MS for n=8 aldehyde in methanol

APPENDIX C

^{1}H AND ^{13}C NMR SPECTRA OF n=8 ALDEHYDE

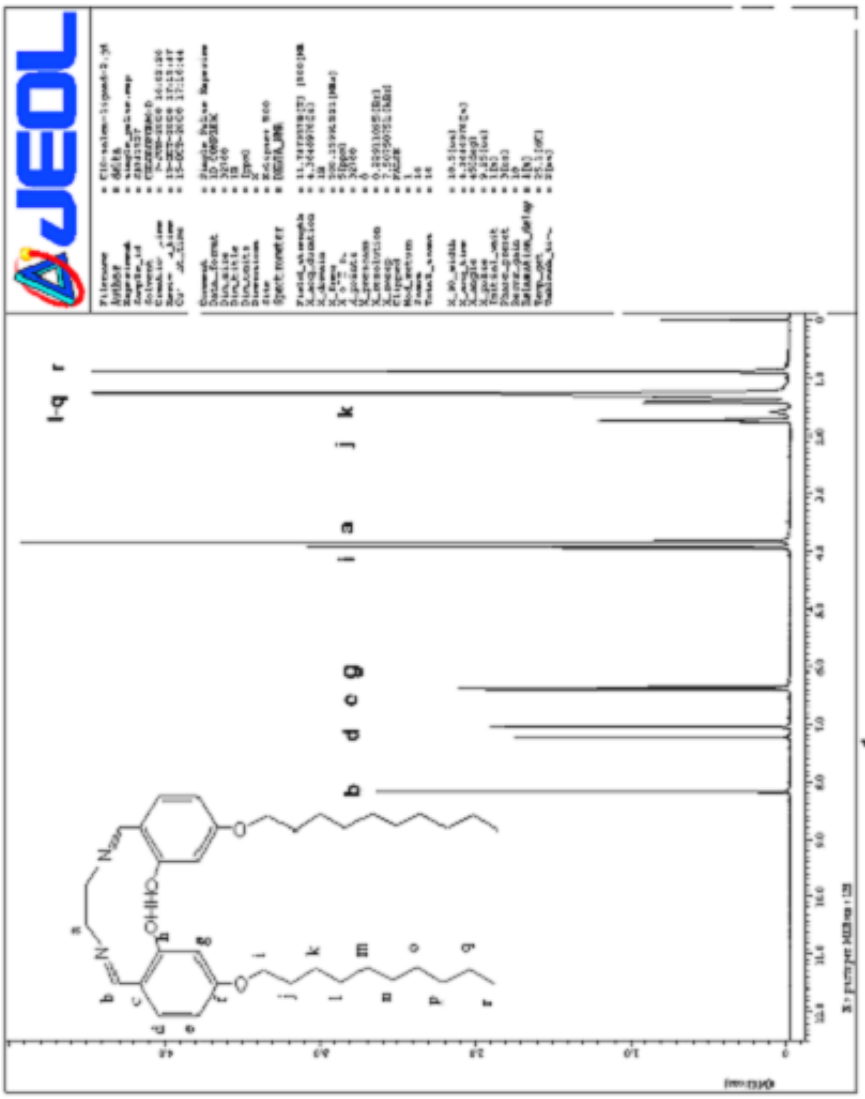

^{1}H-NMR of n=8 salen ligand in chloroform-D

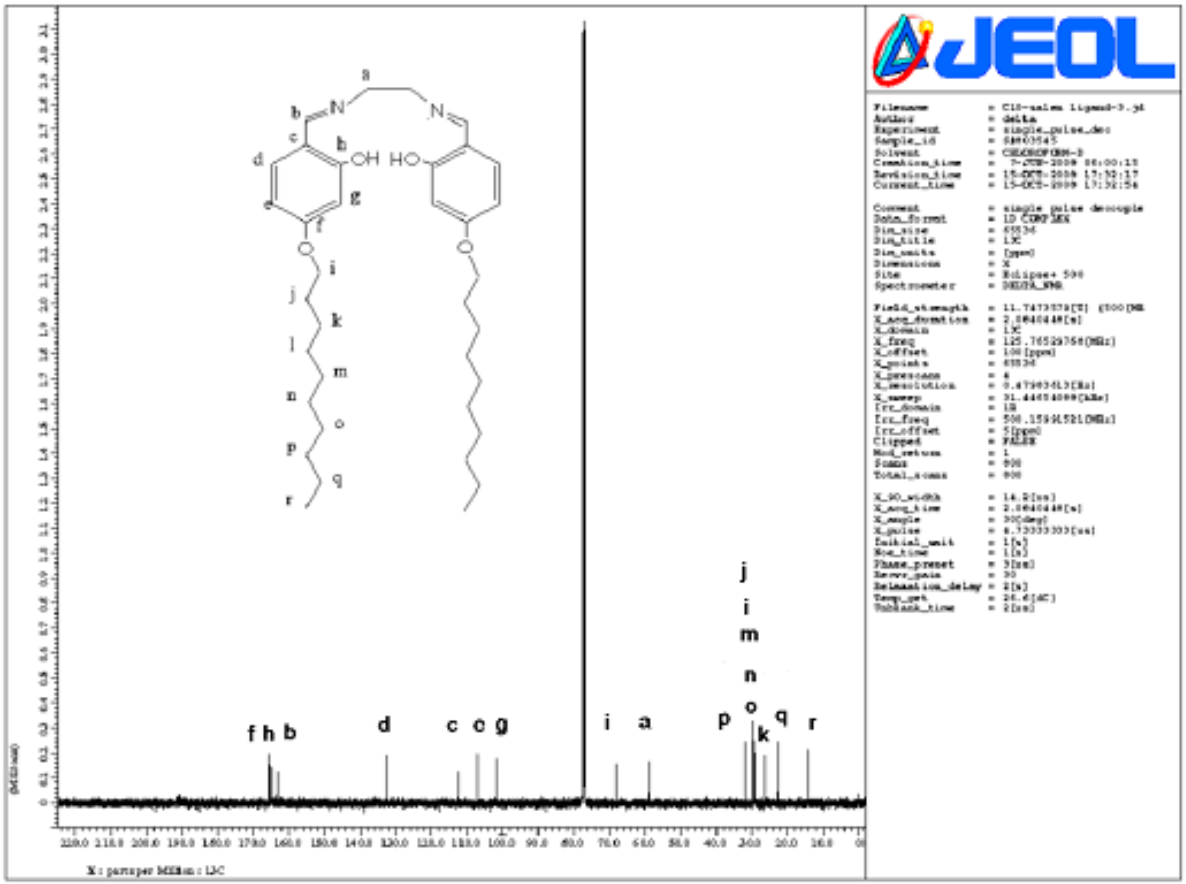

13C NMR sepectrum of n=8 salen ligand chloroform-D

APPENDIX D

MANUSCRIPT 1

Iron(III)-salen complexes with less DNA cleavage activities exhibit more efficient apoptosis in MCF7 cells

Khairul I. Ansari[1], James D. Grant[1], Getachew A. Woldemariam[1], Sahba Kasiri, and

Subhrangsu S. Mandal*,

Department of Chemistry and Biochemistry

The University of Texas at Arlington

Arlington, Texas 76019

[1]These authors contributed equally

*Corresponding author. E-mail: smandal@uta.edu; Fax: 817-272-3808

Abstract

To understand the relation between DNA damage potential with biochemical activities, we synthesized nine different Fe(III)-salen derivatives with varying substituents, analyzed their DNA cleavage properties *in vitro* and biochemical effects on cultured human cells. Our results demonstrated that Fe(III)-salen complexes affect cell viability, induce nuclear fragmentation, activates caspases and apoptosis in cultured human cells. The nature and the position of the substituents in the Fe(III)-salen complexes play critical role in determining their apoptotic efficiencies. Most importantly, our results demonstrated that the *in vitro* DNA cleavage activities of Fe(III)-salen complexes are not essential for their apoptotic activities in human cells. Instead, lesser the DNA cleavage activity more is their apoptotic efficiencies.

Introduction

Apoptosis is a process by which cells maintain a balance between proliferation and death and is often induced by external as well as internal stimuli.[1] Moelcules that interact with nucleic acids, damge DNA and induce apoptosis in human cells find potential applications in medicnal chemistry and antitumour therapy. Notably, most of the anti-tumour agents irrespective of their mechanism of action induce efficient apoptosis in cancer cells and many of them directly interact and/or damage DNA.[2-10] For example Cis-diamminodichloro-platinum(ll) (cisplatin) and cis-diammine (cyclobutane-l, l-dicarboxylato) platinum(ll) (carboplatin), the widely used transition metal based antitumour drugs, induce crosslinking in DNA.[2-8] Similarly, Fe(III)-bleomycin, another well known naturally occurring antitumour

antibiotic, produces free radicals that damage DNA.[11] As DNA interacting molecules find potential applications in novel anti-tumour therapy, intense research efforts are being invested towards developing novel DNA/RNA modifiers and in understanding their molecular mechansim of action.[2, 12, 13]

In general redox active agents that damage DNA *in vitro* are assumed to exhibit apoptotic activities in live cells by inducing oxidative stress and/or DNA damage.[7, 12, 14-17] Metallo-salens with diverse structure and redox characteristics are shown to produce reactive oxygen species under oxidative/reducing environments and damage of DNA/RNA *in vitro*.[18-27] For example iron and copper salen derivatives produce hydroxyl radicals in presence of dithiothreitol and damage DNA.[28, 29] Water soluble cobalt-salen derivatives activate natural oxgen and induce DNA cleavage.[26] Nickel salen derivatives induce crosslinking in DNA, RNA and proteins under oxidative enviroments.[29] Furthermore, various iron-salen derivatives and other metal-complexes have been implicated in efficient assymetric catalysis and in catalyzing hydrolytic cleavage of DNA and RNA.[30-34] Mn(III)-salens that damage DNA *in vitro* are shown to exhibit superoxide dismutase activities. Gust *et al.* showed that diaryl cobalt-salen derivatives posses novel anti-tumour activites.[35] Recently, we reported that Fe(III)-salen cleaves DNA *in vitro* and induces apoptosis in cultured human cells.[36]

Herein, to explore the relation between DNA cleavage activities of metallo-salens with their biochemical activities, we synthesized several Fe(III)-salen derivatives, investigated their DNA cleavage properties and biochemical effects on

cultured human cells (MCF-7). Our results demonstrated that Fe(III)-salen complexes induce efficient apoptosis in MCF7 cells and interestingly, the DNA cleavage potentials of the Fe(III)-salen complexes are not essential for their apoptotic activities.

Results and discussion

In order to understand the relation between DNA damage potential of the redox active molecules with their biochemical activities in human cells, we synthesized nine different Fe(III)-salen derivatives (compds. **1-9**) with different functionalities (hydroxy and methoxy) and diamino bridges (ethylene diamine, *o*-phenylene diamine and 2,3-diamino naphthalene) using a standard protocol (Fig.1).[28, 36] Each of the Fe(III)-salen complexes was characterized by mass spectrometry and elemental (CHN) analysis and the results are consistent with the proposed structures (Fig. 1).

Fe(III)-salen derivatives affect cell viability and induce nuclear fragmentation

Initially we examined the biochemical effects of Fe(III)-salen derivatives (compds. **1-9**) toward MCF7 cell (a human breast cancer cell line). We incubated cells with 20 μM of each of the Fe(III)-salen derivatives separately for 72 hrs and then visualized the cell morphology and viability under differential interference contrast (DIC) settings of a microscope (Fig. 2a). Interestingly, in comparison to the control untreated cells (control panel, Fig. 2a), upon treatment with either of the Fe(III)-salen, Fe(III)-salphen and Fe(III)-salnaphen complexes (compds. **1-3**), cell population decreased dramatically and the remaining cells got clumped, rounded,

and converted into debris indicating signs of cell death (panels 1, 2, and 3, Fig. 2a). Based on the cell morphologies and the population densities, Fe(III)-salphen and salnaphen appeared slightly more effecttive in inducing cell death (cytotoxic) than Fe(III)-salen (compare panels 1-3, Fig. 2a). The methoxy and hydroxy substituted salnaphen complexes showed different cytotoxicity towards MCF7 cells. In case of hydroxy substituted Fe(III)-salnaphen derivatives, only 3,3′-dihydroxy Fe(III)-salnaphen (**4**) was highly effective in inducing cell death whereas 4,4′- and 5,5′-dihydroxy Fe(III)-salnaphen complexes (**5** and **6**) did not show any significant effect on cell viability (panels 4-6, Fig. 2a). However, all three corresponding methoxy substituted Fe(III)-salnaphen derivatives (compds. **7-9**) showed effective cytotoxicity towards MCF7 cells (panels 7-9, Fig. 2a).

To understand the nature of cell death, we performed the nuclear staining of the Fe(III)-salen treated cells with a DNA binding dye DAPI (4',6-diamidino-2-phenylindole). Notably, upon DAPI stanining, cell nucleus appears blue under fluorescence microscope and this technique has been routinely used to visualize the nuclear morphologies.[8] Usually, more intense DAPI staining regions indicates more condensed DNAs (heterochromatin) while less intense DAPI stained regions indicates less condensed DNA (euchromatins).[8] Herein, to visualize the effects on nuclear morphologies, Fe(III)-salen complexes treated cells were stained with DAPI and visualized under fluorescence microscope. Upon DAPI staining, the nucleus of the control untreated cells was visible with distinct nuclear boundary and fairly uniform DNA distribution patterns (control panel, Fig. 2b). However, upon

treatment with the biochemically active Fe(III)-salen complexes (compds. **1-4, 7, 8** and **9**), the DAPI staining patterns of the cell nucleus got affected significantly (Fig. 2b). In most cases, the nucleus lost their well defined boundaries. DNA got heavily condensed (intense DAPI stained regions), and fragmented (intense DAPI stained speckles of nuclear fragments). Furthermore, some of the cell nuclei showed some ring like DAPI stained structures around the nuclear boundaries (eg. in panels 1, 2, 4, and 9, Fig. 2b). Inactive compounds (**5** and **6**) showed no significant effect on the cell nucleus. Notably, the nuclear condensation and fragmentation as well as the ring like DAPI staining patterns are hallmarks of apoptosis indicating that Fe(III)-salen complexes induced apoptosis in MCF7 cells. The apoptotic activities of the Fe(III)-salen complexes were further confirmed by TUNEL (terminal dUTP nicked end labeling) assay (Fig. S1).

Cytotoxicities of Fe(III)-salen derivatives (IC_{50} values)

To quantify the relative cytotoxicity we incubated MCF7 cells with varying concentrations of each of the Fe(III)-salen complexes for 96 hrs and subjected to MTT assay as described previously.[36-38] The percent of viable cells relative to control were plotted against concentration of the Fe(III)-salen complexes to obtain IC_{50} values. IC_{50} values of the biochemically active compounds lie in the range of 0.2 to 22.5 μM (Table 1, Fig. 3 and Fig S2). The IC_{50} values for parent Fe(III)-salen (**1**), Fe(III)-salphen (**2**) and Fe(III)-salnaphen (**3**) are 22, 1.3 and 0.5 μM respectively which suggest that the increase in aromatic functionality in the diimmino bridge (from ethylene diamine to more aromatic ortho-phenylenediamine and 2,3-

diaminonaphthalene) in the Fe(III)-salen complexes significantly increased their cytotoxicity. Notably, increase in aromatic functionalities increases lipophilicity of the molcules as well as may affect their interactions with DNA. In case of Fe(III)-salen complexes, both lipophilicity as well DNA interaction factors may be contributing to the enhanced cytotoxicities of the more aromatic complexes.[26-28, 35, 39-42] In addition, 3,3′-dihydroxy and 4,4′-dimethoxy-Fe(III)-salnaphens (**4** and **8**) also have nanomolar IC_{50}s indicating that these Fe(III)-salen complexes are highly effective in inducing cell death in MCF7 cells (Table 1). Cytotoxicity curves (with extended concentration range, 0 - 60 μM) for the Fe(III)-salen (compd **1**) and the biochemically inactive compds (**5** and **6**) are shown in the supplementary Fig S2. Taken together these studies demonstrated that the nature and the position of the substituents and the nature of diimino bridge in the Fe(III)-salen complexes plays critical roles in determining their cytotoxicity levels (IC_{50} values).

Fe(III)-salen complexes activate caspases-3/7

To confirm the apoptotic activities of Fe(III)-salen derivatives, we analyzed the activation of caspases-3/7 by using a commercially available kit. Notably, to assess the caspase 3/7 activity we used Jar cells (a placental cell line) instead of MCF-7 as MCF-7 cells lack the caspase-3 enzyme.[43] We treated cells with 100 μM Fe (III)-salens (compds. **1-9)** for 0, 8, 16 and 24 hrs and then caspase-3/7 activities were analysed using a commercial caspase-3/7 assay kit. The caspase activities of the biochemically active Fe(III)-salen increased with time with a maxima at 16 hrs and then declined at

higher time points likely due to cell death (data not shown). The relative caspase-3/7 activities (at 16 hr time point) of different Fe(III)-salen complexes were plotted in Fig 4. For a reasonable comparison of caspase-3/7 activation with cytotoxicity, we measured the IC_{50} values for different Fe(III)-salen complexes in JAR cells (Table 1). Although, there is difference in the IC_{50} values for the two different cells lines (MCF7 vs JAR, which is expected due to difference in cell types), caspase activities induced by different biochemically active Fe(III)-salen complexes in JAR cells correlated fairly well with their level of IC_{50} values in JAR cells (Table 1 and Fig. 4). More active (lower IC_{50}) compounds showed higher level of caspase-3/7 activation. For example, Fe(III)-salen, salphen and salnaphen complexes (compds. **1-3**) increased caspases-3/7 activities by 1.7, 9 and 14 fold compared to control untreated cells (JAR cells) and the IC_{50} values (JAR cells) for compds. **1-3** are 22, 0.6 and 0.3 μM respectively. (Fig. 4 and Table 1). Similarly, among the hydroxysalnaphen derivatives, the biochemically active 3, 3′-dihydroxysalnaphen (compd. **4**) induced 18 fold increase (IC_{50}: 0.25 μM in JAR cells) in caspase activity, whereas the inactive compounds (**5** and **6)** induced no significant caspase activity (Fig. 4 and Table 1). The biochemically active methoxysalnaphen derivatives induced caspases-3/7 activities by 5 to 15 fold in comparison to untreated control cells (Fig. 4). These results demonstrated that Fe(III)-salen derivatives that affects cell viability, induce caspase 3/7 activation leading to apoptosis in JAR cells.

Fe(III)-salen complexes with more efficient apoptosis activities induce less DNA cleavage

To correlate the DNA cleavage activities of Fe(III)-salen derivatives with their

apoptotic activities, we performed DNA cleavage assays by incubating different Fe(III)-salen complexes with supercoiled plasmid DNA (pML20-47) with or without a reducing agent dithiothreitol (DTT). In agreement with our previous studies[36, 37], Fe(III)-salen (**1**) induced efficient DNA cleavage in presence of DTT as evidenced by the conversion of supercoiled into nicked circular form of DNA (lanes 3-4, Fig. 5a). Notably Fe(III)-salen itself have some DNA cleavage activity even in the absence of DTT (lane 5, Fig. 5a). The unmodified Fe(III)-salphen (**2**) and salnaphen (**3**) also cleaved DNA in presence of DTT. However, the cleavage efficiency decreased as the aromatic bridge increased from Fe(III)-salen to salphen to salnaphen (Fig. 5a). These results are in contrast to their apoptotic efficiencies where Fe(III)-salnaphen was the most active ($IC_{50:}$ 0.54 μM) and Fe(III)-salen was the least active ($IC_{50:}$ 22.5 μM).

We also performed similar DNA cleavage experiments for different hydroxy and methoxy salnaphen derivatives and the amount of DNA cleaved were quantified and plotted in Fig. 4b. Interestingly, all the hydroxy-Fe(III)-salnaphen derivatives (**4-6**) showed efficient DNA cleavage activity (up to 85 % DNA cleavage) (Fig. 5b). The DNA cleavage abilities of all the hydroxy derivatives were higher than the unmodified Fe(III)-salnaphen (Fig. 5b). These observations are again in contrast to their apoptotic activities (Fig. 5b and 2). The 3,3′-dihydroxy Fe(III)-salnaphen (**4**) which has the least DNA cleavage activity induced most efficient apoptosis. The remaining two hydroxy derivatives (**5-6**) that cleaved DNA efficiently induced no apoptosis in MCF7 cells. Similarly, all three methoxy Fe(III)-salnaphens (**7-9**) that

showed no significant DNA cleavage activities induced efficient apoptosis in MCF7 cells (Fig. 5b and 2).

Conclusion

Understanding the correlation between the DNA damagae potential of small molecules with their biochemical and apoptotic activities is important for designing novel anti-tumour agents. Herein, we synthesized several Fe(III)-salen complexes (compds. **1-9**) with varying substituents and bridging spacers, analyzed their DNA cleavage properties *in vitro* and apoptotic activities in cultures human cells. Cytotoxicity studies demonstrated that unmodified Fe(III)-salen, Fe(III)-salphen and Fe(III)-salnaphen complexes affect cell viability, activate caspases-3/7 and induce nuclear condensation/fragmentation leading to cell death. The activation of caspases-3/7, nculear condensation and fragemntation indicated that Fe(III)-salen complexes induce apoptotic cell death in cultured human cells. Notably the level of caspase activation induced by different Fe(III)-salen complexes (compds **1-9**) were significantly correlated with their cytotoxicity values (IC_{50} values) in JAR cells. These results further support that Fe(III)-salen complexes induce apoptosis in cultured human cells via caspase activation and mitochoindrial pathway.

The comparison of the IC_{50} values for the unmodified Fe(III)-salen, salphen and salnaphen complexes ($IC_{50s:}$ 22, 1.3 and 0.5 μM for compds. **1, 2** and **3** respectively towards MCF7 cells), indicated that the increase in aromatic functionality in the diimino bridges of Fe(III)-salen complexes increases their

cytotoxicities. Analysis of cytotxicities of the hydroxy and methoxy substitueted Fe(III)-salnaphen complexes (compds. **4**-**9**) demonstrated that the position and the nature of substituents play critical role in determining their cytotoxic efficiencies. For example, 3,3′-dihydroxy substitueted Fe(III)-salnaphen (**4**) was highly effective in inducing cell death (IC_{50}.0.2 μM), whereas 4,4′- and 5,5′-dihydroxy Fe(III)-salnaphen complexes (**5** and **6**) were almost inactive toward MCF-7 cells. However, all three corresponding methoxy substituted Fe(III)-salnaphen derivatives (compds. **7-9**) showed effective cytotoxicity towards MCF7 cells ($IC_{50s:}$ 1.5, 0.5 and 1.3 μM respectively). Notably, recent studies indicated that, in comparison to the hydroxy substitued derivatives, methoxy substitueted cobalt-salen complexes are preferentially taken up by cells leading to higher impact on cell growth. [35]This is likely because the methoxy compounds are more hydrophoic compared to their hydroxy compounds that may facilitate cellular permeabilities and uptake efficiencies.[35] Similar mechansim of action may be reflected in the cytotoxic behaviours of our methoxy-substitueted Fe(III)-salnaphen complexes (compds. **7-9**).

The comparison of the *in vitro* DNA cleavage activities of different Fe(III)-salen complexes (compds. **1-9**) with their cytotoxicities were most intriguing. For example, DNA cleavage efficiencies were decreased from Fe(III)-salen to Fe(III)-salphen and Fe(III)-salnaphen complexes (compds. **1**-**3**), while their cytotxicities toward MCF-7 cells were increased in a reciprocal manner (IC_{50} values decreased). The similar results were overserved for various hydroxy and methoxy substitueted

Fe(III)-salenaphen complexes (compds. **4-9**). The lower the DNA cleavage potential of Fe(III)-salen complexes, higher is their cytotoxicities (lower IC_{50} values). These results indicate that the *in vitr*o DNA cleavage activities are not essential for the apoptotic efficiencies of Fe(III)-salen complexes in cultured human cells. Instead, less DNA cleavage active Fe(III)-salen complexes induced more efficient apoptosis.

Although, further studies are needed to address the detail mechansim of differential cytotoxicities, our studies demonstrated that Fe(III)-salen complexes induce apoptosis in cutured human cells with IC_{50}s in the nanomolar to micromolar ranges and the cytottoxic activities does not necessarily depend on their *in vitro* DNA cleavage abilities.

Experimental

General

All reagents for organic synthesis and buffers were purchased from Sigma-Aldrich unless otherwise noted. Tissue culture medium DMEM (Dulbecco's Modified Eagle's Medium), FBS (Fetal Bovine Serum), penicillin and streptomycin were purchased from Sigma-Aldrich. Ferric chloride (anhydrous) was purchased from Spectrum Chemical Manufacturing Corporation. DAPI (4′, 6-diamidino-2-phenylindole) was obtained from Chemicon. MTT (3-(4, 5-dimethylthiazolyl-2)-2, 5-diphenyltetrazolium bromide) was obtained from Tokyo Chemical Industry Co. MCF-7 cell line was purchased from ATCC (American Type Culture Collection). NMR spectra were recorded on JEOL Eclipse 500 (^{1}H, 500 MHz) spectrometer. FT-IR spectra were

recorded by using a Bruker Vector 22 infrared spectrometer. Elemental analyses were performed using a Perkin Elmer Model 2400 CHN analyzer. Mass spectra was taken by using ESI-MS method (positive mode, quadrupole ion trap-MS, MSLCQ Deca XP instrument from Thermo-Fisher Scientific).

Synthesis of Fe(III)-salen and their derivatives (compds. 1-9)

Fe(III)-salen derivatives were synthesized and characterized following a general procedure as described previously.[28,36] In brief, ligands were synthesized by mixing the corresponding salicylaldehyde derivative and diamine in methanol that resulted in dark colored (yellow, orange or red) precipitate of the ligands (yield 80 – 90 %). The respective ligand was mixed with one equivalent of anhydrous ferric chloride in methanol, warmed at 60 °C for 20 min and then cooled down to room temperature. In most cases the metal-complexes were precipitated out upon cooling the reaction mixtures. In some cases the metal complexes were precipitated by adding diethyl ether into the cold reaction mixtures. The products were isolated, recrystallized from methanol and characterized by mass spectral analysis using ESI-MS.

[Fe(III)-salen] chloride (compd. 1): The synthesis of this compound was reported by our lab previously.[36]

Fe(III)-salphen chloride (compd. 2): Two equivalents of salicylaldehyde (2.2 g, 18.1 mmol) was mixed with one equivalent of o-phenylenediamine (920 mg, 8.4 mmol) in methanol that resulted in light orange precipitate of salphen ligand. This ligand (500 mg, 1.6 mmol) was complexed with one equivalent of Fe(III) chloride (295 mg, 1.8 mmol) to obtain compd. **2** (65 % yield). FT-IR (KBr, cm^{-1}): 1600, 1590, 1530, 1450,

1430, 1380, 1320, 1200, 1140, 1110, 910, 880, 850, 800, 730, 600, 530. Observed M/Z value for compd. **2**: 370.18 (M^+, -Cl). CHN analysis: Cacld. (for $C_{20}H_{14}N_2O_2FeCl$. 2.5 H_2O) C: 53.37 %, H 4.26 %, N 6.22 %; Observed: C: 53.32 %, H 3.88 %, N 6.00 %.

Fe(III)-salnaphen chloride (compd. 3): Two equivalents of salicylaldehyde (2.1 g, 17.2 mmol) was mixed with one equivalent of 2,3-diaminonaphthalene (1.3 g, 8.2 mmol) in methanol that resulted in dark yellowish orange precipitate of Salnaphen. This ligand (450 mg, 1.23 mmol) was complexed with one equivalent of Fe(III) chloride (226 mg, 1.4 mmol) to obtain **3** (60 % yield). FT-IR (KBr, cm^{-1}): 1590, 1570, 1540, 1460, 1430, 1385, 1320, 1300, 1200, 1110, 1100, 900, 890, 810, 760, 620, 600. Observed M/Z value for compd **3**: 420.24 (M^+, -Cl); CHN analysis for Salnaphen Fe(III) chloride (**3**) Cacld. (for $C_{24}H_{16}N_2O_2FeCl$. 1.5 H_2O) C: 59.80 %, H 3.97 %, N 5.81 %; Observed: C: 60.05 %, H 3.96 %, N 5.78 %.

3, 3′-Dihydroxysalnaphen Fe(III) chloride (4): Two equivalents of 2, 3-dihydroxybenzaldehyde (2.1 g, 15.2 mmol) was mixed with one equivalent of 2,3-diaminonaphthalene (1.1 g, 6.9 mmol) in methanol that resulted in red precipitate of 3, 3′-dihydroxysalen. This ligand (300 mg, 0.75 mmol) was complexed with one equivalent of Fe(III) chloride (138 mg, 0.85 mmol) to obtain compd. **4** (45 % yield). FT-IR (KBr, cm^{-1}) 3400, 1590, 1500, 1430, 1390, 1300, 1280, 1250, 1129, 890, 802, 760, 500, 590, 530. Observed M/Z value for compd. **4**: 452.27 (M^+, -Cl). CHN analysis

for **4**: Cacld. (for $C_{24}H_{16}N_2O_4FeCl.\ 2\ H_2O$) C: 55.04 %, H 3.85 %, N 5.35 %; Observed: C: 55.42 %, H 3.59 %, N 5.36 %.

4, 4′-Dihydroxysalnaphen Fe(III) chloride (compd. 5): Two equivalents of 2, 4-dihydroxybenzaldehyde (1.8 g, 13 mmol) was mixed with one equivalent of 2,3-diaminonaphthalene (1 g, 6.3 mmol) in methanol that resulted in dark orange brown precipitate of 4, 4′-dihydroxysalen. This ligand (450 mg, 1.3 mmol) was complexed with one equivalent of Fe(III)chloride (243 mg, 1.5 mmol) to obtain compd. **5** (48 % yield). FT-IR (KBr, cm^{-1}) 3395, 1577, 1538, 1435, 1369, 1251, 1213, 1174, 1129, 985, 850, 802, 760, 646, 602, 570. Observed M/Z value for **compd. 5**): 452.27 (M^+, -Cl). CHN analysis for **5**: Cacld. (for $C_{24}H_{16}N_2O_4FeCl.\ 4\ H_2O$) C: 51.50 %, H 4.32 %, N 5.00 %; Observed: C: 51.10 %, H 4.04 %, N 4.96 %.

5, 5′-Dihydroxysalnaphen Fe(III) chloride (compd. 6): Two equivalents of 2, 5-dihydroxybenzaldehyde (2 g, 14.5 mmol) was mixed with one equivalent of 2,3-diaminonaphthalene (1.1 g, 6.9 mmol) in methanol that resulted in dark red precipitate of 5, 5′-dihydroxysalen. This ligand (450 mg, 1.36 mmol) was complexed with one equivalent of Fe(III) chloride (235 mg, 1.4 mmol) to obtain compd. **6** (52 % yield). FT-IR (KBr, cm^{-1}) 3402, 1597, 1537, 1458, 1435, 1385, 1304, 1278, 1223, 1162, 1095, 874, 829, 750, 726, 554. Observed M/Z value for **compd. 6**: 452.27 (M^+, -Cl). CHN analysis for **6**: Cacld. (for $C_{24}H_{16}N_2O_4FeCl.\ 3.5\ H_2O$) C: 52.35 %, H 4.21 %, N 5.09 %; Observed: C: 52.70 %, H 4.07 %, N 5.01 %.

3, 3′-Dimethoxysalnaphen Fe(III) chloride (compd. 7): Two equivalents of 2-hydroxy-3-methoxybenzaldehyde (2.7 g, 17.5 mmol) was mixed with one equivalent of 2,3-diaminonaphthalene (1.2 g, 7.6 mmol) in methanol that resulted in bright orange precipitate of 3, 3′-dimethoxysalen ligand. This ligand (410 mg, 0.96 mmol) was complexed with one equivalent of Fe(III) (186 mg, 1.15 mmol) chloride to obtain compd. **7** (65 % yield). FT-IR (KBr, cm^{-1}): 1707, 1597, 1580, 1545, 1356, 1338, 1248, 1206, 982, 861, 779, 734, 604. Observed M/Z value for compd. **7**: 480.18 (M^+, -Cl). CHN analysis (**compd. 7**) Cacld. (for $C_{26}H_{20}N_2O_4FeCl$. 3.8 H_2O) C: 53.45 %, H 4.76 %, N 4.80 %; Observed: C: 53.27 %, H 3.95 %, N 4.93 %.

4, 4′-Dimethoxysalnaphen Fe(III) chloride (compd. 8): Two equivalents of 2-hydroxy-4-methoxybenzaldehyde (2.1 g, 13.8 mmol) was mixed with one equivalent of 2,3-diaminonaphthalene (1 g, 6.3 mmol) in methanol that resulted in orange colored precipitate of 4, 4′-dimethoxysalen ligand. This ligand (450 mg, 1.1 mmol) was complexed with one equivalent of Fe(III) chloride (194 mg, 1.2 mmol) to obtain compd. **8** (58 % yield). FT-IR (KBr, cm^{-1}): 1607, 1573, 1522, 1457, 1438, 1416, 1373, 1306, 1256, 1219, 1171, 1127, 1023, 976, 834, 751,648. Observed M/Z value for **compd 8**: 480.25 (M^+, -Cl). CHN analysis for **8**: Cacld. (for $C_{26}H_{20}N_2O_4FeCl$. 1.0 H_2O) C: 58.51 %, H 4.15 %, N 5.25 %; Observed: C: 58.43 %, H 3.80 %, N 5.27 %.

5, 5′-Dimethoxysalnaphen Fe(III) chloride (compd. 9): Two equivalents of 2-hydroxy-5-methoxybenzaldehyde (2.89 g, 19 mmol) was mixed with one equivalent of 2,3-diaminonaphthalene (1.5 g, 9.5 mmol) in methanol that resulted in dark reddish brown precipitate of 5, 5′-dimethoxysalen. This ligand (400 mg, 0.94 mmol) was complexed with one equivalent of Fe(III) chloride (192 mg, 1.2 mmol) to obtain compd. **9** (59 % yield). FT-IR (KBr, cm^{-1}): 1621, 1580, 1536, 1461, 1365, 1295, 1264, 1224, 1167, 1036, 823, 744, 718. Observed M/Z value for **compd 9**: 480.18 (M^+, -Cl). CHN analysis for **9**: Cacld. (for $C_{26}H_{20}N_2O_4FeCl$) C: 60.55 %, H 3.91 %, N 5.43 %; Observed: C: 60.07 %, H 3.73 %, N 5.44 %.

Cell culture

Monolayer of human breast cancer cells (MCF-7) were grown and maintained in Dulbecco's modified Eagle's media (DMEM) that was supplemented with heat inactivated fetal bovine serum (FBS, 10%), L-glutamine (1%) and Penicillin/streptomycin (0.1%).[8, 36, 44] Cells were cultured and maintained in humidified incubator with 5 % CO_2 in air at 37 °C. Cells were grown on cover slips for microscopy experiments and in 96 well micro titer plates for cell viability and cytotoxicity assays.

Cell viability assay and DAPI staining

MCF-7 cells were seeded onto a cover slip in a 60 mm plate and grown overnight under normal growth conditions followed by incubation with 20 µM Fe(III)-salen or its derivatives for additional 72 hrs. Control cells were treated with equivalent amount of DMSO. Cells were fixed with 4% -formaldehyde in PBS for 15 minutes, washed twice

with PBS, permeabilized with 0.2% Triton X-100 in PBS for 5 min. Cells were washed three times with cold PBS followed by incubation with DAPI (5 µg per slide) for 10 minutes at room temperature. DAPI stained cells were washed three times with cold PBS, mounted on microscope slide with mounting media (Vectashield H-1000, Vector lab) and visualized under fluorescence microscope.[8]

Cytotoxicity assay (IC_{50} measurement)

The cytotoxicity of Fe(III)-salen and its derivatives was determined by using MTT assay as described previously.[37, 38] In brief, approximately 10,000 MCF-7 (or JAR cells) cells were seeded into each well of a 96 well micro titer plate and incubated 24 hrs in presence of 150 µL DMEM. An additional 50 µL DMEM containing required amount of each Fe(III)-salen to obtain 0.05 to 60 µM final concentration (in 200 µL final volume) in 8 replicate wells were added. Control wells were treated with equivalent amount of DMSO. After 96 hrs of incubation, 20 µL of MTT (5 mg/mL) was added into each well and cell viability was assayed by measuring the formazan absorption at 560 nm as described above. The absorbance (at 560 nm) values were plotted against concentration of Fe(III)-salen complexes to determine the IC_{50}. The experiments were repeated twice with 8 replicates each time.

Caspase-3/7 activity assay

Caspase-3/7 activity was assessed using SensoLyte TM Homogenous AMC Caspase-3/7 Assay Kit (AnaSpec Inc). Briefly, cells were treated with 100 µM Fe (III)-salens for 0, 8, 16, and 24 hrs, lysed, and centrifuged (2500 g for 10 min at 4 °C). The supernatant

was diluted (to 1 μg/μL of protein) and 150 μL extract was mixed with 50 μL of assay buffer containing caspase-3/7 substrate, incubated for 15 min at 37 °C and then fluorescence intensity ($350_{EX}/440_{EM}$) was measured every 10 min (up to 2 hrs) using FLOUstar Omega micro plate reader (BMG labTech). The concentration of activated caspase-3/7 was calculated by using calibration curve with pure standard. The caspase-3/7 activity was finally expressed relative to untreated control cells.

DNA cleavage assay

DNA cleavage reactions were performed by incubating supercoiled plasmid DNA (pML20-47, 0.5 μg) with varying concentration of Fe(III)-salen derivatives in the presence and absence of 1 mM dithiothreitol (DTT) for 1 hr at 37 ^{o}C in 20 mM Tris-HCl (pH 7.4) as described previously.[36] The products were analyzed by agarose gel electrophoresis. The gel was stained with ethidium bromide and visualized by using Alpha Imager-2200 (Alpha Innotech corporation) instrument, and quantified by using Image Quant software.

Acknowledgements

We thank Saoni Mandal and other lab members for critical discussions. This work was supported by grants from Texas Advanced Research Program (00365-0009-2006) and American Heart Association (SM 0765160Y).

Figure Legend

Fig. 1 Structures of Fe(III)-salen complexes (compds. **1-9)**

Fig. 2 Effect on cell viability**:** MCF7 cells were treated with 20 μM of the Fe(III)-salen complexes (in DMSO) for 72 hrs. (a) DIC (differential interference contrast) images of the cells under microscope. (b) Cells stained with DAPI and visualized under fluoresce microscope (Nikon TE200). Controls: cells treated with DMSO; panels 1- 9: cells treated with compds **1-9** respectively.

Fig. 3 Cytotoxicity (IC_{50}) measurements. Approximately 10,000 MCF7 cells (in 96 well microtiter plate) were treated with varying concentrations of Fe(III)-salen complexes for 96 hrs and the viable cells were quantified using MTT assay. The percent viable cells (relative to control DMSO treated) were plotted against concentrations for each compound. The concentration of the metal-complexes at which the conversion of MTT to formazan by viable cells is reduced by 50 % compared to control cells is defined as the $IC_{50.}$ Symbols (empty, shaded and filled triangles) represent the cytotoxicity curves for compds. **1-3** respectively. Symbols (empty, shaded and filled diamonds) represent the cytotoxicity curves for compds. **4-6** respectively. Symbols (empty, shaded and filled circles) represent the cytotoxicity curves for compds. **7-9** respectively.

Fig. 4 Fe (III)-salens induced activation of caspase-3/7. Jar (human placental cell line) cells were treated with 100 μM Fe (III)-salens for 16 hrs and subjected to caspase 3/7 activation assay using a commercially available caspase-3/7 Assay Kit (AnaSpec Inc).

The relative caspase-3/7 activity is compared to the untreated control were plotted for different Fe(III)-salen derivatives. Bars indicated SEM.

Fig. 5 DNA cleavage by Fe(III)-salen complexes. Supercoiled plasmid DNA pML20-47 (0.5 μg) was incubated with varying concentration of Fe(III)-salen complexes in presence of 1 mM DTT at 37 ºC for 1 hr, analyzed by agarose gel electrophoresis and quantified (ImageQuant) (**a**) Agarose gel picture showing the DNA cleavage analysis by compds **1**, **2** and **3**. (**b**): The percent DNA cleaved by compds. **3-9** were quantified and plotted.

Table 1. IC_{50} values of Fe(III)-salen derivatives towards MCF7 and JAR cells.

Compounds	IC_{50} (μM)	
	MCF7	JAR
1	22 (± 0.7)	22 (± 0.8)
2	1.3 (± 0.1)	0.6 (± 0.03)
3	0.5 (± 0.02)	0.3 (± 0.01)
4	0.2 (± 0.06)	0.2 (± 0.05)
5	>100	>100
6	>100	>100
7	1.5 (± 0.2)	1.1 (± 0.03)
8	0.5 (± 0.03)	0.2 (± 0.01)
9	1.3 (± 0.07)	1.0 (± 0.3)

The number in parenthesis indicates the standards error of the means (SEM).

Ansari et al Fig. 1

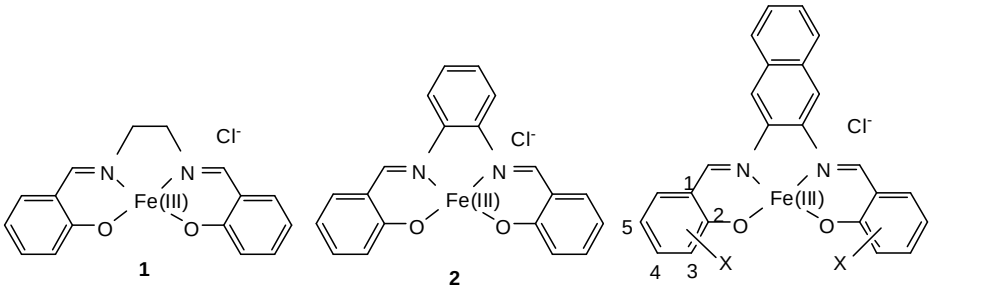

Ansari *et al.* Fig. 2

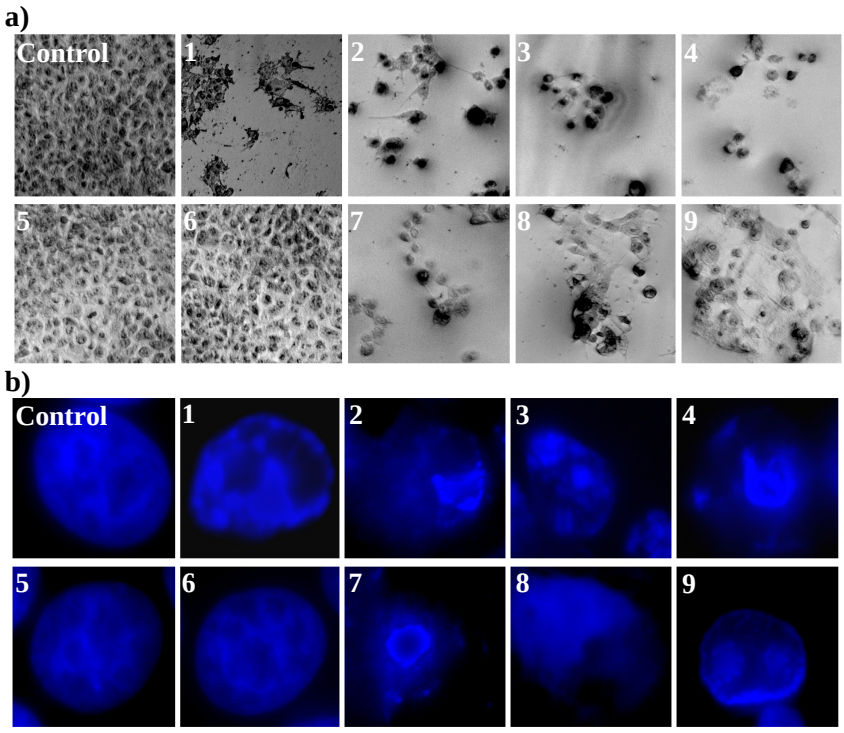

Ansari *et al* Fig. 3

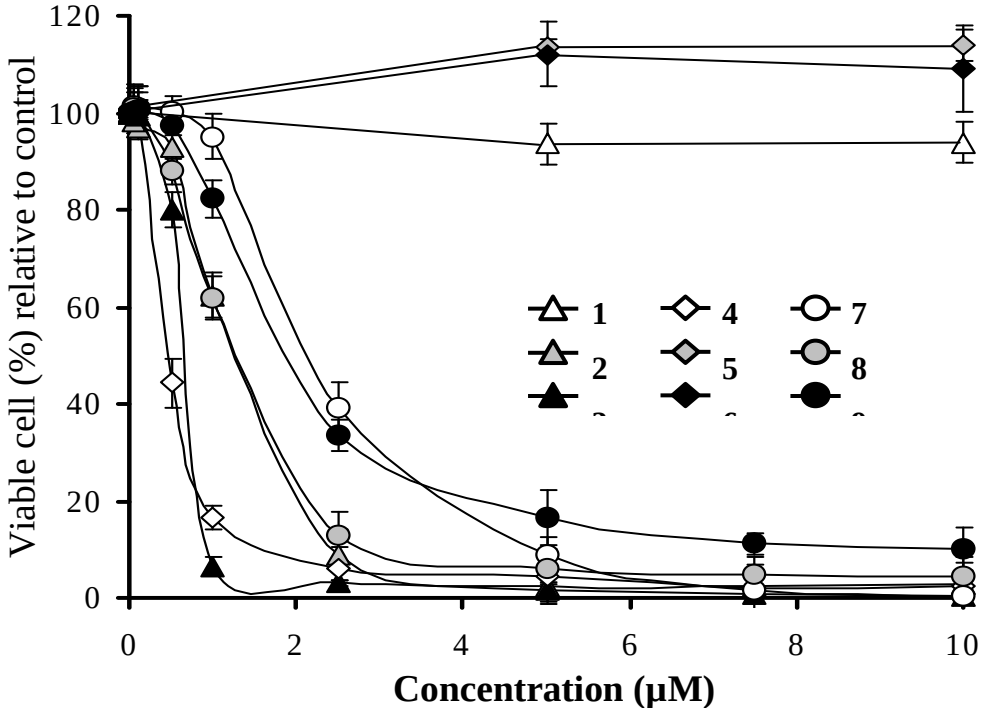

Ansari *et al.* Fig. 4

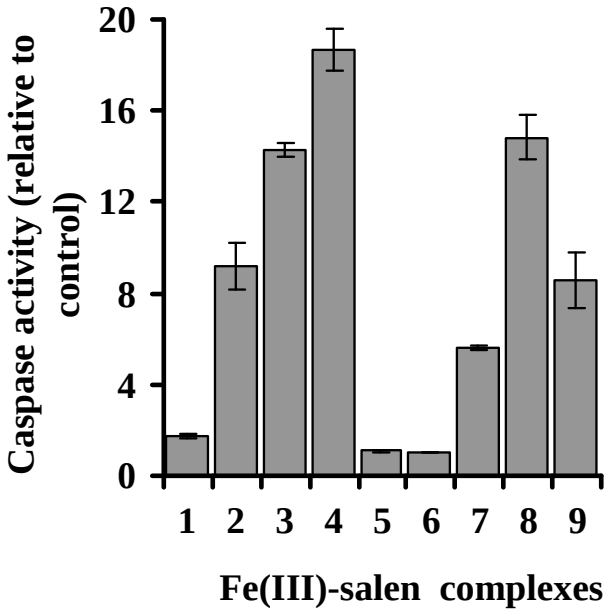

Ansari *et al.* Fig. 5

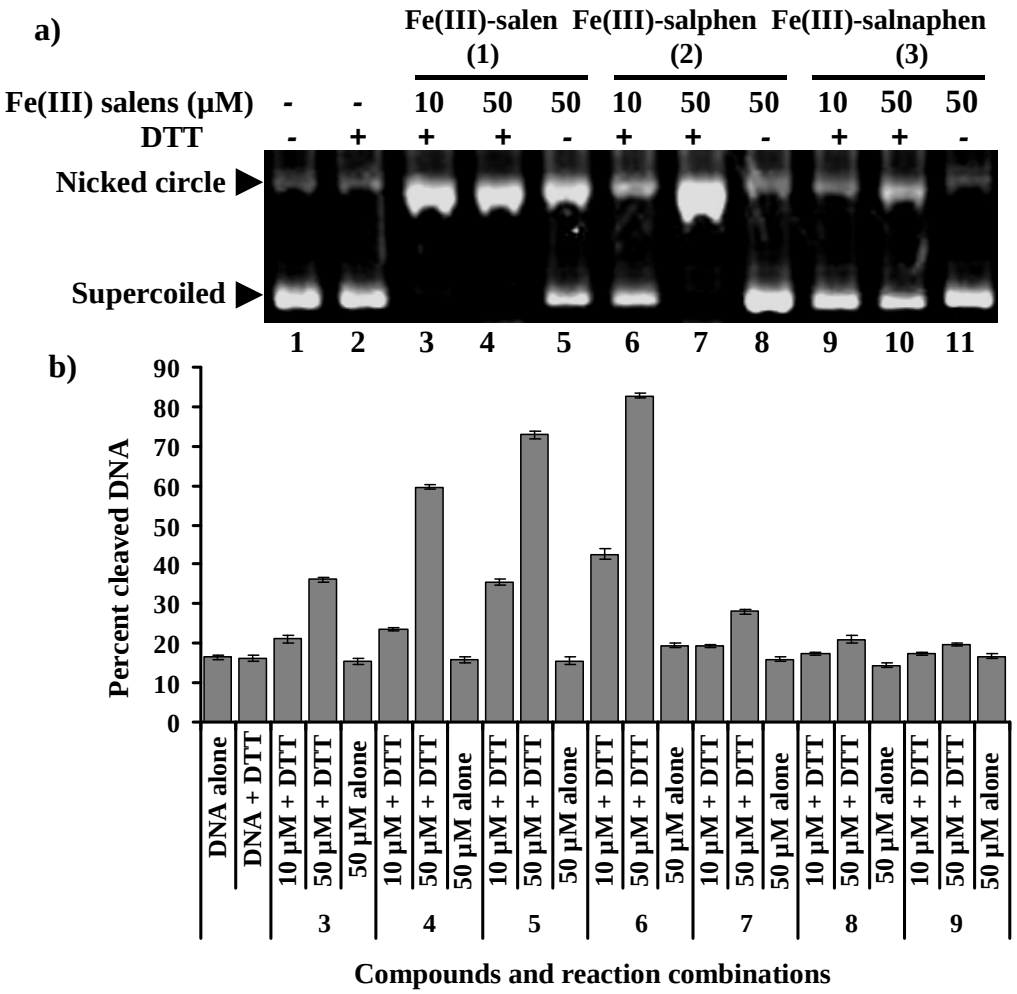

REFERENCES

(1) Sharma, P. S.; Sharma, R.; Tyagi, R. *Curr. Cancer. Drug Targets* **2008**, *8*, 53-75.

(2) Vermeulen, K.; Van Bockstaele, D. R.; Berneman, Z. N. *Cell Prolif.* **2003**, *36*, 131-149.

(3) Tost, J. *Methods Mol. Biol.* **2009**, *507*, 3-20.

(4) Zhang, C. X.; Lippard, S. J. *Curr. Opin. Chem. Biol.* **2003**, *7*, 481-489.

(5) Hanahan, D.; Weinberg, R. A. *Cell* **2000**, *100*, 57-70.

(6) Jagani, Z.; Khosravi-Far, R. *Adv. Exp. Med. Biol.* **2008**, *615*, 331-344.

(7) Desoize, B. *Anticancer Res.* **2004**, *24*, 1529-1544.

(8) Louie, A. Y.; Meade, T. J. *Chemical Reviews (Washington, D.C.)* **1999**, *99*, 2711-2734.

(9) Desoize, B. *Crit. Rev. Oncol. Hematol.* **2002**, *42*, 213-215.

(10) Orvig, C.; Abrams, M. J. *Chemical Reviews (Washington, D.C.)* **1999**, *99*, 2201-2203.

(11) Chitambar, C. R.; Narasimhan, J.; Guy, J.; Sem, D. S.; O'Brien, W. J. *Cancer Res.* **1991**, *51*, 6199-6201.

(12) UL-HAQ, R.; Chitambar, C. R. *Biochem. J.* **1993**, *294*, 873-877.

(13) Monti, E.; Monzini, F.; Morazzoni, F.; Perletti, G.; Piccini, F. *Inorg. Chim. Acta* **1993**, *205*, 181-184.

(14) Sadler, P. J.; Li, H.; Sun, H. *Coord. Chem. Rev.* **1999**, *185-186*, 689-709.

(15) Ho, B. T.; Huo, Y. Y.; Lee, J. H.; Levin, V. A. *Anticancer Drugs* **1991**, *2*, 267-268.

(16) Newman, D. J.; Cragg, G. M.; Snader, K. M. *Nat. Prod. Rep.* **2000**, *17*, 215-234.

(17) Newman, D. J.; Cragg, G. M.; Snader, K. M. *J. Nat. Prod.* **2003**, *66*, 1022-1037.

(18) Tiekink, E. R. *Crit. Rev. Oncol. Hematol.* **2002**, *42*, 217-224.

(19) Berman, J. D. *Rev. Infect. Dis.* **1988**, *10*, 560-586.

(20) Ge, R.; Sun, H. *Acc. Chem. Res.* **2007**, *40*, 267-274.

(21) Rosenberg, B.; Van Camp, L.; Krigas, T. *Nature* **1965**, *205*, 698-699.

(22) Malinowska, K.; Modranka, R.; Kedziora, J. *Pol. Merkur Lekarski* **2007**, *23*, 165-169.

(23) Thatcher, N.; Lind, M. *Semin. Oncol.* **1990**, *17*, 40-48.

(24) Alberts, D. S.; Green, S.; Hannigan, E. V.; Otoole, R.; Stocknovack, D.; Anderson, P.; Surwit, E. A.; Malvlya, V. K.; Nahhas, W. A.; Jolles, C. J. *Journal of Clinical Oncology* **1992**, *10*, 706-717.

(25) Holford, J.; Sharp, S. Y.; Murrer, B. A.; Abrams, M.; Kelland, L. R. *Br. J. Cancer* **1998**, *77*, 366-373.

(26) Treat, J.; Schiller, J.; Quoix, E.; Mauer, A.; Edelman, M.; Modiano, M.; Bonomi, P.; Ramlau, R.; Lemarie, E. *Eur. J. Cancer* **2002**, *38 Suppl 8*, S13-8.

(27) Gelmon, K. A.; Vandenberg, T. A.; Panasci, L.; Norris, B.; Crump, M.; Douglas, L.; Walsh, W.; Matthews, S. J.; Seymour, L. K. *Ann. Oncol.* **2003**, *14*, 543-548.

(28) Janaratne, T. K.; Yadav, A.; Ongeri, F.; MacDonnell, F. M. *Inorg. Chem.* **2007**, *46*, 3420-3422.

(29) Coluccia, M.; Sava, G.; Loseto, F.; Nassi, A.; Boccarelli, A.; Giordano, D.; Alessio, E.; Mestroni, G. *Eur. J. Cancer* **1993**, *29A*, 1873-1879.

(30) Bergamo, A.; Gava, B.; Alessio, E.; Mestroni, G.; Serli, B.; Cocchietto, M.; Zorzet, S.; Sava, G. *Int. J. Oncol.* **2002**, *21*, 1331-1338.

(31) Griffith, D.; Cecco, S.; Zangrando, E.; Bergamo, A.; Sava, G.; Marmion, C. J. *J. Biol. Inorg. Chem.* **2008**, *13*, 511-520.

(32) Hartinger, C. G.; Zorbas-Seifried, S.; Jakupec, M. A.; Kynast, B.; Zorbas, H.; Keppler, B. K. *J. Inorg. Biochem.* **2006**, *100*, 891-904.

(33) Jakupec, M. A.; Arion, V. B.; Kapitza, S.; Reisner, E.; Eichinger, A.; Pongratz, M.; Marian, B.; Graf von Keyserlingk, N.; Keppler, B. K. *Int. J. Clin. Pharmacol. Ther.* **2005**, *43*, 595-596.

(34) BAILES, R. H.; CALVIN, M. *Journal of the American Chemical Society* **1947**, *69*, 1886-1893.

(35) Thiel, W. R.; Angstl, M.; Hansen, N. *Journal of Molecular Catalysis A: Chemical* **1995**, *103*, 5-10.

(36) Bozell, J. J.; Hames, B. R.; Dimmel, D. R. *J. Org. Chem.* **1995**, 2398-2404.

(37) Sivasubramanian, V. K.; Ganesan, M.; Rajagopal, S.; Ramaraj, R. *J. Org. Chem.* **2002**, *67*, 1506-1514.

(38) Wong, T. W.; Lau, T. C.; Wong, W. T. *Inorg. Chem.* **1999**, *38*, 6181-6186.

(39) Dalton, C. T.; Ryan, K. M.; Wall, V. M.; Bousquet, C.; Gilheany, D. G. *Topics in Catalysis* **1998**, *5*, 75-91.

(40) Zhang, W.; Loebach, J. L.; Wilson, S. R.; Jacobsen, E. N. *J. Am. Chem. Soc.* **1990**, *112*, 2801-2803.

(41) Ito, Y. N.; Katsuki, T. *Bull. Chem. Soc. Jpn.* **1999**, *72*, 603-619.

(42) Cowan, J. A. *Curr. Opin. Chem. Biol.* **2001**, *5*, 634-642.

(43) Muller, J. G.; Kayser, L. A.; Paikoff, S. J.; Duarte, V.; Tang, N.; Perez, R. J.; Rokita, S. E.; Burrows, C. J. *Coord. Chem. Rev.* **1999**, *185-186*, 761-774.

(44) Boerner, L. J.; Zaleski, J. M. *Curr. Opin. Chem. Biol.* **2005**, *9*, 135-144.

(45) Meunier, B., Ed.; In *Site Specific Oxidative Scission of Nucleic Acids and Proteins In DNA and RNA Cleavers and Chemotherapy of Cancer and Viral Disease;* Kluwer Academic Publishers: Netherlands, 1996; , pp 119-132.

(46) Demeunynck, M.; Bailly, C.; Wilson, W. D.; Editors **2003**, 336.

(47) Gravert, D. J.; Griffin, J. H. *Inorg. Chem.* **1996**, *35*, 4837-4847.

(48) Mandal, S. S.; Kumar, N. V.; Varshney, U.; Bhattacharya, S. *J. Inorg. Biochem.* **1996**, *63*, 265-272.

(49) Gravert, D. J.; Griffin, J. H. *Inorg. Chem.* **1996**, *35*, 4837-4847.

(50) Sakurai, F.; Inoue, R.; Nishino, Y.; Okuda, A.; Matsumoto, O.; Taga, T.; Yamashita, F.; Takakura, Y.; Hashida, M. *J. Controlled Release* **2000**, *66*, 255-269.

(51) Tsuji, A.; Sakurai, H. *Biochem. Biophys. Res. Commun.* **1996**, *226*, 506-511.

(52) Rajaram, R.; Nair, B. U.; Ramasami, T. *Biochem. Biophys. Res. Commun.* **1995**, *210*, 434-440.

(53) Afonso, V.; Champy, R.; Mitrovic, D.; Collin, P.; Lomri, A. *Joint Bone Spine* **2007**, *74*, 324-329.

(54) Freeman, B. A.; Crapo, J. D. *Lab. Invest.* **1982**, *47*, 412-426.

(55) Day, B. J. *DDT* **2004**, *9*, 557-566.

(56) Maxwell, S. R.; Lip, G. Y. *Br. J. Clin. Pharmacol.* **1997**, *44*, 307-317.

(57) Salvemini, D.; Riley, D. P.; Cuzzocrea, S. *Nat. Rev. Drug Discov.* **2002**, *1*, 367-374.

(58) Liu, R.; Liu, I. Y.; Bi, X.; Thompson, R. F.; Doctrow, S. R.; Malfroy, B.; Baudry, M. *Proc. Natl. Acad. Sci. U. S. A.* **2003**, *100*, 8526-8531.

(59) Peng, J.; Stevenson, F. F.; Doctrow, S. R.; Andersen, J. K. *J. Biol. Chem.* **2005**, *280*, 29194-29198.

(60) Sharpe, M. A.; Ollosson, R.; Stewart, V. C.; Clark, J. B. *Biochem. J.* **2002**, *366*, 97-107.

(61) Decraene, D.; Smaers, K.; Gan, D.; Mammone, T.; Matsui, M.; Maes, D.; Declercq, L.; Garmyn, M. *J. Invest. Dermatol.* **2004**, *122*, 484-491.

(62) Doctrow, S. R.; Huffman, K.; Marcus, C. B.; Musleh, W.; Bruce, A.; Baudry, M.; Malfroy, B. *Adv. Pharmacol.* **1997**, *38*, 247-269.

(63) Kerr, J. F.; Wyllie, A. H.; Currie, A. R. *Br. J. Cancer* **1972**, *26*, 239-257.

(64) Elmore, S. *Toxicol. Pathol.* **2007**, *35*, 495-516.

(65) Segal-Bendirdjian, E.; Hillion, J.; Belmokhtar, C. A. *Bull. Cancer* **2003**, *90*, 9-17.

(66) Renehan, A. G.; Booth, C.; Potten, C. S. *BMJ* **2001**, *322*, 1536-1538.

(67) Thompson, C. B. *Science* **1995**, *267*, 1456-1462.

(68) Desoize, B. *Anticancer Res.* **1994**, *14*, 2291-2294.

(69) Maddika, S.; Ande, S. R.; Panigrahi, S.; Paranjothy, T.; Weglarczyk, K.; Zuse, A.; Eshraghi, M.; Manda, K. D.; Wiechec, E.; Los, M. *Drug Resist Updat* **2007**, *10*, 13-29.

(70) Thomadaki, H.; Scorilas, A. *Crit. Rev. Clin. Lab. Sci.* **2006**, *43*, 1-67.

(71) Fesik, S. W. *Nat. Rev. Cancer.* **2005**, *5*, 876-885.

(72) de Vries, E. G.; Timmer, T.; Mulder, N. H.; van Geelen, C. M.; van der Graaf, W. T.; Spierings, D. C.; de Hooge, M. N.; Gietema, J. A.; de Jong, S. *Drugs Today (Barc)* **2003**, *39 Suppl C*, 95-109.

(73) Gao, Z.; Shao, Y.; Jiang, X. *J. Biol. Chem.* **2005**, *280*, 38271-38275.

(74) Tolcher, A. W. *Hematol. Oncol. Clin. North Am.* **2002**, *16*, 1255-1267.

(75) Lemasters, J. J.; Nieminen, A. L.; Qian, T.; Trost, L. C.; Elmore, S. P.; Nishimura, Y.; Crowe, R. A.; Cascio, W. E.; Bradham, C. A.; Brenner, D. A.; Herman, B. *Biochim. Biophys. Acta* **1998**, *1366*, 177-196.

(76) Ow, Y. L.; Green, D. R.; Hao, Z.; Mak, T. W. *Nat. Rev. Mol. Cell Biol.* **2008**, *9*, 532-542.

(77) Suen, D. F.; Norris, K. L.; Youle, R. J. *Genes Dev.* **2008**, *22*, 1577-1590.

(78) Chowdhury, I.; Tharakan, B.; Bhat, G. K. *Comp. Biochem. Physiol. B. Biochem. Mol. Biol.* **2008**, *151*, 10-27.

(79) Salvesen, G. S.; Riedl, S. J. *Adv. Exp. Med. Biol.* **2008**, *615*, 13-23.

(80) Minn, A. J.; Rudin, C. M.; Boise, L. H.; Thompson, C. B. *Blood* **1995**, *86*, 1903-1910.

(81) Alvarez-Lorenzo, C.; Concheiro, A. *Mini Rev. Med. Chem.* **2008**, *8*, 1065-1074.

(82) Kaparissides, C.; Alexandridou, S.; Kotti, K.; Chaitidou, S. *Journal of Nanotechnology Online* **2006**.

(83) Hamoudeh, M.; Kamleh, M. A.; Diab, R.; Fessi, H. *Adv. Drug Deliv. Rev.* **2008**, *60*, 1329-1346.

(84) Panchapakesan, B.; Wickstrom, E. *Surg. Oncol. Clin. N. Am.* **2007**, *16*, 293-305.

(85) Jain, S. K.; Gupta, Y.; Jain, A.; Bhola, M. *Drug Deliv.* **2007**, *14*, 327-335.

(86) Kashiwagi, H.; Ueno, M. *Yakugaku Zasshi* **2008**, *128*, 669-680.

(87) Al-Jamal, W. T.; Kostarelos, K. *Nanomed* **2007**, *2*, 85-98.

(88) Rui, Y.; Wang, S.; Low, P. S.; Thompson, D. H. *J. Am. Chem. Soc.* **1998**, *120*, 11213-11218.

(89) Gabizon, A.; Shmeeda, H.; Horowitz, A. T.; Zalipsky, S. *Adv. Drug Deliv. Rev.* **2004**, *56*, 1177-1192.

(90) Simoes, S.; Moreira, J. N.; Fonseca, C.; Duzgunes, N.; de Lima, M. C. *Adv. Drug Deliv. Rev.* **2004**, *56*, 947-965.

(91) Fattal, E.; Couvreur, P.; Dubernet, C. *Adv. Drug Deliv. Rev.* **2004**, *56*, 931-946.

(92) Gaspar, M. M.; Perez-Soler, R.; Cruz, M. E. *Cancer Chemother. Pharmacol.* **1996**, *38*, 373-377.

(93) Nobuto, H.; Sugita, T.; Kubo, T.; Shimose, S.; Yasunaga, Y.; Murakami, T.; Ochi, M. *Int. J. Cancer* **2004**, *109*, 627-635.

(94) Babincova, M.; Altanerova, V.; Lampert, M.; Altaner, C.; Machova, E.; Sramka, M.; Babinec, P. *Z. Naturforsch. [C]*. **2000**, *55*, 278-281.

(95) Dudu, V.; Ramcharan, M.; Gilchrist, M. L.; Holland, E. C.; Vazquez, M. *J. Nanosci Nanotechnol* **2008**, *8*, 2293-2300.

(96) Matteucci, M. L.; Thrall, D. E. *Vet. Radiol. Ultrasound* **2000**, *41*, 100-107.

(97) Weissig, V.; Babich, J.; Torchilin, V. *Colloids and Surfaces, B: Biointerfaces* **2000**, *18*, 293-299.

(98) Dagar, S.; Rubinstein, I.; Onyuksel, H. *Methods Enzymol.* **2003**, *373*, 198-214.

(99) Zuhorn, I. S.; Engberts, J. B.; Hoekstra, D. *Eur. Biophys. J.* **2007**, *36*, 349-362.

(100) Torchilin, V. P. *Nat. Rev. Drug Discov.* **2005**, *4*, 145-160.

(101) Wu, Z. H.; Ping, Q. N.; Wei, Y.; Lai, J. M. *Acta Pharmacol. Sin.* **2004**, *25*, 966-972.

(102) Minato, S.; Iwanaga, K.; Kakemi, M.; Yamashita, S.; Oku, N. *J. Control. Release* **2003**, *89*, 189-197.

(103) Koshkina, N. V.; Golunski, E.; Roberts, L. E.; Gilbert, B. E.; Knight, V. *J. Aerosol Med.* **2004**, *17*, 7-14.

(104) Yoo, H. S.; Park, T. G. *J. Control. Release* **2004**, *96*, 273-283.

(105) Lu, Y.; Low, P. S. *Adv. Drug Deliv. Rev.* **2002**, *54*, 675-693.

(106) Ishida, O.; Maruyama, K.; Tanahashi, H.; Iwatsuru, M.; Sasaki, K.; Eriguchi, M.; Yanagie, H. *Pharm. Res.* **2001**, *18*, 1042-1048.

(107) Eavarone, D. A.; Yu, X.; Bellamkonda, R. V. *J. Biomed. Mater. Res.* **2000**, *51*, 10-14.

(108) Parker, N.; Turk, M. J.; Westrick, E.; Lewis, J. D.; Low, P. S.; Leamon, C. P. *Anal. Biochem.* **2005**, *338*, 284-293.

(109) Pires, P.; Simoes, S.; Nir, S.; Gaspar, R.; Duzgunes, N.; Pedroso De Lima,Maria C. *Biochimica et Biophysica Acta, Biomembranes* **1999**, *1418*, 71-84.

(110) Safinya, C. R. *Curr. Opin. Struct. Biol.* **2001**, *11*, 440-448.

(111) de Lima, M. C.; Simoes, S.; Pires, P.; Gaspar, R.; Slepushkin, V.; Duzgunes, N. *Mol. Membr. Biol.* **1999**, *16*, 103-109.

(112) Kawaura, C.; Noguchi, A.; Furuno, T.; Nakanishi, M. *FEBS Lett.* **1998**, *421*, 69-72.

(113) Ross, P. C.; Hui, S. W. *Gene Ther.* **1999**, *6*, 651-659.

(114) Elouahabi, A.; Ruysschaert, J. M. *Mol. Ther.* **2005**, *11*, 336-347.

(115) Hoekstra, D.; Rejman, J.; Wasungu, L.; Shi, F.; Zuhorn, I. *Biochem. Soc. Trans.* **2007**, *35*, 68-71.

(116) Arkin, M. *Curr. Opin. Chem. Biol.* **2005**, *9*, 317-324.

(117) Lum, J. K.; Mapp, A. K. *Chembiochem* **2005**, *6*, 1311-1315.

(118) Pogozelski, W. K.; Tullius, T. D. *Chemical Reviews (Washington, D.C.)* **1998**, *98*, 1089-1107.

(119) Earnshaw, W. C.; Martins, L. M.; Kaufmann, S. H. *Annu. Rev. Biochem.* **1999**, *68*, 383-424.

(120) Goldstein, J. C.; Waterhouse, N. J.; Juin, P.; Evan, G. I.; Green, D. R. *Nat. Cell Biol.* **2000**, *2*, 156-162.

(121) Kawane, K.; Nagata, S. *Methods Enzymol.* **2008**, *442*, 271-287.

(122) Jenuwein, T.; Allis, C. D. *Science* **2001**, *293*, 1074-1080.

(123) Chalah, A.; Khosravi-Far, R. *Adv. Exp. Med. Biol.* **2008**, *615*, 25-45.

(124) Routier, S.; Vezin, H.; Lamour, E.; Bernier, J. L.; Catteau, J. P.; Bailly, C. *Nucleic Acids Res.* **1999**, *27*, 4160-4166.

(125) Gerloch, M.; Lewis, J.; Mabbs, F. E.; Richards, A. *J. Chem. Soc. A* **1968**, 116.

(126) Sharma, Y. S.; Mathur, P. *Transition Metal Chemistry* **1994**, *19*.

(127) Singh, G.; Sharkey, S. M.; Moorehead, R. *Pharmacol. Ther.* **1992**, *54*, 217-230.

(128) Mathis, A.; Wild, P.; Boettger, E. C.; Kapel, C. M.; Deplazes, P. *Antimicrob. Agents Chemother.* **2005**, *49*, 3251-3255.

(129) Zhang, L.; Wu, Q. *J. Biosci.* **2005**, *30*, 599-604.

(130) Mandal, S. S.; Varshney, U.; Bhattacharya, S. *Bioconjug. Chem.* **1997**, *8*, 798-812.

(131) de, B. J.; Hoeijmakers, J. H. *Carcinogenesis* **2000**, *21*, 453-460.

(132) Ansari, A. Z.; Mapp, A. K. *Curr. Opin. Chem. Biol.* **2002**, *6*, 765-772.

(133) Majmudar, C. Y.; Mapp, A. K. *Curr. Opin. Chem. Biol.* **2005**, *9*, 467-474.

(134) Awasthi, S.; Singhal, S. S.; He, N.; Chaubey, M.; Zimniak, P.; Srivastava, S. K.; Singh, S. V.; Awasthi, Y. C. *Int. J. Cancer* **1996**, *68*, 333-339.

(135) Nguyen, S. M.; Lieven, C. J.; Levin, L. A. *J. Neurosci. Methods* **2007**, *161*, 281-284.

(136) Shilatifard, A. *Annu. Rev. Biochem.* **2006**, *75*, 243-269.

(137) Sims, R. J.,3rd; Mandal, S. S.; Reinberg, D. *Curr. Opin. Cell Biol.* **2004**, *16*, 263-271.

(138) Chen, H.; Ke, Q.; Kluz, T.; Yan, Y.; Costa, M. *Mol. Cell. Biol.* **2006**, *26*, 3728-3737.

(139) Woldemariam, G. A.; Mandal, S. S. *J. Inorg. Biochem.* **2008**, *102*, 740-747.

(140) Pavri, R.; Zhu, B.; Li, G.; Trojer, P.; Mandal, S.; Shilatifard, A.; Reinberg, D. *Cell* **2006**, *125*, 703-717.

(141) Zhu, B.; Mandal, S. S.; Pham, A. D.; Zheng, Y.; Erdjument-Bromage, H.; Batra, S. K.; Tempst, P.; Reinberg, D. *Genes Dev.* **2005**, *19*, 1668-1673.

(142) Mandal, S. S.; Chu, C.; Wada, T.; Handa, H.; Shatkin, A. J.; Reinberg, D. *Proc. Natl. Acad. Sci. U. S. A.* **2004**, *101*, 7572-7577.

(143) Mandal, S. S.; Cho, H.; Kim, S.; Cabane, K.; Reinberg, D. *Mol. Cell. Biol.* **2002**, *22*, 7543-7552.

(144) Rokita, S. E.; Burrows, C. J. In *Salen Metal Complexes* Demeunynck, M., Bailly, C., Eds.; Small Molecule DNA and RNA binders, Salen Metal Complexes; Wiley-VCH Verlag GmbH & Co. KGaA: 2003; pp 126-145.

(145) Cronin, M. T.; Schultz, T. W. *Chem. Res. Toxicol.* **2001**, *14*, 1284-1295.

(146) Moridani, M. Y.; Siraki, A.; O'Brien, P. J. *Chem. Biol. Interact.* **2003**, *145*, 213-223.

(147) Abraham, D. J., Ed.; In *Burger's Medicinal Chemistry and Drug Discovery;* John Wiley & Sons: 2003; Vol. 6, pp 5568.

(148) Kerns, E. H.; Di, L. In *Drug-Like Properties: Concepts, Structure Design and Methods from ADME to Toxicity Optimization;* Academic Press Elsevier: 2008; pp 43-47.

(149). Kuz'min, V. E.; Muratov, E. N.; Artemenko, A. G.; Gorb, L.; Qasim, M.; Leszczynski, J. *J. Comput. Aided Mol. Des.* **2008**, *22*, 747-759.

(150) Domanska, U.; Bogel-Lukasik, E.; Bogel-Lukasik, R. *Chemistry--A European Journal* **2003**, *9*, 3033-3041.

(151) Wright, J. S.; Shadnia, H. *Chem. Res. Toxicol.* **2008**, *21*, 1426-1431.

(152) Tollefsen, K. E.; Blikstad, C.; Eikvar, S.; Farmen Finne, E.; Katharina Gregersen, I. *Ecotoxicol. Environ. Saf.* **2008**, *69*, 64-73.

(153) Tanrikulu, Y.; Schneider, G. *Nat. Rev. Drug Discov.* **2008**, *7*, 667-677.

(154) Tang, Y. Z.; Liu, Z. Q. *Cell Biochem. Funct.* **2008**, *26*, 185-191.

(155) Kozubek, A. *Acta Biochim. Pol.* **1995**, *42*, 247-251.

(156) Ben-Sasson, S. A.; Sherman, Y.; Gavrieli, Y. *Methods Cell Biol.* **1995**, *46*, 29-39.

(157) Ellis, R. E.; Yuan, J. Y.; Horvitz, H. R. *Annu. Rev. Cell Biol.* **1991**, *7*, 663-698.

(158) Uchiyama, Y. *Tanpakushitsu Kakusan Koso* **1997**, *42*, 2311-2316.

(159) Glover, D. J.; Lipps, H. J.; Jans, D. A. *Nat. Rev. Genet.* **2005**, *6*, 299-310.

(160) Ewert, K. K.; Ahmad, A.; Bouxsein, N. F.; Evans, H. M.; Safinya, C. R. *Methods Mol. Biol.* **2008**, *433*, 159-175.

(161) Cruz-Campa, I.; Arzola, A.; Santiago, L.; Parsons, J. G.; Varela-Ramirez, A.; Aguilera, R. J.; Noveron, J. C. *Chemical Communications (Cambridge, United Kingdom)* **2007**, 2944-2946.

(162) Sawant, R. M.; Hurley, J. P.; Salmaso, S.; Kale, A.; Tolcheva, E.; Levchenko, T. S.; Torchilin, V. P. *Bioconjug. Chem.* **2006**, *17*, 943-949.

(163) Hafez, I. M.; Ansell, S.; Cullis, P. R. *Biophys. J.* **2000**, *79*, 1438-1446.

(164) Hiraka, K.; Kanehisa, M.; Tamai, M.; Asayama, S.; Nagaoka, S.; Oyaizu, K.; Yuasa, M.; Kawakami, H. *Colloids Surf. B Biointerfaces* **2008**, *67*, 54-58.

(165) Jesorka, A.; Orwar, O. *Annual Review of Analytical Chemistry* **2008**, *1*, 801-832.

(166) Kinnunen, P. K. *Chem. Phys. Lipids* **1991**, *57*, 375-399.

(167) Mora, M.; Sagrista, M. L.; Trombetta, D.; Bonina, F. P.; De Pasquale, A.; Saija, A. *Pharm. Res.* **2002**, *19*, 1430-1438.

(168) Frisken, B. J. *Appl. Opt.* **2001**, *40*, 4087-4091.

(169) Goll, J. H.; Stock, G. B. *Biophys. J.* **1977**, *19*, 265-273.

(170) Dzakpasu, R.; Axelrod, D. *Biophys. J.* **2004**, *87*, 1279-1287.

(171) Mustapa, M. F.; Bell, P. C.; Hurley, C. A.; Nicol, A.; Guenin, E.; Sarkar, S.; Writer, M. J.; Barker, S. E.; Wong, J. B.; Pilkington-Miksa, M. A.; Papahadjopoulos-Sternberg, B.; Shamlou, P. A.; Hailes, H. C.; Hart, S. L.; Zicha, D.; Tabor, A. B. *Biochemistry* **2007**, *46*, 12930-12944.

(172) Everhart, T. E.; Thornley, R. F. M. *Journal of Scientific Instruments* **1960**, *37*, 246-248.

(173) Allen, T. D.; Rutherford, S. A.; Murray, S.; Drummond, S. P.; Goldberg, M. W.; Kiseleva, E. *Methods Cell Biol.* **2008**, *88*, 389-409.

(174) Tsien, R. Y. *Annu. Rev. Biochem.* **1998**, *67*, 509-544.

(175) Bajaj, A.; Kondaiah, P.; Bhattacharya, S. *J. Med. Chem.* **2008**, *51*, 2533-2540.

BIOGRAPHICAL INFORMATION

Getachew Abebe Woldemariam obtained his Ph.D. in Chemistry from The University of Texas at Arlington, December 2008.